Master's thesis

NTNU
Norwegian University of Science and Technology
Faculty of Engineering
Department of Structural Engineering

Hollevik, Lars Jørgen

Fatigue life estimation of Norwegian railway bridges

Master's thesis in Mechanical Engineering
Supervisor: Frøseth, Gunnstein Thomas
December 2020

NTNU
Norwegian University of
Science and Technology

Hollevik, Lars Jørgen

Fatigue life estimation of Norwegian railway bridges

Master's thesis in Mechanical Engineering
Supervisor: Frøseth, Gunnstein Thomas
December 2020

Norwegian University of Science and Technology
Faculty of Engineering
Department of Structural Engineering

NTNU
Norwegian University of
Science and Technology

Fatigue life estimation of Norwegian railway bridges

Norwegian University of Science and Technology

Department of Structural Engineering

Lars Jørgen Hollevik

Abstract

This thesis presents an estimation of the remaining fatigue life of 3 bridges on the Norwegian railway system with a new train load model from [9]. This is done to establish if this load model, based on being conservative, consistent and simple, can be used to replace the existing load models. Fatigue failure is a growing concern regarding steel truss bridges, to replace or refurbish all these bridges would be very expensive and time-consuming. An easy and labour-effective way to prioritise which bridges should be upgraded or replaced would be to estimate the remaining fatigue lifetime of all bridges in the network.

The estimation is done by establishing the influence lines on the bridges by utilising finite element analysis, combining this with the new load model for Norwegian trains and estimating the historic and future fatigue damage accumulated in the bridges by using the rainflow-algorithm.

The results from this estimation shows that the new load model based on being conservative, consistent and simple, results in predictions suggesting large amounts of fatigue damage accumulated on the bridges

The results presented in this thesis are compared with results obtained in an analysis made for Bane NOR in 2018 using a different load model. The comparison shows that the new load model estimates greater damage, a difference in location sustaining the most damage is found, but the percentage of damage over the years are similar between the two models.

A recommendation for further research is to refine the new load model to display a more realistic value for the fatigue damage.

Sammendrag

Denne avhandlingen presenterer resterende livstidsberegning med hensyn på utmattelse for 3 bruer på det norske jernbane systemet ved hjelp av en ny lastmodell foreslått i Frøseth [9]. Dette er gjort for å om den nye lastmodellen, som er basert på å være enkel, konservativ og konsistent, kan erstatte allerede eksisterende modeller. Utmattingsbrudd er en stadig økende fare med hensyn på fagverksbruer i stål, erstatning og overhaling av alle disse bruene vil være kostbart og tidskrevende. En enkel og lite arbeidskrevende måte å prioritere hvilke bruer som skal oppgraderes eller erstattes vil være å estimere resterende livstid med hensyn på utmattelse for alle bruer på det norske jernbanesystemet.

Estimeringen blir gjort ved å etablere influenslinjer på bruen ved hjelp av elementmetoden. Dette kombineres med den nye lastmodellen for norske tog og estimerer historisk og fremtidig utmattelsesskade akkumulert i bruene ved hjelp av rainflow-algoritmen.

Resultatet fra estimeringene viser at den nye last modellen basert på å være konservativ, konsistent og enkel, viser at store mengder utmattelsesskade akkumuleres i bruene.

Resultatene presentert i avhandlingen blir sammenlignet med resultater gitt i en rapport laget av Bane NOR i 2018 hvor det benyttes en annen lastmodell. Sammenligningen viser at den nye lastmodellen estimerer mye større skade, ulik lokasjon for de mest skadede komponentene, men det finnes likheter i hvordan skaden fordeles prosentvis over årene.

Anbefaling til videre forskning er å rafinere den nye lastmodellen til å vise mer realistiske verdier for utmattelsesskade.

Table of Contents

Abbreviations

N	=	number of stress cycles until failure
S	=	Stress range
D	=	total fatigue damage
D_0	=	yearly fatigue damage introduced by past cycles
D_1	=	yearly fatigue damage introduced by future cycles
D_c	=	critical total fatigue damage
S_i	=	stress cycles
δ	=	dirac delta
t	=	fatigue life
p_i	=	load magnitude
n_p	=	number of axles on train
f	=	static loading function
C	=	empirical parameter in fatigue endurance model
b	=	empirical parameter in fatigue endurance model
Φ	=	dynamic amplification factor
l	=	influence line
L	=	length of influence line
ν	=	speed of train
z_0	=	static response
$z(s)$	=	dynamic response
$\Delta\sigma_c$	=	reference fatigue strength
N_x	=	axial force
M_y	=	bending force in weak direction
M_z	=	bending force in strong direction
A_x	=	area of cross-section
A_y	=	shear area about vertical axis
A_z	=	shear area about horizontal axis
W_y	=	sectional modulus of weak axis
W_z	=	sectional modulus of strong axis
σ	=	stress
I_z	=	torsion
I_x	=	second moment of area over horizontal axis
I_y	=	second moment of area over vertical axis
Q_y	=	shear stress in y-direction
Q_z	=	shear stress in z-direction
Q_{tk}	=	characteristic value of the transverse load
r	=	radius of curvature of the bridge
Q_k	=	transverse influence line value
F	=	vertical axle load

F_{th}	=	horizontal force from the centrifugal force
F_{tv}	=	vertical force pair from the centrifugal force
F_{perm}	=	permanent load
$D_{passage}$	=	damage per passage
$D_{pos-passage}$	=	damage per passage in positive direction
$D_{neg-passage}$	=	damage per passage in negative direction
γ_{Mf}	=	partial safety factor for fatigue resistance
a_i	=	traffic mix coefficient

Chapter 1

Introduction

This thesis will concern the topic of estimating the remaining lifetime of steel railway bridges in Norway with respect to fatigue. There are over 2300 railway bridges in the Norwegian railway system, out of which more than 900 are steel bridges [9]. These steel bridges were largely constructed between 1900 and 1960. From the 1960s and up to present day there has been big changes in the design criteria for railway bridges in order to meet the requirements for higher speed and traffic load. These requirements have been caused by higher demand and technological advances made in the railway industry. The increase in loads and frequency leads to a exponential increase in fatigue mechanisms in the bridges. Such increase in fatigue mechanisms will have influence on the expected lifetime the bridge was designed for, and increase the probability of damages and a potential catastrophic collapse.

Railway bridges are costly to upgrade. There is a large cost related to the investment in the upgrade itself, in addition to the cost of delaying and interrupting existing traffic on the distances. It is unfeasible to upgrade or replace all the bridges in the Norwegian railway system as a campaign exercise. Therefore, it is important to monitor and identify fatigue in order to prioritise critical cases for upgrade or full replacement. To make this possible it is necessary to estimate the remaining fatigue-life of each and every bridge in the Norwegian railway network.

An analysis conducted by Bane NOR in 2015 concluded the need for fatigue life calculations to be made on all steel truss and pendulum pillar bridges constructed after the load class 1899. This in order to minimize the number of - and further mapping of need for - manual inspections. Bane NOR engaged a consulting firm to control Norwegian steel railway bridges with regards to fatigue life. Bane NOR owns about 100 railway bridges that are constructed in accordance to the 1899 load class and that spans over 15 meters. A selection of 21 of these bridges, expected to be the most probable to experience fatigue failure was selected for a fatigue life analysis based on train traffic and year of construction.

A fatigue life analysis of 3 of these railway bridges on the Norwegian railway network using a revised load model and traffic frequency definition from [9] will be conducted

in this thesis. Relevant theory and methods for fatigue calculation will be presented in the following chapters. The load-model proposed in [9] and the original model used by Bane NOR for train traffic will be presented. The results from the revised analysis will be compared to the results obtained in the analysis made by Bane NOR in 2018 to highlight advantages and disadvantages associated with each of the two load models.

Chapter 2

Basic Theory

2.1 Theory

The theory in this report is largely based on what is presented in chapter 1 in [9]. [9] shall therefore be considered as reference for this chapter in general.

To estimate the remaining fatigue life of a railway bridge, both crack initiation and crack growth needs to be included in the analysis. This can be determined by a combination of a fatigue endurance model and a damage accumulation model. Basquins relation 2.1,

$$N(S) = CS^{-b} \tag{2.1}$$

is a commonly used fatigue endurance model. N in the model is defined as cycles it takes for a component to go from perfect uncracked material to fatigue failure. S is the stress range the component is repeatedly exposed to. C and b are empirical parameters determined by different tests of different structural details. The fatigue endurance model describes a components repeated exposure to a single stress range. To fully describe the response of a railway bridge, several different stress ranges needs to be combined. This can be done by introducing a damage accumulation model. The Miner's linear damage accumulation rule, shown in equation 2.2 is a such formulation.

$$D = \sum_{i=1}^{k} \frac{1}{N(S_i)} \tag{2.2}$$

Where D is the total fatigue damage accumulated from the stress cycles S_i. When the component reaches a critical level of total fatigue damage D_c, it will fail. The remaining fatigue life depends on how much fatigue damage has been inflicted by past cycles and how much that will be introduced in the future.

$$t = \frac{D_C - D_0}{D_1} \tag{2.3}$$

D_0 denotes the fatigue damage introduced by past cycles. D_1 denotes the yearly fatigue damage introduced in future cycles. This provides the remaining fatigue life t given in years, formulated in equation 2.3.

The stress cycles needs to be established to utilise the formulations stated above. Stress can be inflicted on the bridge as traffic loads and environmental loads. Given that traffic loads will have higher load intensity and application frequency, this will be the critical load regarding fatigue damage, and will be the only load that needs to be modelled. The load can be determined either by physical measurement on the bridge being analysed or by numerical modelling. Numerical modelling will be the preferable choice. Given that this method is cheaper than measurements and give a higher number of data-points than placing measuring devices on the bridges. A numerical model based on an analysis conducted by the finite element method will be used in this report. Here the stress cycles will be modelled by static load moving over the strikers on the bridge. The modelling will be explained in further detail in section 3.1. The static loading can be formulated as in equation 2.4.

$$f(x) = \sum_{i=1}^{n_p} p_i \delta(x - x_i) \tag{2.4}$$

Where δ is the dirac delta function, p_i is the load magnitude and n_p is the number of axles on the train. The influence line $l(x)$ visualize the responses of axial load, bending momentum in weak and strong direction in a predetermined point as the point-load moves over the bridge. By taking the convolution between the influence lines and the static loading function, denoted by the $(*)$ sign, the static response of the bridge can be determined from equation 2.5.

$$z_0(s) = (l * f)(s) = \sum_{i=1}^{n_p} p_i l(s - x_i) \tag{2.5}$$

Where z_0 denotes the static response, l is the influence-line, f is the static loading and s is a shift variable showing the distance the train has moved along the influence line.

By combining the dynamic amplification factor $\Phi(\nu, L)$ with the static response defined in equation 2.5, the total response $z(s)$ of the railway bridge can be defined as

$$z(s) = \Phi(\nu, L) \cdot \sum_{i=1}^{n_p} p_i l(s - x_i) \tag{2.6}$$

The dynamic amplification factor $\Phi(\nu, L)$ is determined for fatigue loads by train speed ν and the length of the influence line analysed L. Dynamic amplification factor for fatigue loads is found by methods further described in [6].

The dynamic total response $z(s)$ is the stress response introduced to the railway bridge by the influence lines.

When conducting fatigue estimation, the normal stress response is considered, giving the following force components to be included; axial force N_x , bending force in weak direction M_y and bending force in strong direction M_z, obtained from $z(s)$ for the different

influence lines of the corresponding force component. The force components are divided by their respective resistance according to 2.7 to get the stress.

$$\sigma = \frac{N_x}{A_x} + \frac{M_y}{W_y} + \frac{M_z}{W_z} \tag{2.7}$$

The resistance being cross section data from the section point analysed, A_x the area of the cross section, W_y and W_z being the sectional modulus of the weak and strong axis of the elements.

The stress cycles S_i mentioned above in the Basquins relation 2.1 and the Miner's accumulation rule 2.2 can be found from the stress σ by a cycle counting algorithm. The cycle counting algorithm is explained in [5].

2.2 Original load model for Norwegian trains

The fatigue life estimations made for Bane NOR where conducted using load model developed through a prior cooperation between Bane NOR and Norges teknisk-naturvitenskaplige universitet (NTNU). This model consists of 13 trains. Four of these trains are taken from the load models described in annex D in Eurocode [7] and describe freight traffic from 85 to the present. The other 8 are divided between passenger and freight traffic and tied to different sections of time, portions of plus minus 30-year intervals from pre 1900s and up to present day. All of the 13 train load models are adjusted in each time era to have a total weight of approximately 225 tons for passenger trains and 750 tons for freight trains. This is done by scaling the number of wagons in the defined load models. A full description of the original load model is attached in the appendix A in figure A1, A2 and A3, taken with permission from the author from 3.3.1 in [3].

2.3 Revised load models for Norwegian trains

Given that train-compositions, locomotives, wagons and train-speeds have been - and are still changing over the years, the rolling-stocks for the different time-eras must be modelled. The rolling-stock is the composition of wagons and locomotives in the trains, both for freight and passenger transport. Such model is proposed in Frøseth [9], which will be referred to as the revised model in this thesis. The load model proposed in Frøseth [9] has a consistency of approximately 40% for freight traffic and 50% for passenger traffic compared to historic traffic on the Norwegian railways. It is a simplification of the Norwegian rolling stock by reducing the amounts of reference trains while still retaining the maximum possible consistency to the historic traffic. An explanation of the new revised load model is presented below, an in dept presentation of the load model can be found in chapter 4 in [9].

The revised load model representing the historic traffic on the Norwegian railway system was developed with three specific properties in mind:

- Conservative
- Simple

- Consistent

A conservative load model with regards to fatigue life estimation will estimate the historic fatigue damage in a structural detail to be as much or more than what is induced by the actual loads from train traffic. This has to be done to ensure that the estimated damage of the structural components are not underestimated and that the bridge is safe for the intervals of time estimated by the analysis. While exact historic traffic data over all bridges in the Norwegian railway system does not exist, estimations on their current levels of fatigue can still be made. These are based on known descriptions of all trains operating on the different sections. The damage from the most damaging trains must be equal to the damage introduced by the reference trains in the load model to introduce more or the same damage as the actual train traffic.

When describing a load model as simple, it is referred to the use and complexity of the model. The load model should contain as few reference trains as possible and have as few restrictions as possible. The reason for keeping a simple load model is that increasing the complexity of a model will increase the possibilities of making errors in the process of fatigue life estimations. Which in turn may lead to considerable over or underestimations of the fatigue life of components due to errors made in the analysis.

The results from a fatigue assessment of a consistent load model will provide consistent fatigue damage in all structural details. To introduce a consistent level of fatigue damage in all structural details the load model must be calibrated to all types of structural details. Providing an unbiased evaluation of all components in the bridge being analysed. If the load model is calibrated for a specific structural component the analysis will be prioritised toward this structural detail. This bias might lead to a detailed analysis of this type of component and provide an accurate result, but the analysis might overlook other more damaged details. An inconsistent load model might lead to a wrongful prioritisation in further surveillance of critical parts or an underestimation of damage in parts deemed wrongfully not critical. To prioritise the correct critically damaged structural components, the load model must be consistent.

The load model is divided into different classes and presented as reference-trains for passenger and freight trains. All these reference trains consist of a locomotive (L) and a set of up to 4 base wagons (A,B,C,D). The reference trains are presented in 4 periods: 1900-1930, 1930-1960, 1960-1985 and 1985- present. All of these reference-trains are collected from [9] in tables 4.B.1 and 4.B.2 with approval from author. They are presented in tables 2.1 and 2.2.

Table 2.1: Reference trains for passenger traffic. Axle loads given in tonnes and axle pitch given in metres. Table is cited with approval from author[9].

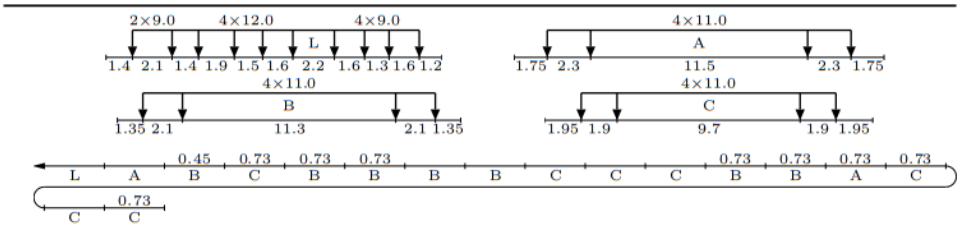

Train 1, period: 1900–1930, speed: 34 km/h, total length: 306.2 m, total weight: 686.8 tn. $a_1 = 5.7$

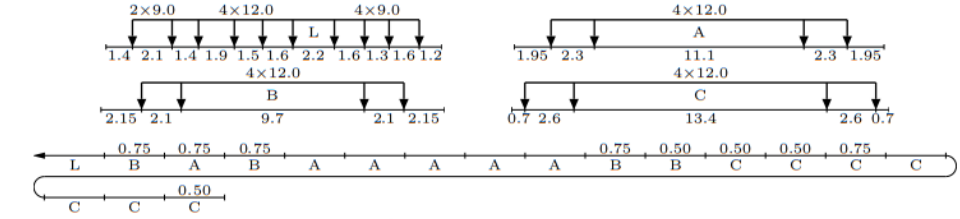

Train 2, period: 1930–1960, speed: 63 km/h, total length: 348.2 m, total weight: 762.0 tn. $a_2 = 5.4$

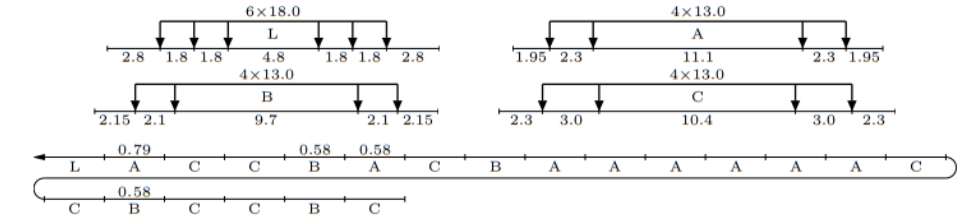

Train 3, period: 1960–1985, speed: 71 km/h, total length: 415.2 m, total weight: 1071.6 tn. $a_3 = 2.4$

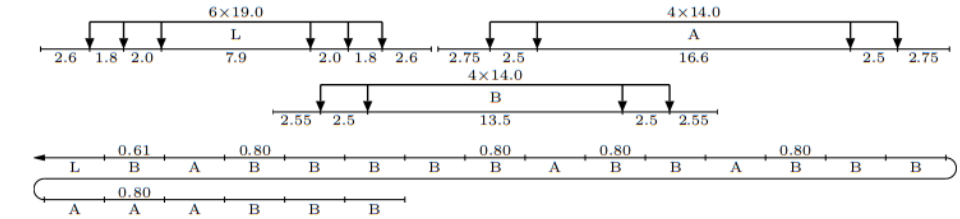

Train 4, period: 1985–, speed: 144 km/h, total length: 513.7 m, total weight: 1156.2 tn. $a_4 = 2.8$

Train composition given by the loop, the identifier at the bottom and the load modifier at the top.

Table 2.2: Reference trains for freight traffic. Axle loads given in tonnes and axle pitch given in metres. Table is cited with approval from author[9].

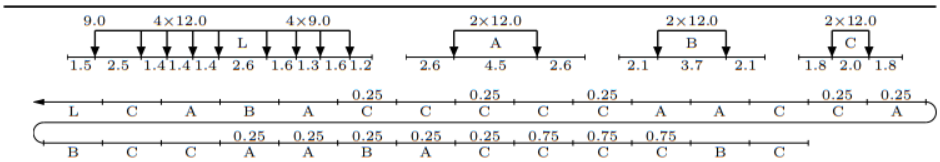

Train 5, period: 1900–1930, speed: 5 km/h, total length: 209.7 m, total weight: 543.0 tn. $a_5 = 10.7$

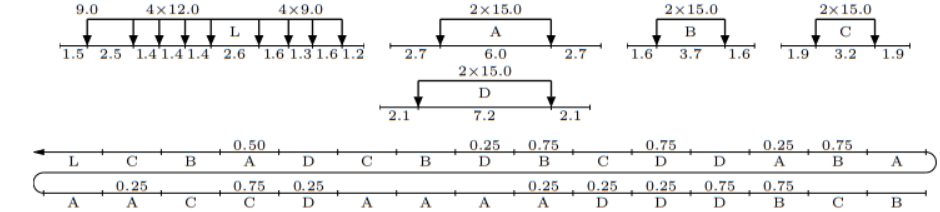

Train 6, period: 1930–1960, speed: 12 km/h, total length: 293.7 m, total weight: 745.5 tn. $a_6 = 9.4$

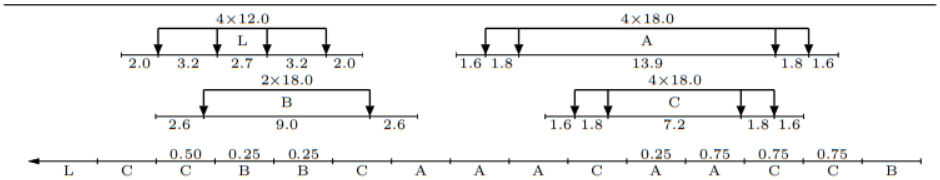

Train 7, period: 1960–1985, speed: 24 km/h, total length: 243.2 m, total weight: 750.0 tn. $a_7 = 20.2$

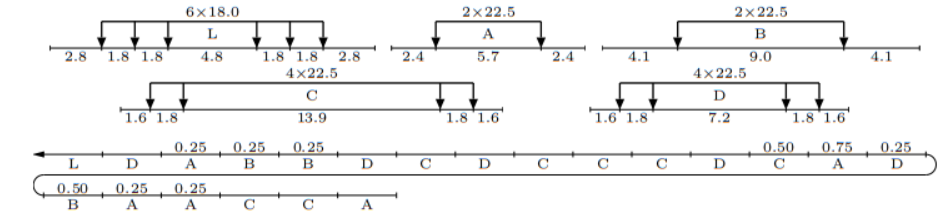

Train 8, period: 1985–, speed: 5 km/h, total length: 336.6 m, total weight: 1233.0 tn. $a_8 = 15.0$

Train composition given by the loop, the identifier at the bottom and the load modifier at the top.

Chapter 3

Method

An overview of the method used for obtaining the input data, the method used to conduct the construction analysis and the method for calculating the fatigue life of the bridges from the results of the structural analysis will be presented in this chapter.

3.1 Structural analysis

This section presents the structural analysis conducted on the 21 bridges in order to extract the influence lines needed to perform the fatigue life analysis. This analysis was conducted by a consulting firm commissioned by Bane NOR. All data and calculations from this analysis was made available by Bane NOR with regards to this thesis.

The structural analysis was conducted by importing the geometry and the cross-sectional properties for the bridges into either the software modules RM-Bridges or Sofistik. RM-Bridges and Sofistik are sophisticated structural analysis programs based on the finite element method. In broad strokes these analysis programs take the geometry and the cross-sectional properties of the bridges as input, static and dynamic characteristic loading is simulated and the output of the analysis are the influence lines for the different loading cases. The geometry of the bridges being analysed were modelled in an excel sheet, where all of the structural components were described based on original drawing of the bridge. The structural components on the bridges were discretised in a systematic manner, explained below. This was done to make the fatigue calculations and the post-processing of the analysis easier.

The cross-sectional properties for the different structural components were calculated and defined in an excel sheet containing the cross-sectional area A_x, the shear area about the vertical and transverse axis A_y, A_z, the torsion I_z and the Second moment of area over local vertical and transverse axis I_y, I_x.

The geometry of the bridge was discretised by a value called bridge element number and a value for the beam element number. The bridge element number consists of a 4 digit number, the first denoting partly the beam type (e.g truss, grillage) and partly on which side of the construction the element is, the second value denoting different geometrical

locations on the designated side and the last two denoting the placement of the element along the side, visualized in figure 3.1.

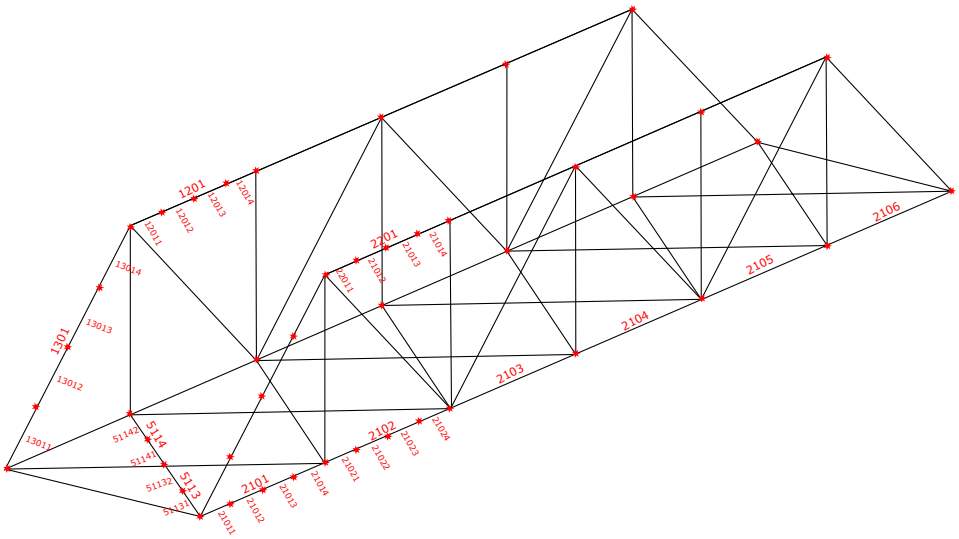

Figure 3.1: Visualisation of the discretisation of some bridge and beam elements on a simplified model of the lerelva bridge.

As seen in figure 3.1 The beam element numbers were organised in a same way as the bridge elements but containing an extra value denoting the placement of the beam element along the bridge element.

Each bridge was assigned a permanent load. This load is assigned to model the weight of the bridge by applying a negative force on all the nodes based on cross-sectional properties and material properties. This way, static weight on top of the element is taken into account as well, such as the weight of the train tracks and the sleepers.

Depending on whether or not the bridge exhibits curvature, there was modelled either one- or three- unit forces on the bridge during the simulation. If there is no curvature on the bridge the simulation only applied a moving point-load of 1 kN consisting of two wheel loads of 0.5 kN with a axle length distance between. These loads were inflicted on each of the train tracks. This was done by placing the loads on the longitudinal grillages or equivalent structural components of the bridges which were located directly beneath the train tracks. This point-load was stepped over the bridge with a pre-set stepping distance of 10 cm. This was done over the full length of the bridge. The responses from the start- and end-node of the element from each point-load step over the bridge was then extracted for each element on the bridge, creating the influence lines for the elements. The influence lines extracted were exported to an lst-file Infl_{ijk} with three dimensions which was organized in the following manner:

i - beam element number

j - start or end node of element

k - response

The responses extracted consisted of: Normal stress in local x-direction N_x, shear stress in local y-direction Q_y, shear stress in local z-direction Q_z, torsional moment M_x, bending moment in local y-direction M_y and bending moment in local z-direction M_z.

There will be a centrifugal force contribution if a bridge has horizontal curvature caused by the train traveling along the radius of the bridge. This force was simulated by two moving point loads over the bridge. The centrifugal force was decomposed into a vertical force pair and a horizontal force. This was done because only the response from the vertical force pair was subjected to dynamic effects, explained in further detail below and in NS-EN 1991-2, pt. 6.5.1 see [6]. These two moving point-loads were stepped across the bridge in the same manner as the vertical axle load and has the same attack point. The difference is that the horizontal force was directed in towards the centre of the curvature of the bridge and the vertical force pair are directed in opposite vertical directions to simulate the overturning moment from the centrifugal force. The directions of the force vectors are demonstrated in 3.2. These two centrifugal force influence lines from the horizontal load and the vertical load pair were extracted in the same way as the vertical load component, to lst-files Infl_tv$_{ijk}$ and Infl_th$_{ijk}$. These two lists were organised in the same way as for Infl$_{ijk}$ described above.

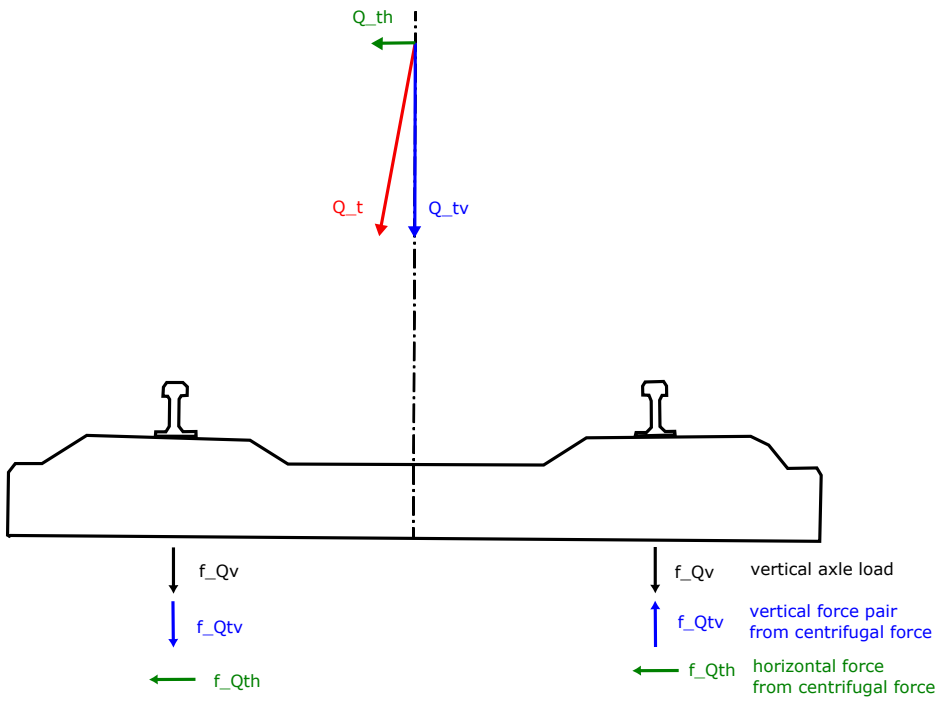

Figure 3.2: Decoupling of transverse loads.

3.2 Calculation procedure

In this section the different stages of the calculation procedure of the fatigue life estimation will be presented. First a brief overview of the process followed by an explanation of each step in the following sub sections.

- Importing data
- Calculating influence lines for normal stress
- Defining load models for trains.
- Establish stress time series from trains in load model
- Establish yearly traffic
- Calculation induced damage from historic traffic
- Estimate future induced damage
- Calculate remaining fatigue life

This chapter will only present the method used to obtain the results. Results and analysis will be presented in chapter 4.

3.2.1 Importing data

Four outputs are obtained from the structural analysis conducted in either RM-Bridge or Sofistik software, as explained above. These are the geometric properties, the cross-sectional properties, the permanent loads on the structure and the influence lines of the different element on the structure. All of which are important in the fatigue life calculations.

The influence lines and the permanent loads are organised in the same way. An lst-file with three dimensions as described in section 3.1 above, each containing the permanent load or influence line for the response from the unit-load moving across the bridge at the specified points on the bridge. The data imported from these lst-files to the calculations are the force components for the axial force N_x and the bending moment for the strong M_y and weak axis M_z. Each influence line imported from the structural analysis contains the response from the force component along the the bridge as demonstrated in figure 3.3.

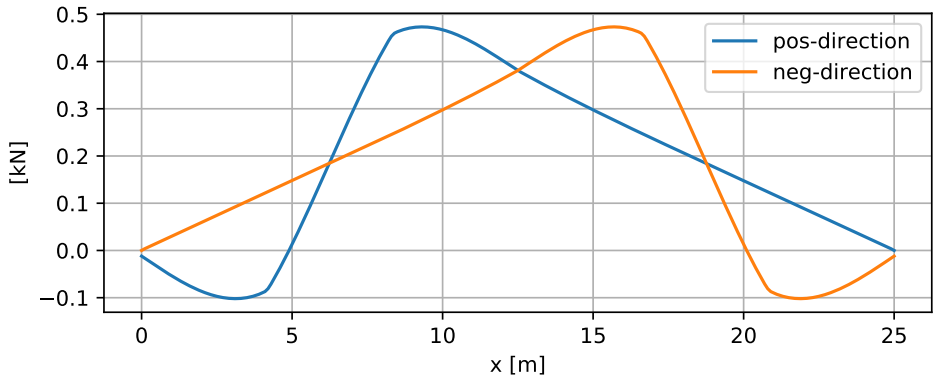

(a) Influence line, N_x, Element 23021 Section Point 1

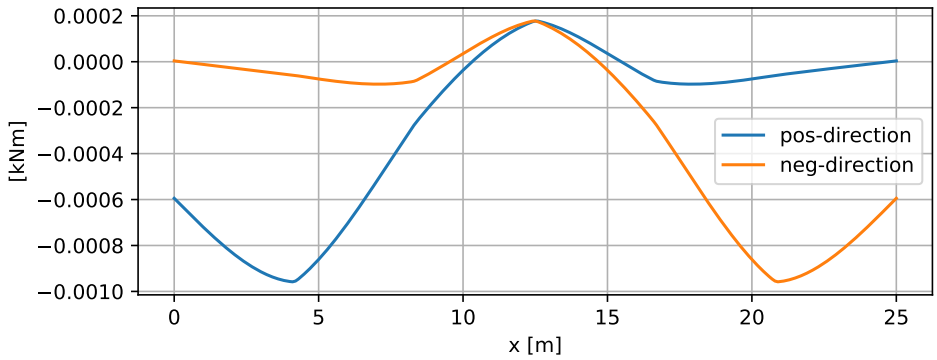

(b) Influence line, M_y, Element 23021 Section Point 1

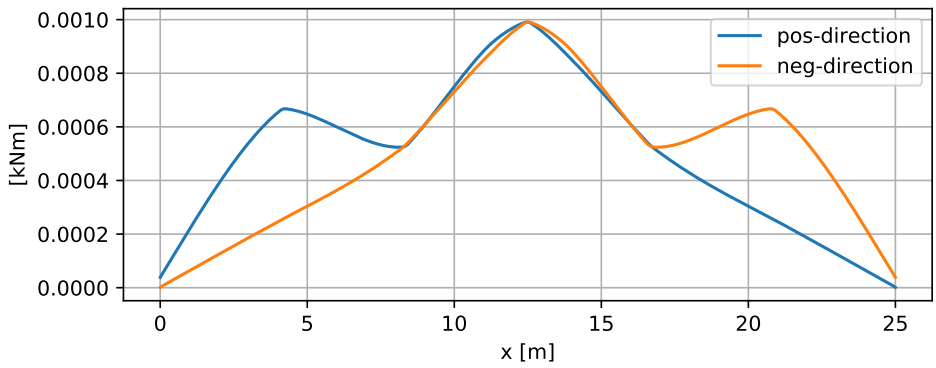

(c) Influence line, M_z, Element 23021 Section Point 1

Figure 3.3: Influence lines for vertical axle load by axial force N_x, bending moment for strong axis M_y and bending moment for weak axis M_z for section point 1 in element 23021 on the Lerelva bridge, in both positive and negative direction.

The cross-sectional properties are imported to the calculations in a 3 dimension data structure W_{ijk}.

- i: cross section
- j: section point
- k: area/sectional modulus for the corresponding force component.

Making it efficient to extract the correct cross-sectional properties for influence line calculation, and to analyse all section points with regards to which rivet is most prone to failure in any given beam.

The geometric properties of the bridge are imported as a list with 9 columns. This list describes all the different beam elements: Beam number, element number, start- and end node number, member length, structural group, cross section, determinant length and structural category. These are in turn used to determine the detail category, cross-sectional properties and dynamic amplification factor.

3.2.2 Calculating influence lines for normal stress

The normal stress contributions from each force component in the influence lines are calculated by dividing the force component with its corresponding resistance according to equation 2.7 presented in chapter 2. This is done by identifying the cross section and section point of the beam element being analysed from the geometric properties and extracting the corresponding cross-sectional properties of A_x, W_y and W_z . These cross-sectional properties are used in calculating the normal stress from the influence lines corresponding to the all the section points in the cross section of the beam element.

If the bridge has a horizontal curvature the influence lines from the centrifugal force must be considered. The centrifugal force is decomposed as shown in figure 3.2 because only the vertical component of the force will have dynamic effects on the bridge and must be multiplied by the dynamic amplification factor $\phi(\nu, L)$, introduced in equation 2.6. The centrifugal forces are related to the speed and radius of curvature according 3.1 from NS-EN 1991-2, pt. 6.5.1 see [6].

$$Q_{tk} = \frac{\nu^2}{127 \cdot r} \cdot Q_k \tag{3.1}$$

Where Q_{tk} is the characteristic value of the transverse load, ν is the speed of the train in $[\frac{km}{h}]$, r is the radius of curvature in $[m]$ and Q_k is the transverse influence line value. To extract the influence line contribution from the vertical and horizontal components of the centrifugal force, the influence lines Infl_tv and Infl_th are multiplied with the speed squared divided by the radius according to equation 3.1.

3.2.3 Establishing stress series for elements.

The response of a single axle is collected from the influence lines. To satisfy the fatigue estimation formulas given in the theory section, the influence line must be combined with the static load function in equation 2.4 to provide the static response of the bridge given

in equation 2.5. The static load function is formulated by combining the load magnitude of the axles combined with the axles positions along the train. Such a static load function can be seen in figure 3.4, being the load vector for the T4 reference train defined below.

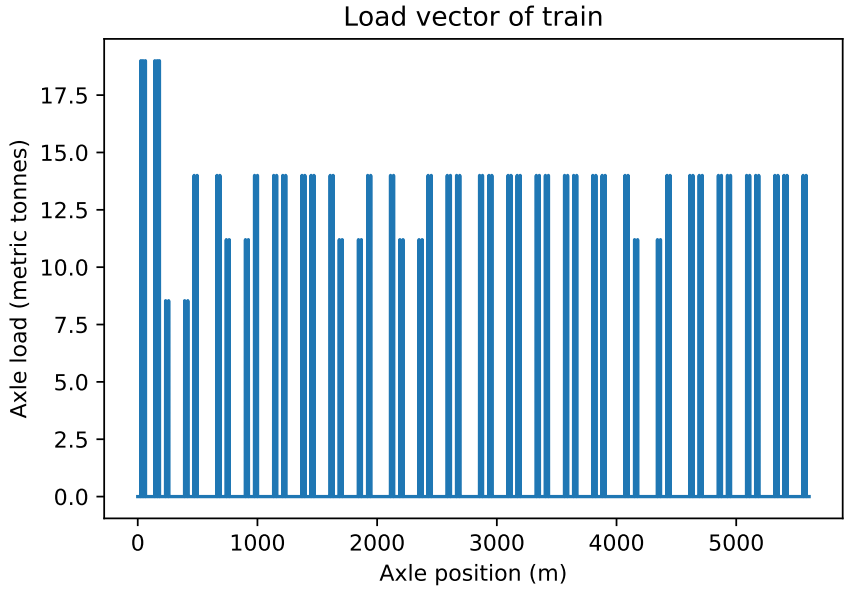

Figure 3.4: Static load function of T4 reference train, found in [9].

The static response z_0 from the elements on the bridge can be found by using equation 2.5. This is done by taking the convolution between the static load models defined by the reference trains above and the influence lines imported from the structural analysis. The dynamic response $z(s)$ is found by multiplying the static response z_0 with the dynamic amplification factor Φ as described in equation 2.6.

The different influence line contributions must be treated differently, given that only some of the contributions will have dynamic effects on the bridges. There are 4 possible normalised influence line contributions forming the response, if there is horizontal curvature on the bridge. These are the influence lines for vertical axle load F, horizontal force F_{th} from centrifugal force, vertical force pair F_{tv} from centrifugal force and permanent load F_{perm}. All components except F_{perm} are affected by the static load model, the static response for these components are found by taking the convolution between the influence and the static load model as described above. The static response from the vertical axle load and the vertical force pair from the centrifugal force are the only components that are affected by dynamic effect and are the only two components multiplied by the dynamic amplification factor to establish the dynamic response of the bridge. The stress time series for the particular reference train over the bridge is established by summing the response form F_{perm}, the static response from the convolution between train and F_{th} and the dynamic response from the convolution between F and F_{tv} and the train load vector

multiplied by Φ. An exemplification of this procedure is presented below.

The stress series for the train passing over the bridge in both directions must be found to perform a realistic fatigue analysis of the bridge. The influence lines imported from the construction analysis are defined as moving in the positive direction. From this definition the act of reversing the direction of the influence lines will provide the response of the trains moving over the bridge in negative direction. This is easily done by reversing the array of the influence lines when calculating the responses in python. Stress series for negative direction is calculated in the same way as for positive, the only difference being the reversing of the direction of the influence lines. The stress series for all elements are calculated in both positive and negative direction and will be used in the fatigue calculations described in section 3.3.

As seen in the figures for the reference trains above, several trains have a high max speed. Some of these max speeds exceed the speed limit for the bridges as can be found in table 3.4. Therefore, if the max speed of a reference train is above the speed limit of the bridges, the max speed is set to be the speed limit of the bridge being analysed when calculating the dynamic amplification factor Φ of the different reference trains.

Exemplification of establishing stress time series for reference train T4;

Taking the convolution of the influence lines for the vertical axle load shown in figure 3.3 and the static load function as shown in 3.4 will as explained above and in the theory section provide the static response z_0 for this train at this given point of the bridge. The static and the dynamic response of the T4 reference train on the element 23021 is demonstrated in figure 3.5. The dynamic response is found by multiplying the static response by the dynamic amplification factor as explained in equation 2.6.

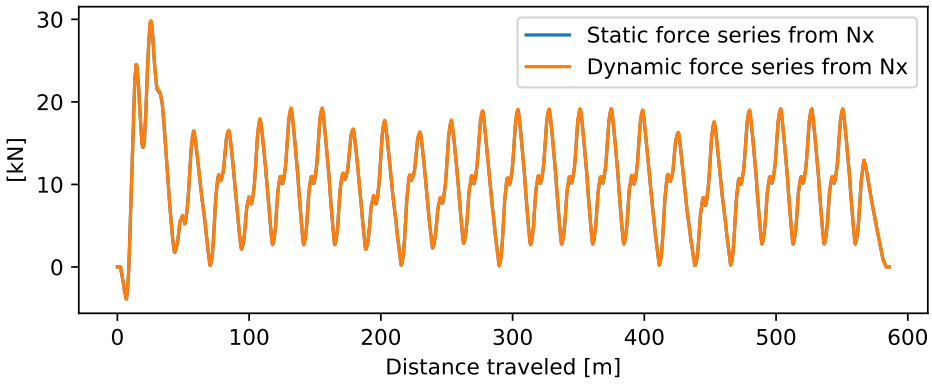

(a) Nx

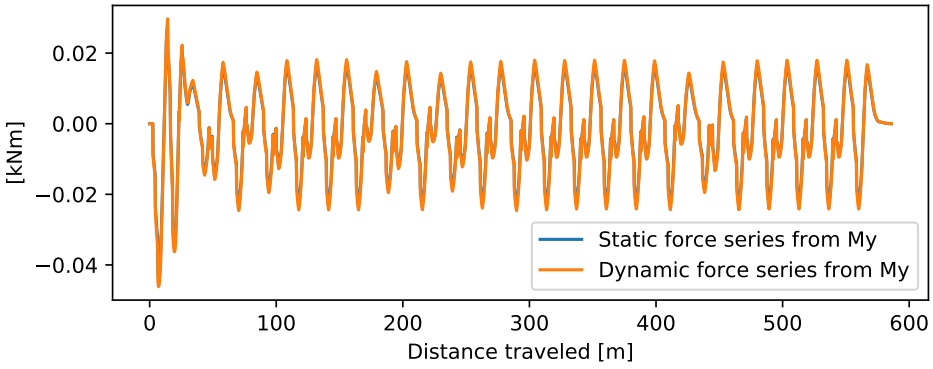

(b) My

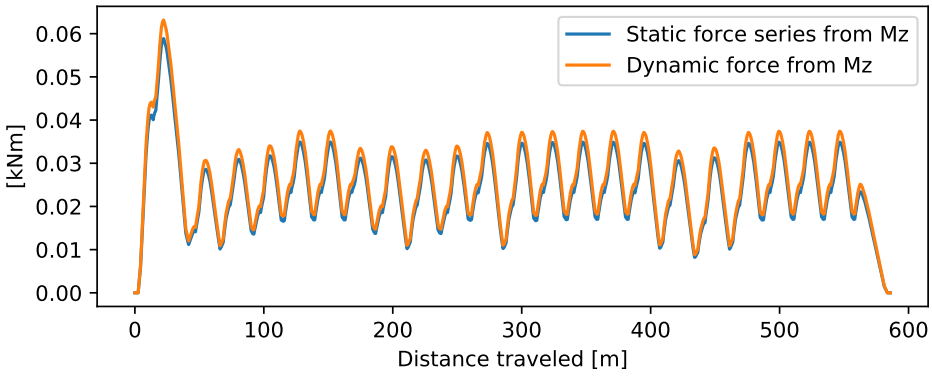

(c) Mz

Figure 3.5: Static and dynamic response for vertical axle load by axial force N_x, bending moment for strong axis M_y and bending moment for weak axis M_z for section point 1 in element 23021 on the Lerelva bridge, in positive direction.

This total stress response is calculated for all force components additional to the response for vertical axle load shown in 3.5 by summing the different stress contributions as explained above. The normal stress contribution form N_x, M_y, M_z and total normal stress for selected element can be seen in figure 3.6.

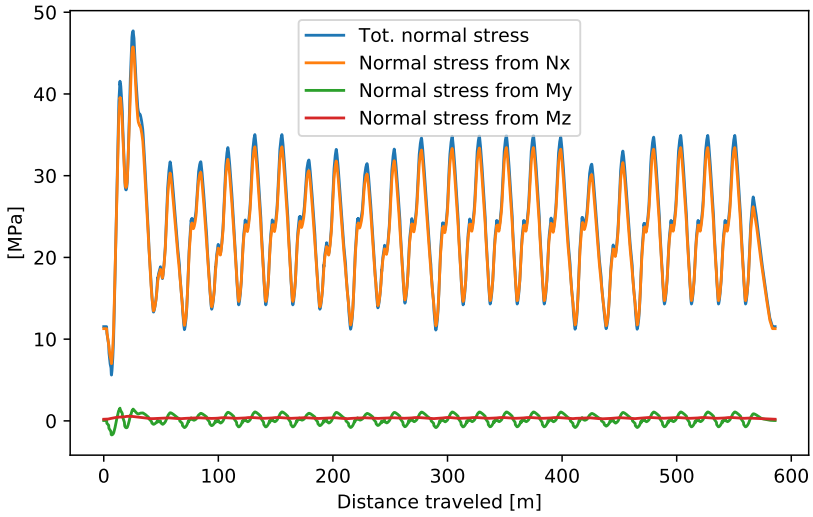

Figure 3.6: The total normal stress in positive direction on Element 23021 Section Point 1 of the Lerelva bridge caused by T4 reference train.

3.3 Obtaining fatigue damage per train passage.

The rainflow cycle counting algorithm is used to extract the stress cycles [$\Delta\sigma_1$,$\Delta\sigma_2$,....,$\Delta\sigma_n$] from the dynamic stress response $z(s)$. To find the total fatigue damage from these cycles the Miner's damage accumulation rule from equation 2.2 needs to be applied to the stress cycles and the cycles until failure N. The cycles until failure N for each stress cycle $\Delta\sigma$ is found through the endurance curves, described in further detail below in 3.4. The fatigue damage per passage $D_{passage}$ of the reference trains can be found by implementing the steps described above on the dynamic stress response of the reference trains. The fatigue damage is calculated for the trains passing in both negative $D_{neg-passage}$ and positive direction $D_{pos-passage}$, by stress cycle counting and miners sum of the total normal stress series in negative and positive direction defined in section 3.2.3.

$$D_{passage} = \frac{D_{pos-passage} + D_{neg-passage}}{2} \tag{3.2}$$

To account for the traffic going in both directions the damage per passage $D_{passage}$ is defined as in equation 3.3. The fatigue damage calculation is performed by using functions

defined in the python package fatpack, which performs both the stress cycle extraction and the Miner's accumulation for the dynamic stress response.

3.4 Endurance curves

The endurance curves are a set of log -log curves giving the relations between stress ranges $\Delta\sigma$ and cycles until failure N. These curves are used in combination with the rainflow ranges to establish cycles until failure N. The N value is used in the Miner's accumulation to find the damage introduced into the element. These curves are defined by their detail category number which refers to the fatigue resistance $\Delta\sigma_c$ in MPa at $N = 2 \times 10^6$ load cycles.

As seen in figure 3.7 there are 4 such curves defined. These are to be used for different parts of the bridges. Two types of curves are presented in figure 3.7; the trilinear EC3_71 curves taken from the Eurocode [7] and the linear ds85 curves taken from [11]. The EC3_71 can according to [11] be assumed to be a conservative lower boundary in fatigue calculations for riveted construction component. This curve is used as the benchmark in the estimations conducted in this report. The ds85 linear curve is a endurance curve defined for riveted construction details with a calculated shear force in the rivets lower than the minimum slip resistance. According to [11] the minimum value of slip resistance per rivet is 12 kN for rivets riveted by hand, by pneumatic hammer or by unknown technique with less than 15 rivets in the connection. This value will be used in this report given that the riveting method for most of these bridges are unknown.

There are two curves for each of the detail categories ds85 and EC3_71. This corresponds to the two different partial safety factors for fatigue resistance γ_{Mf} defined in the Eurocode [7], for a safe life assessment method these are defined to be 1.15 for structural details with a low consequence of failure and 1.35 for structural details with high consequence of failure. The structural details with low consequence of failure are categorised as secondary and the structural details with high consequence of failure are categorised as primary in this report. The partial safety factor is introduced to the calculations by dividing the detail category of the endurance curve by the partial safety factor to obtain the endurance curve including the safety factor.

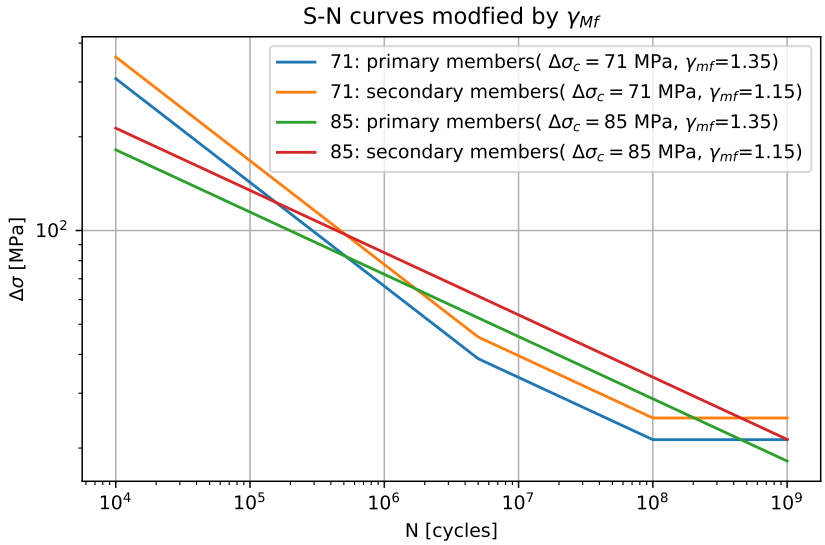

Figure 3.7: Endurance curves for detail category ds85 and EC3_71 modified by γ_{Mf}.

Initially all elements are analysed using the EC3_71 curves. Further considerations are made based on the result of this initial analysis:

- If the results from the initial analysis provide a sufficiently long fatigue life for the element and a sensible result, no further analysis is made.

- If the results from the analysis provide low or no remaining fatigue life for the element further considerations will be made:
  - Analyse the element with the ds85 endurance curve if the shear force on the rivets are less than 12 kN.

By analysing all the elements on the bridge and using this algorithm the results from the initial fatigue life estimation can be organised fast according to remaining fatigue life. This provides a fast way to identify and organise fatigue prone components on the bridges. By identifying these failure prone components early in the analysis, more time can be used on establishing the correct fatigue parameters and more detailed assessment of these components.

3.5 Yearly passages

Table 3.1 show the yearly passages of freight and table 3.2 show the yearly passages passenger trains in years between 1900 to present day on a series of sub-lines on the Norwegian railway system. The sub-lines presented in table 3.1 and 3.2 are the sub-lines where

the bridges being analysed are localised, as can be seen visualised in table 3.4. The given time in table 3.1 and 3.2 does not match the intervals made for the reference trains. The intervals for the reference trains are given in table 2.1 and 2.2 as 1900-1930, 1930-1960, 1960-1985 and 1985- present and are based on the likeness of trains in these periods. The total fatigue damage is a summation of the fatigue damage per passage over the years. Therefore, the number of passages for the different intervals of the reference trains needs to be calculated. This is done by linear interpolation of values of the years not specified in the tables 3.1 and 3.2.

Table 3.1: Yearly passages of freight trains for the sub-lines relevant to the bridges analysed.

Line	Subline		**Freight trains**						
	Terminal A	Terminal B	1900	1920	1940	1960	1980	2000	2018
Hovedbanen	Lillestrøm	Eidsvoll	1460	2190	4745	5840	8760	8760	6935
Kongsvingerbanen	Lillestrøm	Kongsvinger	730	2920	2920	4015	4745	7300	7665
Østfoldbanen	Ski	Sarpsborg	730	730	1460	4015	7300	8030	5475
Dovrebanen	Eidsvoll	Hamar	1460	3650	3650	5840	9490	8030	6570
	Hamar	Dombås	1460	2920	2920	3650	6570	7300	5840
	Dombås	Støren	0	3650	2920	2190	5110	5840	5110
	Støren	Trondheim	730	5110	5110	2920	5840	6570	6935
Randsfjordbanen	Hokksund	Hønefoss	2190	2190	2190	2190	8760	2920	3285
Bergensbanen	Hønefoss	Myrdal	0	2190	2190	2190	4380	5110	6570

Table 3.2: Yearly passages of passenger trains for the sublines relevant to the bridges analysed.

Line	Subline		**Passenger trains**						
	Terminal A	Terminal B	1900	1920	1940	1960	1980	2000	2018
Hovedbanen	Lillestrøm	Eidsvoll	3650	4380	9490	12775	16060	33580	73730
Kongsvingerbanen	Lillestrøm	Kongsvinger	3650	3650	5840	11315	8760	17520	17520
Østfoldbanen	Ski	Sarpsborg	7300	6570	8030	13870	26280	30660	29930
Dovrebanen	Eidsvoll	Hamar	3650	4380	5840	10220	12410	24820	18250
	Hamar	Dombås	2190	2920	5110	6570	8760	5110	9490
	Dombås	Støren	0	1460	2190	2920	2920	4380	3650
	Støren	Trondheim	1460	6935	7300	11315	18980	15695	22630
Randsfjordbanen	Hokksund	Hønefoss	2190	2920	4380	8030	6205	7300	3650
Bergensbanen	Hønefoss	Myrdal	0	2190	2920	4380	3650	3650	3650

The linear interpolation is done by equation 3.3 between the values stated in table 3.2 and 3.1.

$$y = y_1 + (x - x_1)\frac{y_2 - y_1}{x_2 - x_1} \tag{3.3}$$

The dataset gathered from the linear interpolation of freight and passenger trains in tables 3.1 and 3.2 are displayed in the graphs in figures 3.8 and 3.9. The plots of these datasets show the the number of yearly passages of both freight and passenger trains of the sub-lines afflicting the analysed bridges on a yearly basis from 1900 to 2018. These values will be used to estimate the already inflicted fatigue damage D_0 for all components points on the bridges.

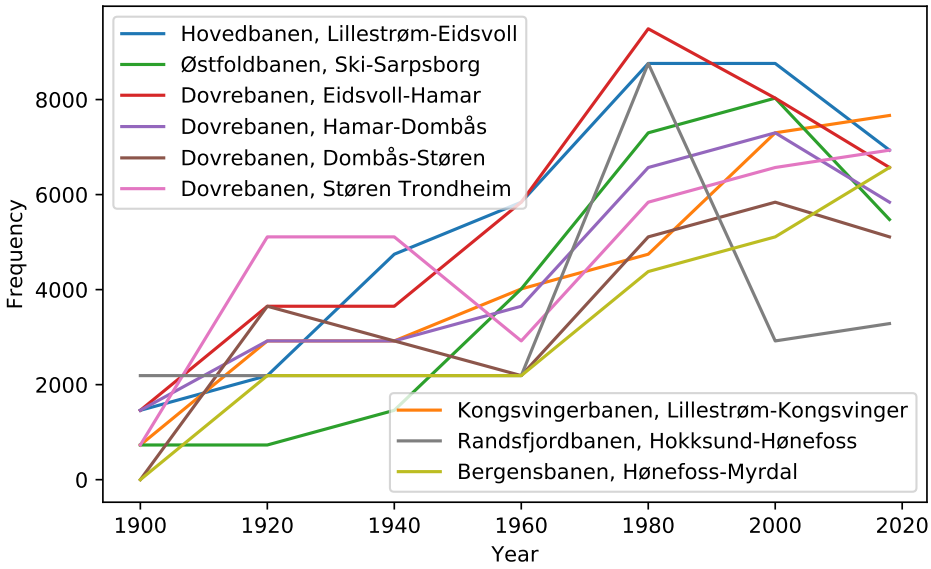

Figure 3.8: Linearly interpolated train passages for freight trains on selected lines on the Norwegian railway network from 1900 to 2018.

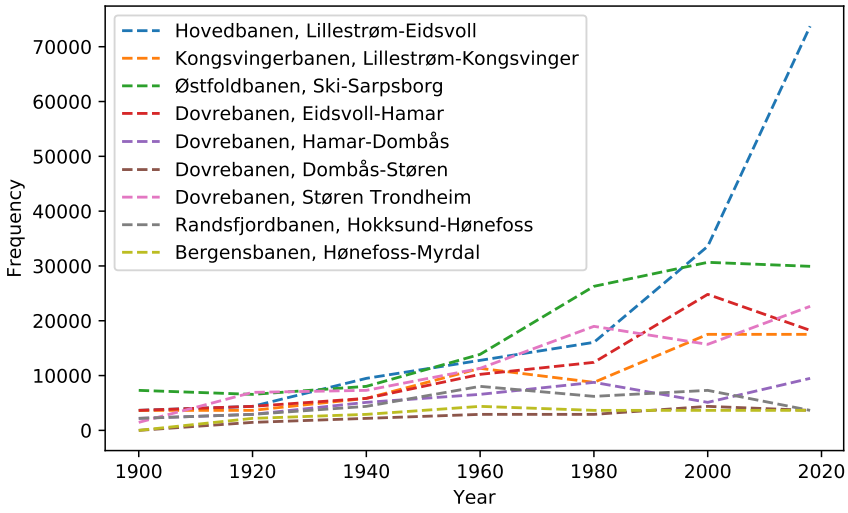

Figure 3.9: Linearly interpolated train passages for passenger trains on selected lines on the Norwegian railway network from 1900 to 2018.

The number of train passages n_i done in the previously defined time periods for the reference trains can be found by summing the passages in the different time periods, found by the interpolation conducted above. Which provides the 8 different n values for each sub-line presented in table 3.3. Given that the year of construction and the start of the time period for the first reference trains T5 and T1 does not correspond. These values are interpolated and summed up for each bridge to provide the correct frequency given the year of construction.

Table 3.3: Number of passages n_i within the different time intervals defined for the reference trains.

Train	Year	Type	Lillestrøm-Eidsvoll	Lillestrøm-Kongsvinger	Ski-Sarpsborg	Eidsvoll-Hamar	Hamar-Dombås	Dombås-Støren	Støren-Trondheim	Hokksund-Hønefoss	Hønefoss-Myrdal
T1	1900-1930	Passenger	142170	67525	24638	132130	88878	31938	158500	86870	46903
T2	1930-1960	Passenger	307695	99098	68985	217905	163700	71723	260340	166440	101290
T3	1960-1985	Passenger	38430	113610	151840	298750	195460	74095	399220	173280	98185
T4	1985-present	Passenger	1397585	230950	236885	691490	222220	129940	601060	200480	120450
T5	1900-1930	Freight	67251	119170	215350	90155	75190	72818	112420	67890	44895
T6	1930-1960	Freight	127290	123735	187975	90885	81395	95448	171915	65700	65700
T7	1960-1985	Freight	191260	249840	542390	298750	137060	100560	118810	152205	89243
T8	1985-present	Freight	271620	479610	900330	255620	229400	174900	191500	116500	142410

Table 3.4: Overview of sub-lines bridges being analysed are located on combined with speed-limits and construction year.

Bridge	Stretch	Year of construction	Speed for passenger trains	Speed for freight trains
Børke bru over Lerelv	Lillestrøm- Eidsvoll	1929	90	90
Fetsund bru	Lillestrøm- Kongsvinger	1919	80	70
Hobøl viadukt	Ski- Sarpsborg	1913	85	80
Bru over Åkerselva	Eidsvoll- Hamar	1920	105	100
Bru over Brummund elv	Hamar- Dombås	1913	110	95
Talleraas bru	Hamar- Dombås	1912	90	70
Svanå	Dombås- Støren	1918	130	130
Hesthagen	Dombås- Støren	1913	120	120
Bru over Aalma	Dombås- Støren	1915	100	100
Byna	Dombås- Støren	1916	90	80
Igla elv	Dombås- Støren	1912	75	70
Sokna ved Lundamo	Støren- Trondheim	1917	50	50
Lerelva	Støren- Trondheim	1919	80	70
Møstadbekken	Støren- Trondheim	1916	120	110
Katfoss bru	Hokksund- Hønefoss	1909	70	70
Bru over Sokna	Hønefoss- Myrdal	1908	130	120
Langvannsoset	Hønefoss- Myrdal	1907	95	90
Solheimselva	Hønefoss- Myrdal	1908	110	110
Saulidelva	Hønefoss- Myrdal	1906	110	100
Bru over Todøla	Hønefoss- Myrdal	1906	115	105
Usta ved Breifoss	Hønefoss- Myrdal	1907	75	70

3.6 Calculation of previously introduced fatigue damage

In equation 2.3 the value D_0 is presented as fatigue damage introduced by past cycles. This value can be established by the summation of the yearly introduced fatigue damage. Already established are total number of passages made by both freight and passenger trains n_i in table 3.3 and the damage per passage found $D_{passage}$ in 3.3 by cycle counting. From these values D_0 can be found by the equation 3.4.

$$D_0 = \sum_{i=1}^{8} a_i \cdot n_i \cdot D_{passage-i} \tag{3.4}$$

Where a_i is a coefficient that describes the traffic mix of the given reference trains, presented in table 2.1 and 2.2 taken from [9].

3.7 Estimate the future yearly damage D_1

In equation 2.3 the value D_1 is presented as the yearly fatigue damage introduced by future stress cycles. This value must be estimated. D_1 is calculated the same way as the different segments of the D_0. As can be seen in equation 3.5 the D_1 is the sum of the damage introduced from the freight trains and the passenger trains, although the n_i value will differ with the different scenarios proposed. The damage per passage $D_{passage}$ and traffic mix coefficients a_i will be assumed to be equal to the values in the period 1986-present.

$$D_1 = a_8 \cdot n_{8-future} \cdot D_{passage-8} + a_4 \cdot n_{4-future} \cdot D_{passage-4} \tag{3.5}$$

When considering the future traffic, the development of the yearly frequency of the traffic must be estimated. In order to obtain results that can be compared to the result from the original report, the future traffic development must be the same percentage-wise. Defining the future traffic development as 2% increase in traffic from freight trains and 5% increase in traffic from passenger trains.

The values for n_{2018} are given in table 3.2 and 3.1. The $n_{8-future}$ and $n_{4-future}$ values used to calculate D_1 are calculated by increasing the n_{2018} for freight and passenger traffic by the factor stated above.

3.8 Estimation of remaining fatigue life t

The remaining fatigue life t of the different elements analysed is found by equation 2.3. Given the three different estimated scenarios for D_1, three different t values are calculated. Failure will occur if the preciously introduced fatigue damage D_0 described in equation 3.4 is greater than 1 [8]. Therefore, the critical fatigue damage D_C is defined as 1.

Chapter 4

Analysis

In this chapter, a detailed explanation of the steps used to obtain the results will be presented. The process of quality testing the theoretical method for calculating the results and the calculation used to find the results for the updated method is presented.

The analysis can be summarised in a few steps; the calculation of results for the original load-model, comparison and conformation of these results with regards to the original report to validate the calculations and calculating the new results for the revised load model.

4.1 Replicated results from original load model

The calculations used to estimate the fatigue life of the bridges needs to be controlled. This is done to ensure that the calculations in this report is correct. The way this is conducted is by replicating the results from the prior report made for Bane NOR, using the same load model and influence lines. In this way the only error source for deviations between the result from this step of the analysis and the original report is the calculations. It is not necessary to do a full analysis of all the 21 bridges with the old load model to ensure the validity of the calculations, but the results replicated should include all the force components and the highest grade of complexity in the calculations.

The Lerelva bridge was chosen for such a control calculation. This bridge was chosen because it was one of the most damaged bridges with a horizontal curvature. The horizontal curvature of the bridge provides an extra influence line contribution from the centrifugal forces provided by the train traveling along the radius of the bridge. This centrifugal force is decomposed into a horizontal and a vertical component as explained in chapter 3.2.2.

The first step being to replicate the results of a single element to verify that the calculations and load models are correct. Then replicating several elements both with critical damage and remaining lifetime within reasonable limits of the results of the original report to verify the validity of the calculations made in the first element. The replication of most damaged element of the Lerelva bridge will be presented in detail, and the two other elements with the lowest estimated fatigue life for the different constructional categories

will be presented briefly. Replications of results on other bridges were also performed but will not be presented.

The first element chosen is the most damaged element on the bridge over Lerelva. This element is located at the longitudinal grillage of the bridge. Given that the influence lines and the cross-section data are input data not altered from the report, but the load models are build using the pacril package, a different way of defining the load models than the original report, giving a potential error source. Therefore, the first comparable results that can expose any possible errors in the recreated models and calculations are the Stress time series. This will ensure that the normal stresses for N_x, M_y and M_z are correctly modelled for the vertical and the transverse loads. The calculated stress time series for the normal stress in the most damaged element by train LMP4 is presented in figure 4.1.

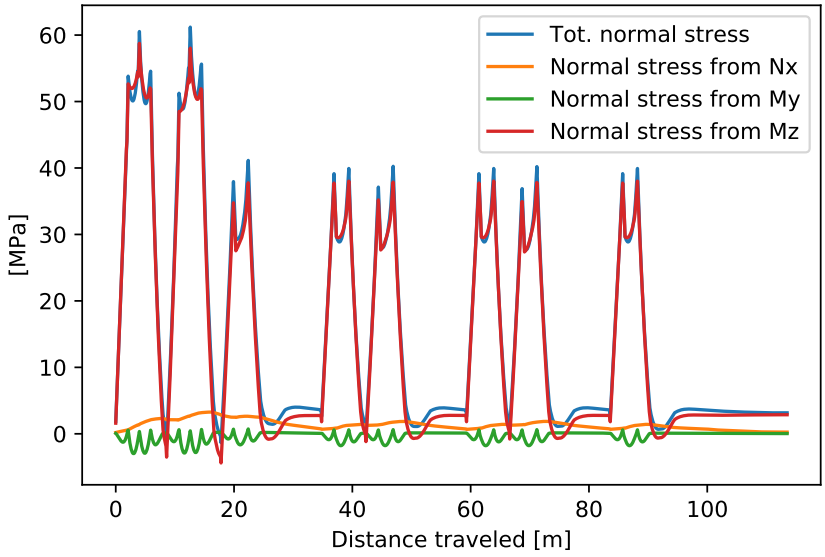

Figure 4.1: Reproduced stress time series for normal stress - Longitudinal grilliage - total and individual contributions from force components for train LMP4 passing in positive x-direction.

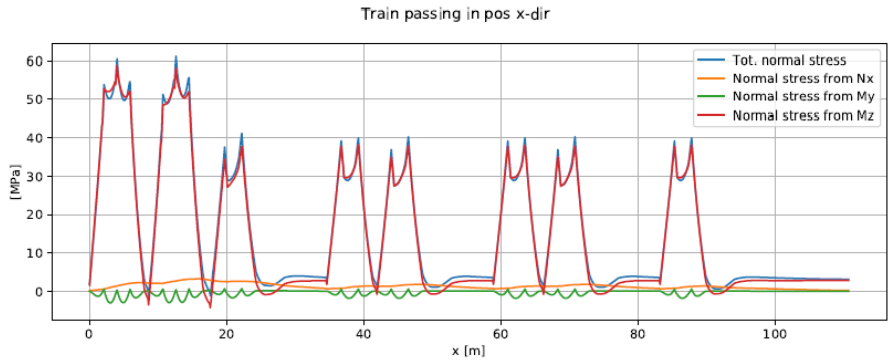

Figure 4.2: Original stress time series for normal stress - Longitudinal grilliage - total and individual contributions from force components for train LMP4 passing in positive x-direction. Taken from [3] with permission from author.

By comparing the stress time series in figure 4.1 reproduced in the calculations for this report with the stress time series LMP4 train in figure 4.2 taken from the original report it can be observed that the graphs in these two figures are identical. The same comparison can be made with all the stress time series from the calculated and the original report and the comparison will show that the results are the same. The stress time series in the reproduced calculations are modelled correctly. This provides that the influence lines are imported in the same way as in the original report and the new definition of the original load model are corresponding with the load model used in the original report.

Historic fatigue							Future fatigue			
	ϕ	$D_{train,posx}$	$D_{train,negx}$	D_{1year}	D_{tot}	% of D_{hist}	ϕ	$D_{train,posx}$	$D_{train,negx}$	D_{1year}
LM5EC	1.153	5.28e-06	5.28e-06	5.02e-03	0.166	15.10	1.153	5.28e-06	5.28e-06	5.02e-03
LM6EC	1.153	3.64e-06	3.66e-06	5.95e-03	0.196	17.91	1.153	3.64e-06	3.66e-06	5.95e-05
LM7EC	1.153	3.25e-06	3.32e-06	3.56e-03	0.118	10.73	1.153	3.25e-06	3.32e-06	3.56e-03
LM8EC	1.153	3.17e-06	3.17e-06	2.59e-03	0.085	7.78	1.153	3.17e-06	3.17e-06	2.59e-03
LMF2	1.153	1.94e-07	2.05e-07	8.95e-04	0.010	0.90	nan	nan	nan	nan
LMF3	1.153	5.94e-07	6.03e-07	2.68e-03	0.08	7.34	nan	nan	nan	nan
LMF4	1.153	1.75e-06	1.75e-06	7.84e-03	0.196	17.89	nan	nan	nan	nan
LMP2	1.164	9.90e-08	1.03e-07	6.82e-04	0.008	0.68	nan	nan	nan	nan
LMP3	1.164	1.67e-07	1.83e-07	1.18e-03	0.035	3.23	nan	nan	nan	nan
LMP4	1.164	5.13e-07	5.25e-07	3.50e-03	0.088	7.98	nan	nan	nan	nan
LMP5	1.164	5.13e-07	5.17e-07	3.47e-03	0.115	10.45	1.164	5.13e-07	5.17e-07	3.47e-03

Table 4.1: Detailed damage by train for element 31031 on Lerelva bridge from original report. Taken from [**?**] with permission from author.

By comparing the replicated results in table 4.2 and the results given in the original report i table 4.1 for element 31031 a small difference in damages per passage D_{train} can be found for all trains in both positive and negative direction. When comparing the damage per passage in negative $D_{train,negx}$ and positive direction $D_{train,posx}$ and the yearly damage biggest difference in found between yearly damage D_{1year} of the LM5EC train with a percentage of error of 9.36%. The mean error of $D_{train,posx}$ is 3.87%, for $D_{train,negx}$ is 0.17% and for D_{1year} it is 2.81%. The total accumulated historic damage from the cal-

Historic fatigue							Future fatigue			
	ϕ	$D_{train,posx}$	$D_{train,negx}$	D_{1year}	D_{tot}	% of D_{hist}	ϕ	$D_{train,posx}$	$D_{train,negx}$	D_{1year}
LM5EC	1.153	5.44e-06	5.03e-06	5.49e-03	0.171	14.15	1.153	5.44e-06	5.03e-06	5.49e-03
LM6EC	1.153	3.68e-06	3.73e-06	6.04e-03	0.199	18.00	1.153	3.68e-06	3.73e-06	6.04e-03
LM7EC	1.153	3.49e-06	3.41e-06	3.74e-03	0.123	10.27	1.153	3.49e-06	3.41e-06	3.74e-03
LM8EC	1.153	3.23e-06	3.21e-06	2.62e-03	0.087	7.15	1.153	3.23e-06	3.21e-06	2.62e-03
LMF2	1.153	2.06e-07	2.11e-07	9.34e-04	0.010	0.93	nan	nan	nan	nan
LMF3	1.153	5.90e-07	5.87e-07	2.64e-03	0.079	7.14	nan	nan	nan	nan
LMF4	1.153	1.77e-06	1.72e-06	7.81e-03	0.195	17.63	nan	nan	nan	nan
LMP2	1.164	1.01e-07	1.05e-07	6.93e-04	0.008	0.69	nan	nan	nan	nan
LMP3	1.164	1.83e-07	1.68e-07	1.18e-03	0.035	3.20	nan	nan	nan	nan
LMP4	1.164	5.45e-07	5.54e-07	3.71e-03	0.093	8.36	nan	nan	nan	nan
LMP5	1.164	5.37e-07	5.32e-07	3.60e-03	0.118	12.48	1.164	5.37e-07	5.32e-07	3.60e-03

Table 4.2: Calculated detailed damage by train for element 31031 on the Lerelva bridge.

culations $D_{hist,calculated}$ is 1.12000 and the total accumulated historic damage from the original report $D_{hist,report}$ is 1.09618 as seen in table 4.3 for element 31031. When the mean error percentage for the damages described above is as low and no striking difference in total accumulated historic damage, it is assumed that the method of calculations is sufficient with regards to reproducing results and to be used for further analysis.

Table 4.3: Summary of results from reproduction of original analysis.

Element	$D_{histrep}$	$D_{histcalc}$	$L_{restrep}$	$L_{restcalc}$
31031	1.0962	1.1200	0	0
13051	0.9263	1.0247	5.0	0
41121	0.5290	0.5572	26.9	31.24

Reasons for the difference in damage per passage D_{train}, accumulated damage D_{tot} and ultimately remaining Fatigue life L_{rest} as seen in table 4.3 can be many. A small differences that can be pointed out such that the Φ used in the calculations are 1.15287911 rather than 1.53 and 1.16433665 rather than 1.164 but it is not likely that these are the deciding factors in the difference in damage. Disregarding the difference in accuracy of the dynamic amplification factor the other cause off the difference is found in the application of the rainflow algorithm.

There are different ways to implement the rainflow counting method. In the original report the rainflow algorithm is based on a three-point criteria which identifies half- and full RF cycles. The rainflow algorithm that is used in this report is the rainflow algorithm explained in [5]. This method is based on a four-point criteria and only counts full RF-cycles. There are several reasons for using the four-point criteria rather than the three-point. The main difference between the two criteria is how the residual is treated, but according to [10] these two methods will provide nearly identical results. The four-point criteria is selected in further analysis in this thesis because it has been conventionally used in fatigue life calculations for railway bridges and truncated stress series. This choice has little influence on the overall results presented in this thesis.

4.2 Results from the revised load model

The results from the calculations made with the revised load model presented in section 2.3 is presented in this section. Given that all section points of all elements in the bridge are analysed a selection must be made of which elements that are to be presented. First the general data from the most damaged elements of the bridge in each structural category is presented. Then the most damaged elements from the 3 different cross-sections which has obtained the most historic fatigue are presented in detail. First by representing the general data for the element from the tabulated results. Then the detailed result of fatigue damage per train is presented and a figure demonstrating the accumulation of fatigue damage per train, for passenger trains, for freight trains and the total accumulation over the years from construction up to 2018. The general data from the 150 most damaged elements of the bridges are presented in the Appendix.

4.2.1 Results from Lerelva bridge.

Table 4.4: Tabulated result of the most damaged element in each structural category on the Lerelva bridge.

beam	element	pt	pos	L_{rest}	D_{hist}	$\Delta\sigma$	section	category
2302	23024	SP 1	1	-37.870251	17.226789	71	Fag-Di2	primary
3224	32242	SP 1	1	-29.500993	7.425879	85	LB1	secondary
2406	24061	SP 1	0	-29.123579	6.377029	71	Fag-Ve4	primary
2301	23011	SP 2	0	-34.770533	5.461222	71	Fag-Di1	primary
2101	21011	SP 2	0	-36.624840	5.153397	71	Fag-UG1	primary
2303	23031	SP 2	0	-27.138895	4.714777	71	Fag-Di3	primary
1104	11044	SP 1	1	-37.342907	4.398081	71	Fag-UG2	primary
2204	22041	SP 4	0	-32.773849	4.108346	71	Fag-OG1	primary
4114	41141	SP 2	0	-20.613928	2.435083	85	TB	secondary
2405	24051	SP 1	0	-10.311956	1.465863	71	Fag-Ve12	primary
1405	14051	SP 5	0	-6.759290	1.265500	71	Fag-Ve11	primary
3123	31231	SP 16	0	10.632520	0.754187	85	LB2	secondary
5135	51351	SP 1	1	16.062385	0.715453	85	Vi-Di3	primary
1406	14061	SP 4	0	53.622843	0.344190	71	Fag-Ve2	primary
5114	51142	SP 1	1	90.673659	0.304369	85	Vi-Di1	primary

Detailed results: Truss diagonal, Element 23024

Table 4.5: General data

	beam: 2302 element: 23024 section point: 1 position: 1
L_{rest}	-37.870251
D_{hist}	17.226789
$\Delta\sigma_C$	71
γ_{Mf}	1.35
cross-section	Fag-Di2
category	primary

Table 4.6: Results per train for element 23024

Train	Φ	D_{pos}	D_{neg}	D_{tot}	% of D_{hist}
T1	1.028731	3.503791e-07	4.395780e-07	0.191673	1.112645
T2	1.055693	4.378201e-07	4.733920e-07	0.640507	3.718087
T3	1.063618	7.013961e-07	6.644375e-07	0.654322	3.798281
T4	1.072805	9.733448e-07	9.562711e-07	1.623741	9.425674
T5	1.004262	3.136095e-07	4.734886e-07	0.259447	1.506067
T6	1.009959	3.480757e-07	4.968554e-07	0.682705	3.963043
T7	1.020030	1.429032e-06	1.331189e-06	3.312213	19.227106
T8	1.004262	3.463908e-06	3.402710e-06	9.862181	57.249096

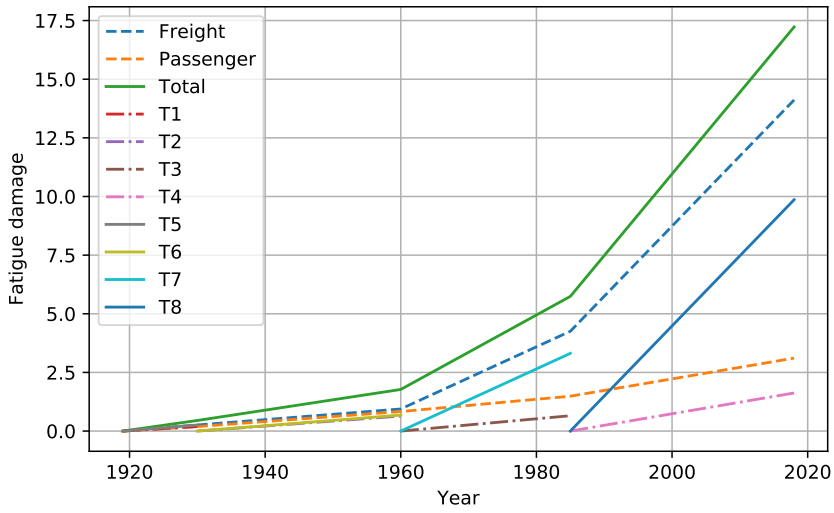

Figure 4.3: Accumulated fatigue damage from construction year to 2018 from trains on element 23024.

Detailed results : Longitudinal grillage, Element 32242

Table 4.7: General data

	beam: 3224 element: 32242 section point: 1 position: 1
L_{rest}	-29.500993
D_{hist}	7.425879
$\Delta\sigma_C$	85
γ_{Mf}	1.15
cross-section	LB1
category	secondary

Table 4.8: Results per train

Train	Φ	D_{pos}	D_{neg}	D_{tot}	% of D_{hist}
T1	1.115091	4.089648e-08	3.821304e-08	0.019195	0.258488
T2	1.145120	2.532138e-08	2.528534e-08	0.035572	0.479027
T3	1.154005	4.443065e-08	4.381366e-08	0.042275	0.569292
T4	1.164337	3.562021e-08	3.601291e-08	0.060278	0.811729
T5	1.088105	5.535880e-08	5.630895e-08	0.036808	0.495671
T6	1.094365	1.443269e-07	1.474189e-07	0.235731	3.174452
T7	1.105465	4.827759e-07	4.869968e-07	1.163709	15.670993
T8	1.088105	2.049984e-06	2.010807e-06	5.832311	78.540345

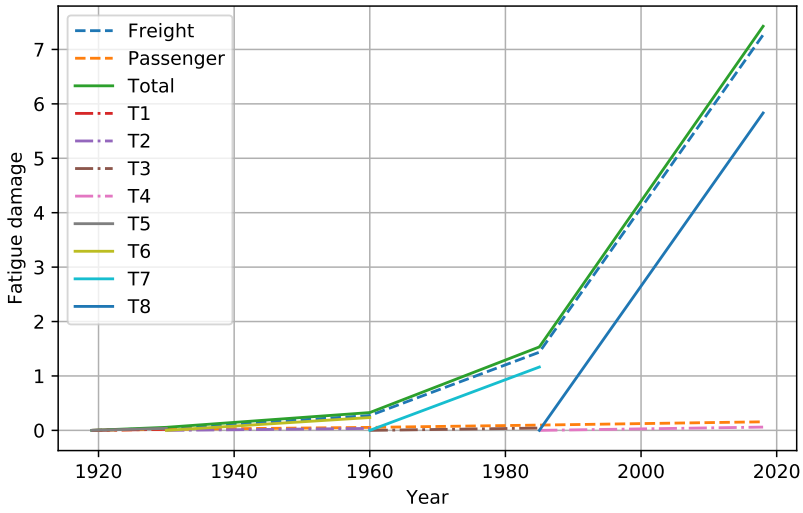

Figure 4.4: Accumulated fatigue damage from construction year to 2018 from trains on element 32242.

Detailed results: Vertical truss, Element 24061

Table 4.9: General data

	beam: 2406 element: 24061 section point: 1 position: 0
L_{rest}	-29.123579
D_{hist}	6.377029
$\Delta\sigma_C$	71
γ_{Mf}	1.35
cross-section	Fag-Ve4
category	primary

Table 4.10: Results per train

Train	Φ	D_{pos}	D_{neg}	D_{tot}	% of D_{hist}
T1	1.028731	4.588967e-08	4.640442e-08	0.022394	0.3512
T2	1.055693	6.950359e-08	7.057845e-08	0.098466	1.5441
T3	1.063618	1.132772e-07	1.156752e-07	0.109683	1.7200
T4	1.072805	2.568877e-07	2.492492e-07	0.425906	6.6788
T5	1.004262	5.246154e-08	5.430563e-08	0.035193	0.5519
T6	1.009959	5.146362e-08	5.314394e-08	0.084523	1.3254
T7	1.020030	4.403502e-07	4.416736e-07	1.058412	16.5973
T8	1.004262	1.572869e-06	1.589848e-06	4.542452	71.2315

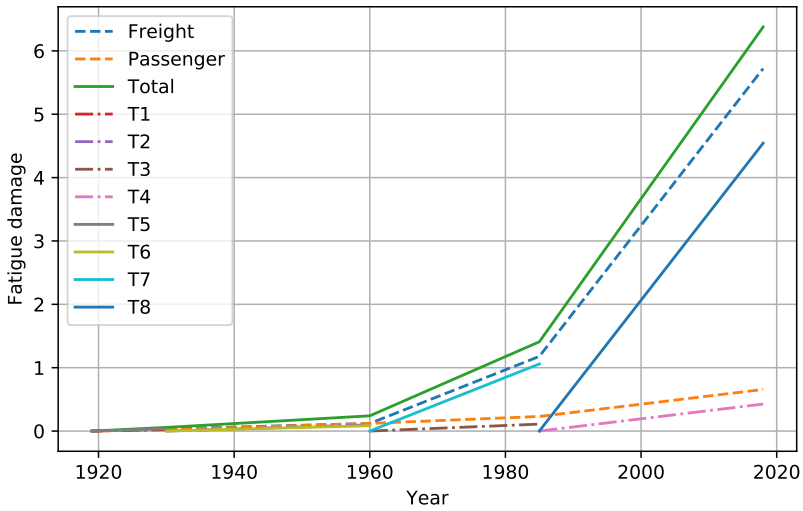

Figure 4.5: Accumulated fatigue damage from construction year to 2018 from trains on element 24061.

4.2.2 Results from the Brummund bridge

Table 4.11: Tabulated result of the most damaged elements of each structural category on the bridge over the Brummund river.

beam	element	pt	pos	L_{rest}	D_{hist}	$\Delta\sigma$	section	category
3202	32023	SP 3	0	-46.866003	29.063693	85	LB2	secondary
3204	32041	SP 2	1	-49.173126	13.220983	71	LB1	secondary
4123	41231	SP 7	0	-30.409299	2.834454	85	TB	secondary
1102	11021	SP 7	1	-28.096167	2.331692	85	HB2	primary
1105	11051	SP 5	0	-10.503097	1.274743	85	HB1	primary

Detailed results: Longitudinal grillage, Element 32023

Table 4.12: General data

	beam: 3202 element: 32023 section point: 3 position: 0
L_{rest}	-46.866003
D_{hist}	29.0636933
$\Delta\sigma_C$	85
γ_{Mf}	1.15
cross-section	LB2
category	secondary

Table 4.13: Results per train

Train	Φ	D_{pos}	D_{neg}	D_{tot}	% of D_{hist}
T1	1.126921	1.620031e-07	1.691025e-07	0.055006	0.189
T2	1.156950	3.003880e-07	2.976581e-07	0.264330	0.910
T3	1.165835	1.079497e-06	1.090911e-06	0.509074	1.752
T4	1.213389	1.848384e-06	1.925088e-06	1.173958	4.039
T5	1.099935	2.268665e-07	2.299415e-07	0.125776	0.433
T6	1.106195	7.762921e-07	7.834179e-07	0.596677	2.053
T7	1.117296	1.908682e-06	1.924060e-06	5.305687	18.255
T8	1.099935	6.027374e-06	6.197668e-06	21.033184	72.369

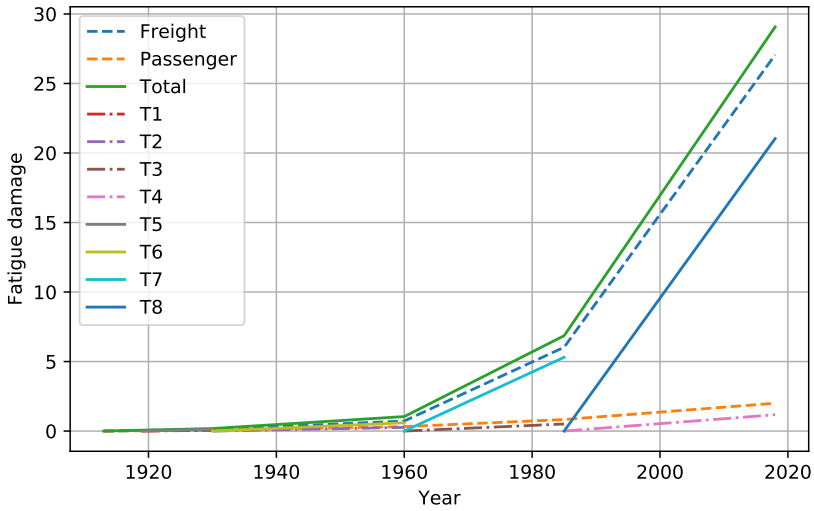

Figure 4.6: Accumulated fatigue damage from construction year to 2018 from trains on element 32023.

Detailed results: Transverse grillage, Element 41231

Table 4.14: General data

	beam: 4123 element: 41231 section point: 7 position: 1
L_{rest}	-28.096167
D_{hist}	2.834454
$\Delta\sigma_C$	85
γ_{Mf}	1.15
cross-section	TB
category	secondary

Table 4.15: Results per train

Train	Φ	D_{pos}	D_{neg}	D_{tot}	% of D_{hist}
T1	1.124789	2.603034e-08	2.508045e-08	0.008491	0.300
T2	1.154817	4.827506e-08	4.722638e-08	0.042211	1.489
T3	1.163702	1.138456e-07	1.180736e-07	0.054397	1.919
T4	1.211256	2.721628e-07	2.864386e-07	0.173785	6.131
T5	1.097802	2.256158e-08	2.113238e-08	0.012031	0.424
T6	1.104062	2.655563e-08	2.422035e-08	0.019425	0.685
T7	1.115163	1.821845e-07	1.797626e-07	0.501046	17.677
T8	1.097802	5.937530e-07	5.821082e-07	2.023069	71.374

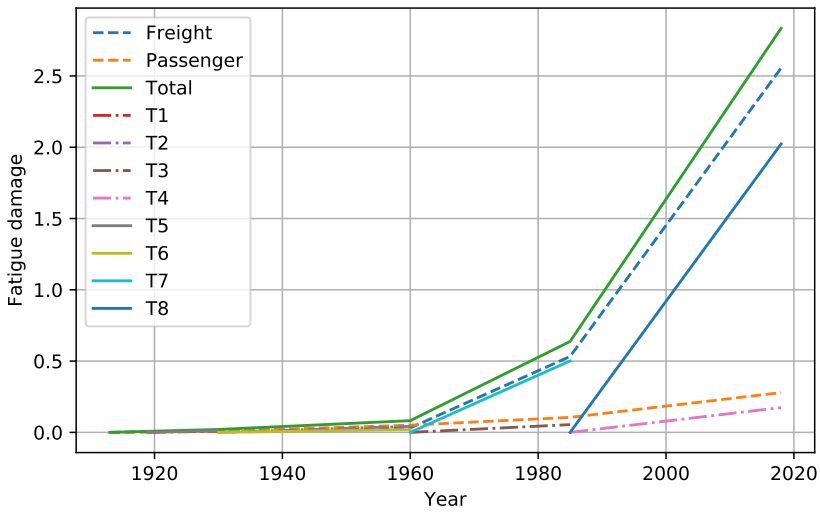

Figure 4.7: Accumulated fatigue damage from construction year to 2018 from trains on element 41231.

Detailed results: Main girder, Element 11021

Table 4.16: General data

	beam: 1102 element: 11021 section point: 7 position: 1
L_{rest}	-28.096167
D_{hist}	2.331692
$\Delta\sigma_C$	85
γ_{Mf}	1.35
cross-section	HB2
category	primary

Table 4.17: Results per train

Train	Φ	D_{pos}	D_{neg}	D_{tot}	$\%of D_{hist}$
T1	1.042538	4.145354e-08	4.491701e-08	0.014349	0.616
T2	1.072567	6.012218e-08	6.452751e-08	0.055094	2.363
T3	1.081452	7.302575e-08	7.287835e-08	0.034222	1.468
T4	1.129006	9.373224e-08	1.014509e-07	0.060723	2.604
T5	1.015552	2.951693e-08	3.772088e-08	0.018513	0.794
T6	1.021812	3.477198e-08	4.433430e-08	0.030263	1.298
T7	1.032913	1.430013e-07	1.445621e-07	0.398076	17.072
T8	1.015552	4.930851e-07	5.068872e-07	1.720452	73.786

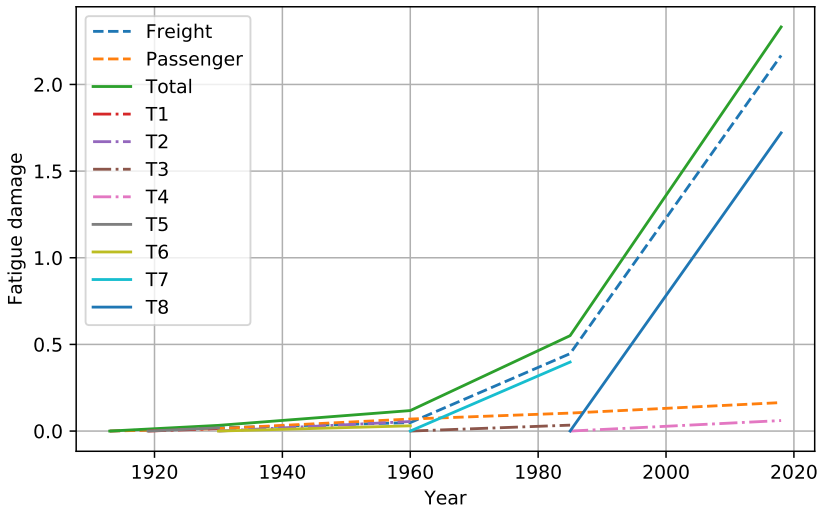

Figure 4.8: Accumulated fatigue damage from construction year to 2018 from trains on element 11021.

4.2.3 Results form the Saulidaelva bridge

Table 4.18: Tabulated result of the most damaged elements of each structural category on the Saulidaelva bridge.

beam	element	pt	pos	L_{rest}	D_{hist}	$\Delta\sigma$	section	category
8108	81081	SP 2	0	-31.309430	72.194534	71	LB-Diag	secondary
1403	14034	SP 2	1	-27.908922	26.254915	85	Fag 5-6	primary
4103	41031	SP 2	1	-29.441462	21.558387	71	LB	secondary
3702	37024	SP 2	1	-30.325728	19.762234	71	T Diag2_1	secondary
1401	14014	SP 3	1	-29.868767	16.548838	71	Fag 1-2	primary
7103	71034	SP 2	1	-28.071015	13.773518	71	BF Diag	secondary
1405	14054	SP 1	1	-26.785851	12.819067	85	Fag 9-10	primary
1306	13064	SP 5	1	-28.136028	10.304999	71	Diag 6-7	primary
1107	11074	SP 4	1	-26.140671	5.248105	71	UG 4-8	primary
1305	13054	SP 7	1	-23.592967	5.215899	71	Diag 7-10	primary
3108	31084	SP 1	1	-22.351950	4.955813	71	Tverr Stag	secondary
1308	13084	SP 5	1	-25.105947	4.231207	71	Diag 2-3	primary
3301	33014	SP 4	1	-20.393018	3.544946	85	T End 1	secondary
3704	37044	SP 1	1	-19.768642	3.366709	71	T Diag2_2	secondary
7106	71061	SP 4	0	-17.844311	2.983568	71	BF Stag2	secondary
1105	11054	SP 4	1	-20.488111	2.795006	71	UG 8-10	primary
1203	12031	SP 2	0	-20.775310	2.794058	71	OG 6-10	primary
3303	33034	SP 2	1	-16.837043	2.439751	71	T Diag1_1	secondary
1302	13021	SP 7	0	-14.103353	1.865005	71	Diag 3-6	primary
7105	71054	SP 3	1	-10.659407	1.670094	71	BF Stag1	secondary
3309	33094	SP 3	1	-2.853343	1.111717	85	T End 2	secondary
1201	12011	SP 1	0	1.386074	0.959558	71	OG 2-6	primary
3503	35034	SP 2	1	2.393446	0.914344	71	Tverr1	secondary

Detailed results: Diagonal longitudinal grillage, Element 81081

Table 4.19: General data

	beam: 8108 element: 81081 section point: 2 position: 0
L_{rest}	-31.309430
D_{hist}	72.194534
$\Delta\sigma_C$	71
γ_{Mf}	1.15
cross-section	LB-Diag
category	secondary

Table 4.20: Results per train

Train	Φ	D_{pos}	D_{neg}	D_{tot}	$\%of D_{hist}$
T1	1.029408	1.857881e-06	1.969114e-06	0.493648	0.684
T2	1.056899	3.027281e-06	3.004613e-06	1.649620	2.285
T3	1.064989	6.194695e-06	5.868483e-06	1.421308	1.969
T4	1.107971	1.229139e-05	1.232266e-05	4.150668	5.749
T5	1.004500	9.397753e-07	9.652610e-07	0.440832	0.611
T6	1.010295	1.932124e-06	2.172059e-06	1.267331	1.755
T7	1.020546	9.539254e-06	9.604691e-06	17.255478	23.901
T8	1.004500	2.132673e-05	2.128792e-05	45.515650	63.046

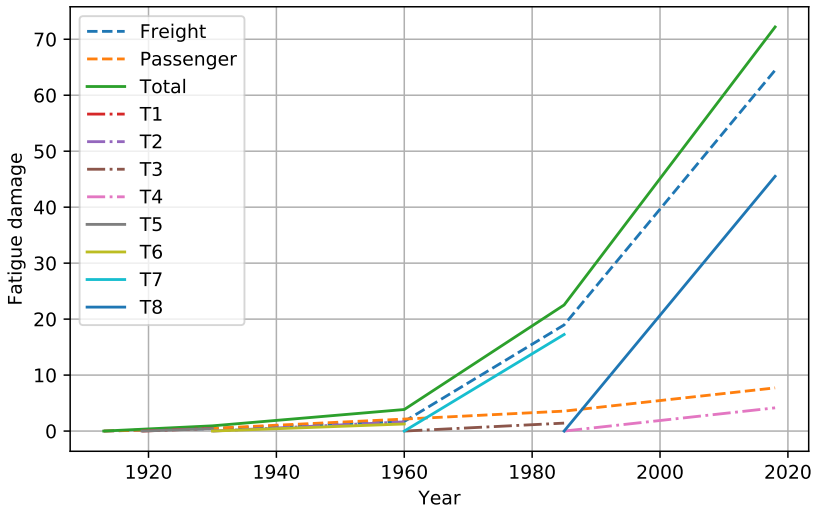

Figure 4.9: Accumulated fatigue damage from construction year to 2018 from trains on element 81081.

Detailed results: Vertical truss, Element 14034

Table 4.21: General data

	beam: 1403 element: 14034 section point: 2 position: 1
L_{rest}	-27.908922
D_{hist}	26.254915
$\Delta\sigma_C$	85
γ_{Mf}	1.35
cross-section	Fag 5-6
category	primary

Table 4.22: Results per train

Train	Φ	D_{pos}	D_{neg}	D_{tot}	$\%of D_{hist}$
T1	1.029408	3.575829e-07	3.726619e-07	0.094195	0.359
T2	1.056899	7.258668e-07	7.464895e-07	0.402664	1.534
T3	1.064989	2.396970e-06	2.314906e-06	0.555163	2.115
T4	1.107971	8.808117e-06	8.370863e-06	2.896891	11.034
T5	1.004500	2.466476e-07	2.663232e-07	0.118703	0.452
T6	1.010295	2.820269e-07	3.119095e-07	0.183402	0.700
T7	1.020546	2.596771e-06	2.653915e-06	4.732728	18.026
T8	1.004500	8.012784e-06	8.157587e-06	17.271168	65.783

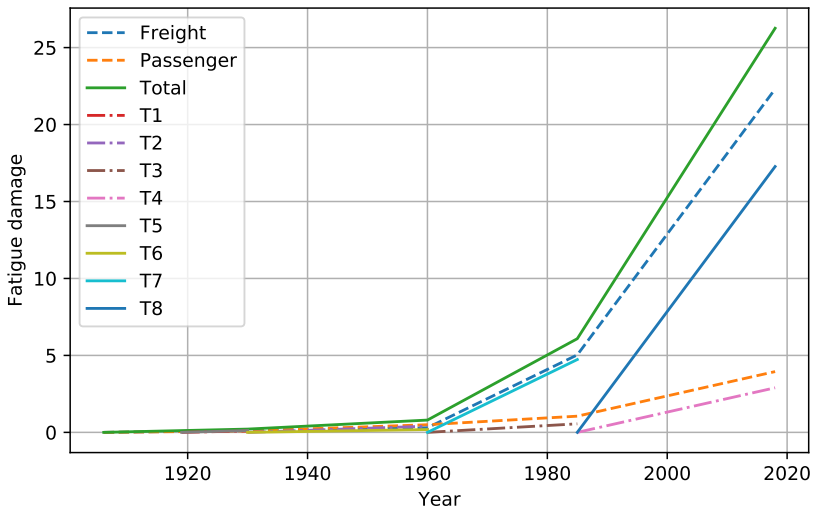

Figure 4.10: Accumulated fatigue damage from construction year to 2018 from trains on element 14034.

Detailed results: Longitudinal grillage, Element 41031

Table 4.23: General data

	beam: 4103 element: 41031 section point: 2 position: 1
L_{rest}	-29.441462
D_{hist}	21.558387
$\Delta\sigma_C$	71
γ_{Mf}	1.15
cross-section	LB
category	secondary

Table 4.24: Results per train

Train	Φ	D_{pos}	D_{neg}	D_{tot}	$\%of D_{hist}$
T1	1.093645	1.573678e-07	1.552691e-07	0.040327	0.187
T2	1.123674	4.280321e-07	4.199713e-07	0.231915	1.076
T3	1.132559	1.909955e-06	1.937227e-06	0.453283	2.103
T4	1.180112	6.427748e-06	6.378433e-06	2.159506	10.017
T5	1.066658	2.526726e-07	2.418143e-07	0.114426	0.531
T6	1.072918	1.019103e-06	1.028210e-06	0.632190	2.933
T7	1.084019	2.512122e-06	2.533525e-06	4.547916	21.096
T8	1.066658	6.217323e-06	6.308787e-06	13.378825	62.059

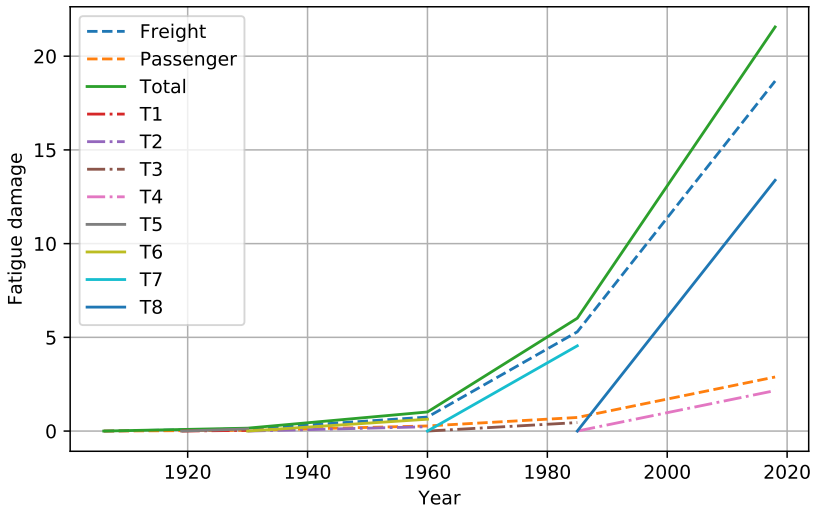

Figure 4.11: Accumulated fatigue damage from construction year to 2018 from trains on element 41031.

4.3 Analysis of Lerelva bridge

In this section the results presented in the section above will be explained, elaborated on and compared to results from the original report. This will be done both with regards to placement and scope of the damage as well as which periodic trains are the most damaging using the different load model. First the general data and the outline and general trends seen in the results will be presented and discussed. Then the detailed data presented from the few selected elements will be discussed. The locations on the bridge is defined by using a local x,y,z axis system. The x-direction describing the length of the bridge, starting at 0 at the start of the bridge and ending at 25 meters. The z-direction being 0 along the mid-line parallel to the train tracks, defining left and right side in direction of the traffic. The y-direction defining the height above or under the wind diagonal. The location of the elements and visualisation of the different parts of the bridge is found in the figures C1 in the appendix displaying the discretisation of the Lerelva bridge.

The first thing that is clearly noticed is the extreme values of the fatigue damage induced D_{hist}. Given that a failure is expected to occur if the fatigue damage value exceeds a value of 1, the values for D_{hist} seen in table 4.4 and further results can be categorized as extreme. The scope of these values will not be the subject of this analysis, but the values must be commented. In order to correctly estimate fatigue lifetime using the revised load model these values must be corrected to a realistic damage level. Research is currently being done in the Department of Structural Dynamics at NTNU to establish a factor to convert the conservative maximum amount of fatigue damage to a realistic value for further use when implementing the revised load model in fatigue life estimation.

The more interesting parts of the result are the trends seen from the revised model compared to the old load model. Which structural components are the most damaged with the new model compared to the old? What is the percentage of damage of the different time periods? Are there differences in freight and passenger trains? Which trains cause the most damage on the bridges? All of which will be discussed below.

4.3.1 Trends observed in the general data

The first observation from the general data, presented in table 4.4, is that the connection between the second diagonal truss and lower truss is the most damaged component on the bridge. Looking at the trends found by sorting the general data after fatigue damage in table B1 in the appendix shows a clear pattern with regards to the location and cross-sectional properties of these elements.

Starting at the most and third most damaged elements seen in table B1 in the appendix which is located at on the second diagonal truss connecting with the first lower horizontal truss on the right side of the Lerelva bridge. The second most and forth most damaged point is located on the same position the opposite side of the right truss, the fifth diagonal truss connected to the lower horizontal truss. The next four elements in the list are located in the same spots as the most and the third most damaged elements, but located on the left side of the bridge. This making the first observation from the general data is that the connection between second diagonal truss and the horizontal truss on any side and in any direction of the bridge is the spots accumulating the most damage with the revised load model.

From table B1 containing the general data of the 150 most damaged elements it can be seen that the 80 first elements on the list consist of elements located on the beam numbers 2302, 2305, 1302 and 1305 and have the same cross-section. These are all located on the second diagonal trusses of the bridge. The trend of these trusses be seen from the general data is the element at the bottom, connected to the horizontal truss, accumulating the most damage and in gradually decrease in accumulated damage along the diagonal truss. The second observation is that the most damaged structural components of the bridge are the second diagonal trusses on the bridges.

The next structural components that has sustained substantial amounts of damage are the longitudinal grillages. The most damaged components are all located on the longitudinal grillage on the right side, in negative z-direction. The damaged components are located in two areas along this one grillage and has accumulated from 7.42 to 7.3 in fatigue damage. The area with the most damaged components on the right longitudinal grillage are located on the furthest end of the bridge 23-24 meters along the bridge defined in positive x-direction. The second most damages area being located at the start of the bridge, 2-3 meters in positive x-direction. Further down the list at a damage of 6.2 to 5.8 we find the equivalent points on the left longitudinal grillage located 1 meter in positive z- direction. To summarise the third observation made from the general data is that the second most damaged structural detail is the longitudinal grillage, with most damage accumulated in the right grillage on the areas of 2-3 and 23-24 meters in positive x-direction.

The third most damaged structural component sustained a historic fatigue damage value of 6.37. This component is located near the top of the vertical truss located at the center of right side of the bridge. The forth observation made from the general data of

the Lerelva bridge is that the vertical truss on the right side of the bridge is the third most damaged structural detail with the most damaged element 24061 located in the height of 3 meters in positive y-direction on the truss.

The general trend found from the most damaged elements calculated with the new load model for the Lerelva bridge is damage first appearing in the right side of the bridge, the spots are mirrored in the left side, but less damage is accumulated here. The reason for the most damaged components being on the right side is because the curvature of the bridge is defined in the right direction in the analysis. Making the transverse load from the train going along the curvature affect the right side of the bridge more. The most damaged detail of the primary category, essential bearing structure, is the second diagonal truss, the primary structural detail with the element accumulating the second most damage is the vertical truss located in the center of the bridge and the most damaged structural detail of secondary category, non bearing structural detail, is the right longitudinal grillage.

4.3.2 Trends observed in the detailed data in element 23024

Starting with the most damaged element 23024, representing the trend in the second diagonal truss. By first looking at the dynamic amplification factor Φ for the different trains in table 4.6 it can be observed that this is significantly larger for the passenger trains (T1-T4) than the freight trains (T5-T8). This is not a surprising value, given that the speed for the passenger trains are much larger than the speeds of the freight trains.

Furthermore, looking at the damage per passage in positive D_{pos} and negative D_{neg} direction in table 4.6 it is interesting to establish if there is differences in damages from the trains in each period regardless of frequencies and the a_i factor of the trains. It can be seen that the damage is very similar for the first two periods in time, the 1900-1930 represented by T1- and T5-trains and the 1930-1960 represented by the T2- and T6-trains. A gradual increase in damage is seen for all the trains over the different time periods. Looking at the increase in damage of T2 to T3 compared to the increase from T6 to T7 we see that the new value for freight trains are approximately the double of the values for passenger trains in the same time period. Comparing the T4 values to the T8 values it can be seen that the value for the freight train T8 is over 3 times larger than the passenger train T4. This means that the damage of one freight train running over the track will cause over 3 times the damage of a passenger train on the diagonal trusses of this bridge.

The trend of freight trains causing the most damage is continued and amplified when considering the total accumulated fatigue damage D_{tot}. The values of D_{tot} of the two first periods with T1, T5 and T2, T6 are similar in broad strokes. However, the values of D_{tot} for the freight trains T7 and T8 are over 5 and 6 times as big as the corresponding values for T3 and T4. This is mainly caused by the traffic mix factor a_i. Given that the frequencies n_i for for passenger trains for the Støren-Trondheim subline are drastically bigger than the values for freight trains as presented in table 3.3.

A summary of the most important observations from the most damaged element 23024 can be seen in the figure 4.5. The freight train in period 1985-2018 provides the most fatigue damage as can be seen in table 4.6 the damage from this period is 57% of the historic damage accumulated in the element. The freight trains in the period 1960-1985 are the second biggest contributor with 19.2% accumulated damage. The passenger trains in the period 1985-2018 are also a considerable contributor to the general accumulated

fatigue damage with 9.4%. This probably due to the massive increase in traffic in these years. The rest of the periods show marginal influence in the general accumulated fatigue damage.

4.3.3 Trends observed in the detailed data in element 32242

In the most damaged secondary category element 32242 on the longitudinal grillage the same tendencies are not surprisingly found in the dynamic amplification factor Φ as in the most damaged element 23024, but as explained above this value is largely affected by the speed of the train.

However, there is a different pattern is seen in the damage per passage in positive D_{pos} and negative D_{neg} direction seen in table 4.8. All the passenger trains T1-T4 has the approximately same values of 2-4 $\cdot 10^{-8}$. Whereas the freight trains start of just a little higher and increase drastically over the decades from 5 $\cdot 10^{-8}$ to 2 $\cdot 10^{-6}$. This shows that a passage of a freight trains will affect the longitudinal grillage more than a passage of a passenger train. This is further confirmed when looking at figure 4.4, D_{tot} and $\%of D_{hist}$ in table 4.8. When multiplying by the traffic mix coefficient and the frequencies the tendencies seen from the D_{pos} and D_{neg} are amplified. This results in a contribution of under 1% for load model periods T1-T5 and most of the damage being accumulated in the 1985-2018 period from freight trains. Although there being 3 times as many passenger trains compared to freight trains running on the subline. A notable difference is seen when comparing the damages found in element 23024 and element 32242. The freight traffic is responsible for all the damage affecting the element 32242 compared to element 23024 where the passenger trains were the reason for approximately 18% of the damage.

4.3.4 Trends observed in detailed data in element 24061

The same trends are seen in the dynamic amplification factor Φ in table 4.10 for the vertical truss element 24061 as the other elements with the Φ being larger for trains with greater speeds. Further when considering the damage per passage D_{pos} and D_{neg} a difference from the longitudinal grillage element 32242, the development is similar to that found in the diagonal truss in element 23024. The passenger trains increase in the damage per passage in an almost linear fashion from 3.2 $\cdot 10^{-8}$ to 8.5 $\cdot 10^{-8}$. Nothing like the development found in the freight trains. The development for the freight trains regarding damage per passage starts similarly to the values for the passenger trains on a low level for the first period, this low level is continued in the second time period, but a substantial increase in damage is seen for the T7 period and a similar leap in size is seen when comparing the T7 and T8 period for the damage per passage seen in table 4.10. When considering the total damage for a period it can be seen that this trend is amplified by the a factor and the frequencies of the trains like the two other elements. The accumulated damage for this element is much lower than that of the diagonal truss but expresses a trend in between the trend seen in the previous elements. The freight trains in T7 and T8 cause the majority of damage also in this element.

4.3.5 Comparison of trends in the revised and original model for the Lerelva bridge

The trends found in the results from the estimations made with the revised load model show that the freight train of the last two periods, 1960-1985 and 1985-2018 does the most damage. The diagonal truss is the overall most damaged structural part followed by the longitudinal grillage.

A comparison of these simple trends with the results presented in the Lerelva-report [2] is given in this section. In table 6 in appendix C in the Lerelva-report shows the general data of all elements in the analysis with a fatigue lifetime under 100 years, organized in ascending order from least to most fatigue lifetime. The trends of interest in this table are the location of the elements and which elements are the most damaged using the original load model versus the revised model.

The most damaged element in the original report is located at the longitudinal grillage in 1 meter in z direction, at exactly the opposite side in both x and z direction of the second most damaged structural category component on the longitudinal grillage found in the simulation with the revised load model. The further development of damage done to elements of the category longitudinal grillage is the same as seen in the results for the revised model with elements on the opposite ends of the same side being the most damaged. The general trend following these critically damaged elements are elements along the left longitudinal grillage being more damaged than the elements located on the right longitudinal grillage in the analysis using the original load model.

The second most damaged structural component in table 6 described above is the diagonal truss on the left side, also this located at the opposite side of the most damaged element found with the revised load model although only in the z-plane. The further development of elements in the truss category is also the same as seen in the revised load model but on the opposite side. As the most damaged elements in the results from the revised load model were the two ”second diagonal trusses” on the right side in the results from this report it is the two ”second diagonal trusses” on the left side.

The third most damaged elements are located on the vertical truss in the connection below the fifth diagonal truss at the centre-point of the bridge. The elements of this structural category which are damaged with a fatigue life of under 50 years are located around the connection of the two diagonal trusses described above on the left side trusses.

However, looking at the detailed results for element 31931 on the longitudinal grillage in the Lerelva report [2] in chapter 8 of appendix C, in table 8.2 and figure 8.3 it can be seen that the distribution of damage is quite different than the results shown in table 4.8 and figure 4.4. The freight trains make up for 59% of the damage rather than the 97% of the damage found using the revised model in element 32224 also located on the longitudinal grillage.

Comparing the results from the two different elements in the diagonal trusses, element 13051 from the original report and element 23024 from the results presented in 4.6 and 4.5 it can be seen that tendencies in the results are more equal than in the comparison of the two longitudinal grillage elements. The results from the original report found in table 9.2 and figure 9.3 in the Lerelva report [2] show a more equal distribution between damage from passenger and freight trains. The historic fatigue damage from the passenger trains are 47.5% of the total historic damage in the original report, compared to 18% in

the estimations presented in this report. The percentage of damage from the freight trains are larger in the revised load model despite the damage per passage being larger for freight trains in the original report. This is most likely caused by the a-factor first being included in the D_{tot} calculations.

The trends seen in the general data is that the most damaged elements in the original report are placed on the left side, the number of elements from different sections of the bridge are greater. The larger spread in elements might be because of the way the results are presented in the original report versus the results obtained using the revised load model. The trends in the detailed data show a difference in percentage of contribution of fatigue damage between the two models. The revised model has a significantly higher contribution from the freight trains compared to the original report despite having a lower damage per passage.

4.4 Analysis of the Brummund river bridge

The analysis of the Brummund river bridge will be conducted in the same manner as for analysis of the Lerelva bridge. First general trends will be discussed, followed by discussion of the detailed results from the most damaged element of the 3 most damaged structural categories. Then a comparison to the original report followed by a summary of the trend, differences and similarities of the models. The locations on the bridge is defined by using a local x,y,z axis system. The x-direction describing the length of the bridge, in this case 0 meters in x-direction being the start of the bridge and 15.9 meters in x-direction being the end of the bridge. The z-direction is defined along the mid-line of the bridge, positive being on the right side and negative being on the left side of the train tracks. The y-direction describing the height defined as 0 at the lowest part of the bridge, the wind diagonals. The locations of the elements and visualisation of the different parts of the bridge is found in the figures D1 in the appendix displaying the discretisation of the Brummund river bridge.

4.4.1 Trends observed in the general data of the Brummund river bridge.

The general data is listed in table 4.11, where the most damaged elements of the different structural components are presented and in table B2 in the appendix presenting the 150 most damaged elements of the bridge. From table B2 the first trend is easily identified. The longitudinal grillage LB2 is the most damaged structural component by far. There are several elements sustaining the same amount of damage. The most damaged elements are located in the far side of the bridge, this element is located at 14.5 meters in x-direction and at the positive side in z-direction. The second most damaged location on the longitudinal grillages is located at the start of the bridge at 2 meters in x-direction at the negative side in z-direction. The trend of table B2 is that the following elements on and around these elements on both positive and negative z-direction sustain the same amount of damage. The most damaged sectors of the bridge are the longitudinal grillages at 1-2.5 meters in x-direction and 13.5-15 meters in x-direction. The further development is elements around

5.5 and 11.5 meters in x-direction. The last segment found in table B2 is elements on both side at the midpoint at 8 meters in x-direction.

The damaged element in each area is located on both sides of the bridge with the same value of damage ranging from 29 to 15. The damaged segments are found with equal damage value and are "mirrored" in z- and x-direction, with exception of elements which are located at the middle of the bridge in x-direction and can only be mirrored in z-direction.

However, looking further in table 4.11 it can be seen that the most damaged component of each structural category range from 29 for the longitudinal grillage to 2 for the transverse grillage, being the secondary bearing of the bridge. The damage is 2 and 1 for the main girders of the bridge, being the primary bearing of this bridge. These two structural components will be further examined below. Further it can be seen that no structural parts of the bridge has remaining fatigue lifetime D_{hist} over 1.

4.4.2 Trends observed in the detailed data in element 32023

The detailed results for element 32023 is presented in subsection 4.2.2, the placement of this element is at the far end of the right longitudinal grillage. The element is a secondary element, a structural component with low consequence in case of failure. In table 4.13 it can be seen that the Φ is as expected, gradually increasing for passenger trains as caused by increase in weight and speed, and an increase and decrease given the increase and decrease in speeds for freight trains. Looking at the damage per passage D_{pos} and D_{neg} a gradual increase and larger values for the freight trains compared to the passenger trains in the same time periods. The total damage seen in figure **??** is as the trend is expected to be with the new load model, largely affected by damage from the T8 freight train, 72% of the damage is accumulated in the period 1985-present. However, the passenger trains are not to be neglected, 4% of the damage accumulated in this element is from passenger trains in the period 1985-present. Low to no amounts of damage is done by passenger or freight trains before 1930.

4.4.3 Trends observed in element 41231

Element 41231 is located on the transverse grillage of the bridge, a secondary structural component. The damage accumulated in this element is considerably lower than accumulated in element 32023 and has a value of 2.83 as seen in table 4.14. Looking at table 4.15 it can be seen that the Φ has the same development as seen in element 32023. The damage per passage is lower than what was seen in element 32023. The development seen in the passenger trains is a steady increase for both D_{pos} and D_{neg} from period T1 to T4. For the freight trains it is constant at $2 \cdot 10^{-8}$ for T5 and T6 and increases for T7 and T8. The D_{tot} seen in table 4.15 and visualized in figure 4.7 displays the same trends as seen prior for the new load model, 71% damage from modern freight trains in period 1985-present, 17.7% for freight trains in period 1960-1985 and 6.1% from modern day passenger trains.

4.4.4 Trends observed in the detailed data in element 11021

Element 11021 is the second element of 5 on the left main girder. This element is of primary category, meaning it is the primary load bearing structure of the construction. Looking at table 4.17 it can be seen that the Φ-factor is smaller than than in element 32023 and 41231. The damage per passage D_{pos} and D_{neg} for the passenger trains starts of low for T1 and increases steady up to T4. The D_{pos} and D_{neg} values for the freight trains starts of low and is increased by over a factor of 10 from T5 to T8. The total damage displays a similar percentage wise damage as for element 32021 except for the passenger trains. The percentage damage from the passenger trains are 7%, the distribution over the years shows that 2.3% of the damage is sustained in the time period 1930-1960, but the period 1900-1930 displays marginal amounts of damage. The general trend is the same as seen before with 73% of the damage being provided from the T8, modern day freight train in the period 1985-present.

4.4.5 Comparison of trends in the revised and original model for the bridge over the Brummund river

The results from the calculations made by Bane NOR is presented in detail in the Brummund-report [1]. These results will be referenced to and compared with the results calculated with the new load model presented in the sections above.

To compare the general trends of the two models table 4.11 is compared to table 9-2 in the Brummund-report [1]. This shows the sorted list of the different elements with the most fatigue damage in each structural component. The lists are similar with regards to the order of the structural components. The longitudinal grillage being the most damaged, followed by the transverse grillage and least damaged being the main girders of the bridge. Considering the general trends found from table B2 in the appendix compared with the tabulated results of the simulation with the original load model found in appendix C table 6 in the Brummund- report[1]. These two tables show the same pattern, only consisting of longitudinal grillage LB2 elements, starting of with the same elements and following the same pattern. The general trends of the two simulations are similar except for the magnitude in the damage from the new load model.

Comparing the detailed results sin element 31022 in table 8.2 in appendix C in the Brummund -report and the detailed results from element 32023 in table 4.13 it can be seen that the contributions from passenger train in the original report is larger, with 10.9% of historic damage from modern trains compared to 7% being the contribution from passenger trains in total for the revised load model. This trend is also found in the other detailed elements. The % of D_{hist} for passenger trains of element 41211 in table 10.2 in appendix C in the Brummund-report is 20.5% for modern train is the time period 1985-present compared with 6.1% from the revised model in element 41231. This further confirms the trend as seen in the Lerelva bridge that the revised model is less damaged from the passenger trains. However, the order of the damaged elements is the same regardless of this difference in the distribution of the damage between freight and passenger trains.

4.5 Analysis of the Saulidelva bridge

The analysis of the Saulidelva bridge will be conducted in the same manner as for analysis of the Lerelva bridge and the Brummund river bridge. First general trends will be discussed, followed by discussion of the detailed results from the most damaged element of the 3 most damaged structural categories. Then a comparison to the original report followed by a summary of the trend, differences and similarities of the models. The location of the elements and visualisation of the different parts of the bridge is found in the figures E1 in the appendix displaying the discretisation of the Saulidelva bridge.

4.5.1 Trends observed in the general data.

The general data of the Saulidelva bridge is found in table 4.18 and in section B3 in the appendix. From table B3 in the appendix is can be seen that the four most damaged elements has the cross-sectional properties of the diagonal longitudinal grillage, found in the vicinity of the same area on the bridge. The largest amount of historic damage D_{hist} accumulated in any component on this bridge is a value of 79.2. This component is located on the diagonal longitudinal grillage just short of the midpoint of the bridge, connecting to the brake structure of the bridge. The second most damaged component is located just past the midpoint of the bridge at the connection the other side of the brake structure. The two next elements on the list are connected to the brake structure at the same points as the two most damaged components, all being connected to the brake structure in the middle of the bridge. These components are the secondary bearing of the bridge.

The next four elements in table B3 are vertical trusses located at the first and third quarter-points on the bridge. Showing a considerably lower damage value than the components described above, but still large value of 26,25 in historic damage. The vertical trusses being in the primary bearing structure of the bridge.

The third most damaged section of the bridge seen from table 4.18 are the longitudinal grillage. Looking at table B3 in the appendix it can be seen that the elements with the most damage in this section are 4 elements. These elements are located in two different parts of the bridge. Two of them are located on either side of the connection with the first transverse grillage on the right longitudinal grillage. The other two are located at the opposite side of the right longitudinal grillage on either side of the connection with the last transverse grillage. The further development of elements on the longitudinal grillage elements on either side of the already established two sectors, but the damage mainly observed on the right longitudinal grillage. This is due to the curvature of the bridge being defined in the right direction in the analysis.

Further damage is seen in the transverse grillage. As seen in table 4.18 the most damaged element in the transverse grillage is element 37024 followed by element 37084 seen in table B3. These elements are found in the diagonals located underneath the right longitudinal grillage at 3 meters and 6 meters in positive x-direction.

The trends of the Saulidelva bridge found from the general data is that the diagonal longitudinal grillages connected to the brake structure at the centre of the bridge are the most damaged element. Further the vertical trusses and the longitudinal grillages on the right side of the bridge are severely damaged, probably caused by the right curvature of the bridge. The affected locations are around the midpoint of the bridge, at the quarter-points

on either side of the bridge and at the connection of the first and last transverse grillage on the right side.

4.5.2 Trends observed in the detailed data in element 81081

The placement of element on the diagonal longitudinal grillage is explained in the section above. This element is the secondary bearing of the structure. From table 4.20 it can be seen that the Φ follows the speed of the train, increasing for higher speeds and decreasing for lower speed trains. From the damage per passage in positive and negative direction the development is a gradual increase for the passenger trains and for the freight trains, although the freight trains i T5 and T6 has lower damage per passage than the passenger trains i T1 and T2. The damage per passage for the freight train in T7 and T8 are larger than the damage per passage in passenger trains in T3 and T4. The total historic damage D_{tot} shown in figure 4.9 and table 4.18 show a slightly different development than what is seen in the Brummund bridge. The main contribution of the damage is still from the modern freight trains in period 1985-present day, but the contribution is at 63% not at the around 70% as seen above. The passenger trains have contributed more to the damage with 5.7 % of the total damage being caused by modern day passenger trains. The trains from the period 1900-1930 for both freight and passenger trains exhibit very low amounts of damage.

4.5.3 Trends observed in the detailed data in element 14034

Element 14034 is the located near the top of the vertical truss located at the quarter-point of the bridge on the right side. From table 4.22 it can be seen that the Φ is equal to the Φ factor seen for element 14034. The damage per passage is relatively equal for the freight and passenger trains with exception of the period 1930-1960 where the damage per passenger train passage is over double the size of the damage per passage of the freight train. Looking at the total damage accumulated per time period D_{tot} in table 4.22 and the figure 4.10 it can be seen that the contribution from the modern day freight train T8 is larger than in element 81081 and the damage from the passenger trains are considerably larger with 11% of the total damage being accumulated by passenger train traffic from 1985-present day. The damage accumulated from trains traveling on the bridge before 1930 is very low in this element as well.

4.5.4 Trends observed in the detailed data in element 41031

Element 41031 is located on the longitudinal grillage at the connection of the first transverse grillage. from table 4.24 it is seen that the Φ is higher than for the other two elements analysed above. This is probably caused by more dynamic behaviour in the longitudinal grillages located directly beneath to the train tracks. The Damage per passage starts of low and gradually increases for both passenger and freight trains, the damage per freight train being slightly larger than the damage per passenger trains in all periods. The total damage follows the same pattern seen in element 14034 with 62% damage caused by modern day freight trains and 10% damage caused by modern day passenger trains. Also, in this

element there is under 1% damage from both passenger and freight trains in the period 1900-1930.

4.5.5 Comparison of trends in the revised and original model for the Saulidelva bridge

The results from the calculations made by Bane NOR is presented in detail in the Saulidelva-report [4]. These results will be referenced to and compared with the results calculated with the new load model presented in the sections above.

The tables 4.18 and table 9-2 in the Saulidaelva - report [4] showing the most damaged elements of each structural group from the Saulidelva bridge for the two different load models. Both of these tables show the similar order of the damaged elements. A difference between the two tables being that the original model estimates the element 14054, the vertical truss at the center-point of the bridge to be among the three most damaged structural groups of the bridge, in table 4.18 it can be seen that this is the seventh most damaged structural category in the analysis using the revised model. Further considering the tabulated results of the elements sorted after historic damage from the most damaged element and descending in table A.3 in the appendix and table 6 in appendix C in the Saulidelva-report [4]. Starting off these two tables are very similar. Both establishing element 81081 as the most damaged element by far, followed by elements in the vertical trusses 14034 and 14074. But as discussed above the original report establishes element 14054 as one of the most damaged elements. The revised model establishes the several other elements on the bridge as more damaged than this particular element. The revised model establishes several other elements of the secondary category as more damaged than the vertical truss at the midpoint of the bridge, although the element 14014 in the first vertical truss primary category structural components are found in the list before element 14054. Given that the damage for element 14054 is still large in the results from the revised load model, with a accumulated damage of 12.8 either the revised load model has underestimated this particular element or the original load model and the analysis from the Saulidelv-report has underestimated the other elements being ranked as more damaged in the results from the revised model.

When comparing the detailed results for element 14032 from table 8.2 in appendix C in the Saulidelva-report and the results presented in table 4.22 it is seen that the percentage-wise contribution of damage by modern day freight trains are larger for the modern day freight trains in the original report compared to the revised model, 71% of the historic damage is caused by freight trains from 1985-present day in with the original load model versus 63% in the revised model. The contribution from passenger trains are larger in the original load model and trains before 1930 show over 1% of the total damage for both freight and passenger trains compared to being below 1% for all passenger and freight trains in all elements in the revised load model.

Looking at the detailed result for element 81081 in table 10.2 in appendix C in the Saulidelva-report compared to results from the revised model in table 4.20 it can be seen that the percentage wise contribution of the freight trains and the passenger trains distributed differently for the two load models. In the original model the damage done by modern day freight trains are 52% compared to 63% from the revised model. More dam-

age is seen in earlier trains in the original model, 9.3% of the damage is caused by freight trains from the 1930-1960 compared to 1.8% seen from the revised model. The passenger trains in the original report are also more evenly distributed, with 6% from modern day trains, 5% from 1960-1985 and 2.6% from 1930-1960 compared to 5.7% from modern day trains and 2% from both 1960-1930 and 1960-1985. The trains in the period 1900-1930 show 1.5% damage in the original load model whereas the revised model show under 1% damage for train in the period 1900-1930.

4.6 Most damaged components in railway bridges.

Which structural components are the most damaged with the new model compared to the old? The most damaged structural components found from these 3 bridges are of different cross-sectional properties, placement and bearing category. The most damaged element in the Lerelva bridge is the second diagonal truss, which is a primary structural bearing component. The most damaged element in the bridge over the Brummund river is the longitudinal grillage in the start and end of the bridge, which is a secondary bearing component. The most damaged element in the Saulidelva bridge is the diagonal grillage near the midpoint of the bridge, which is a secondary bearing component.

Compared to the estimation made with the old load model for the Lerelva bridge, the difference in the results is that the primary bearing diagonal truss was highlighted as the most damaged element.

The general trend from the fatigue life analysis conducted using the old load model was that critical damage mainly was found in structural components in the secondary bearing of the bridge. The reason for this might be the old load model not being consistent for all structural components. The estimations of the most damaged structural components performed using the new load model show both primary and secondary bearing elements, especially the difference in priority shown from the analysis of the Lerelva bridge. This shows that the new load model can estimate critical fatigue damage in both primary and secondary bearing elements.

4.7 Significance of historic traffic

The trends for historic traffic found in the detailed results as described above, show a clear pattern of historic significance in terms of fatigue damage. The most prominent trend found in all the detailed results analysed in this thesis is that the damage accumulated for both individual groups passenger trains and freight trains in the period 1900-1930 is below 1% of the historic fatigue damage. The three bridges that has been analysed in this thesis were built in 1906, 1913 and 1919, and are thereby not filling the interval 1900-1930. The T1 and T5 trains will have some affect if a detailed individual bridge study is to be performed, but in a large overall analysis for priority of overhaul and maintenance the effect is negligible, as a overall result under 1% is marginal and can be neglected to save computing cost.

The next trend found from the detailed results is that modern day freight trains induce most damage on the bridges. The damage accumulated by the freight trains range from

50% to 80% of the historic damage inflicted on the bridge. Passenger trains accumulate 5-10% of the total historic fatigue damage on the bridges. Compared to the results from the original load model it can be seen that the the distribution of historic damage is similar for freight train damage, but the historic damage is more evenly distributed over the decades for the old load model.

Chapter 5

Conclusion

In this report the remaining fatigue life of 3 railway bridges has been estimated. The calculations are based on historic traffic and a load model proposed in Frøseth [9] for the Norwegian railway system.

This paper evaluates a new load model for trains in fatigue life estimation for railway bridges. This load model is designed to be consistent, conservative and simple, and proposed as a new standard for fatigue life estimation of railway bridges on the Norwegian railway system and similar systems. The evaluation uses the new load model for analysis of fatigue for railway bridges and compare the results with an old extensive load model.

The new load model shows that the modern-day freight trains accumulate 50-80% of the historic fatigue damage. However, the damage from passenger trains cannot be neglected, as this represents 5- 10% of the historic damage. The fatigue damage accumulated from train traffic in the period 1900-1930 in all elements analysed is less than 1% of the historic fatigue damage. Given the continued low contribution from the train traffic in this time period it is recommended not to include this time period in fatigue life estimation when using the new load model for analysis.

Both primary and secondary structural bearing components can be critically damaged. An advantage of the new model is that it seems not to be biased towards secondary or primary bearing components. The calculations show that the new load model has the ability to identify critical damage in both secondary and primary bearing component, compared to the old model that mostly identified critical damage in primary bearing components.

The new model can be used to determine which structural components in a bridge that are subject to most damage. In its current form it cannot be used for accurate determination of fatigue life and thereof to prioritise maintenance and replacements of Norwegian railway bridges. The reason for this is that the results from estimations conducted with the new load model show an overestimation of the fatigue damage in all elements, but the overestimation is consistent. The load model can be used to identify the most damaged parts of a bridge, due to the consistent overestimation of the fatigue damage. Providing the opportunity to monitor these given parts.

Further research is needed to refine the revised load model in order for the results

to be corrected with regards to the magnitude of the values. This to reflect a realistic historic fatigue damage accumulation on bridges on the Norwegian railway system. When a correction factor is found and included in the load model a new analysis should be made to further evaluate the applicability of this load method.

Appendix

A Original load model

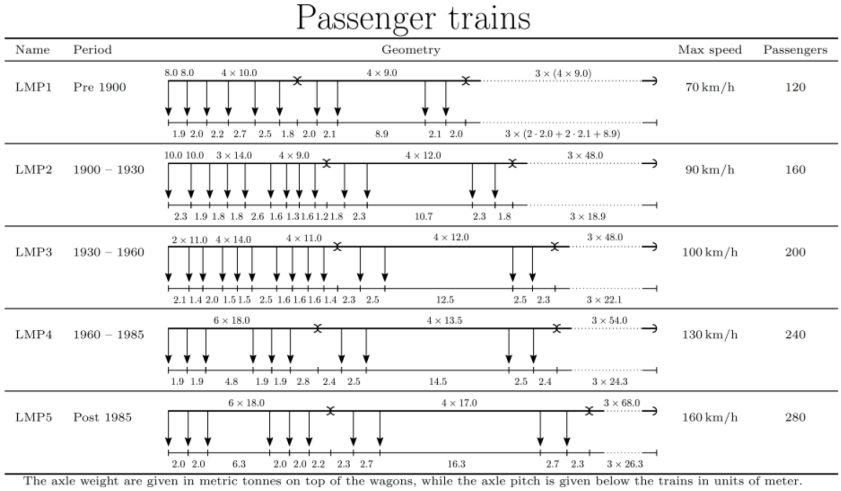

Figure A1: Load model for passenger trains used in fatigue estimation by Bane NOR in 2018.

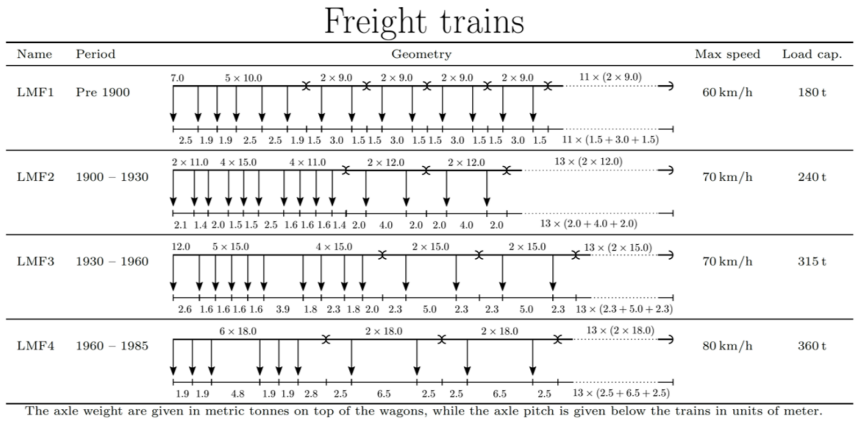

Figure A2: Load model used for historic freight trains in fatigue life estimation by Bane NOR in 2018.

Type 5 Locomotive-hauled freight train

$\Sigma Q = 21600\text{kN}$ $V = 80\text{km/h}$ $L = 270{,}30\text{m}$ $q = 80{,}0\text{kN/m}'$

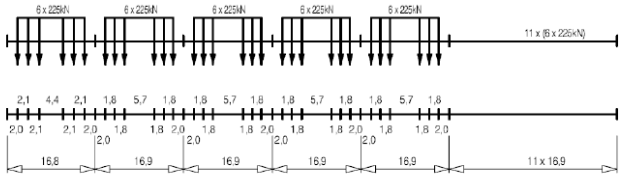

Type 6 Locomotive-hauled freight train

$\Sigma Q = 14310\text{kN}$ $V = 100\text{km/h}$ $L = 333{,}10\text{m}$ $q = 43{,}0\text{kN/m}'$

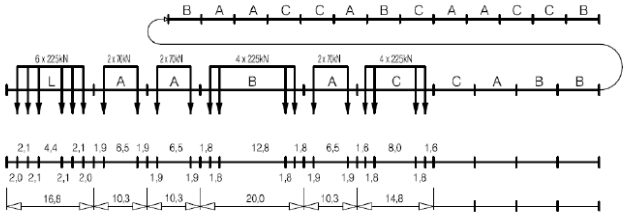

Type 7 Locomotive-hauled freight train

$\Sigma Q = 10350\text{kN}$ $V = 120\text{km/h}$ $L = 196{,}50\text{m}$ $q = 52{,}7\text{kN/m}'$

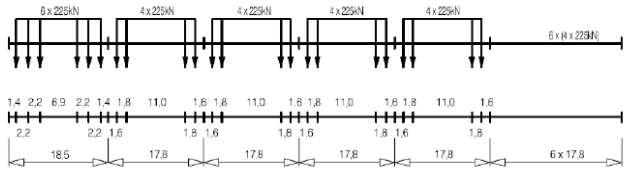

Type 8 Locomotive-hauled freight train

$\Sigma Q = 10350\text{kN}$ $V = 100\text{km/h}$ $L = 212{,}50\text{m}$ $q = 48{,}7\text{kN/m}'$

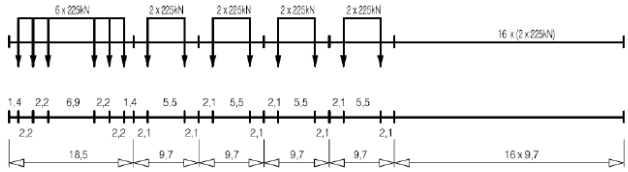

Figure A3: Load model used for modern freight trains in fatigue life estimation by bane NOR in 2018.

B Tabulated results of the 150 most damaged elements from the bridges.

B.1 Tabulated results from Lerelva bridge.

Table B1: Tabulated result of the 150 most damaged elements on the Lerelva bridge.

beam	element	pt	pos	L_{rest}	D_{hist}	$\Delta\sigma_C$	section	category
2302	23024	SP 1	1	-37.870251	17.226789	71	Fag-Di2	primary
2305	23051	SP 1	0	-37.839810	17.138040	71	Fag-Di2	primary
2302	23024	SP 2	1	-37.889069	17.106813	71	Fag-Di2	primary
2305	23051	SP 2	0	-37.809825	17.034368	71	Fag-Di2	primary
1305	13051	SP 3	0	-37.081017	16.015360	71	Fag-Di2	primary
1302	13024	SP 3	1	-37.064053	15.966386	71	Fag-Di2	primary
1305	13051	SP 4	0	-37.041596	15.919421	71	Fag-Di2	primary
1302	13024	SP 4	1	-37.028911	15.842774	71	Fag-Di2	primary
2302	23024	SP 1	0	-37.358860	15.398819	71	Fag-Di2	primary
2302	23023	SP 1	1	-37.358860	15.398819	71	Fag-Di2	primary
2305	23051	SP 1	1	-37.352331	15.316010	71	Fag-Di2	primary
2305	23052	SP 1	0	-37.352331	15.316010	71	Fag-Di2	primary
2302	23024	SP 2	0	-37.341328	15.276476	71	Fag-Di2	primary
2302	23023	SP 2	1	-37.341328	15.276476	71	Fag-Di2	primary
2305	23051	SP 2	1	-37.269335	15.174501	71	Fag-Di2	primary
2305	23052	SP 2	0	-37.269335	15.174501	71	Fag-Di2	primary
1305	13051	SP 3	1	-36.467846	14.455898	71	Fag-Di2	primary
1305	13052	SP 3	0	-36.467846	14.455898	71	Fag-Di2	primary
1302	13024	SP 3	0	-36.409832	14.382122	71	Fag-Di2	primary
1302	13023	SP 3	1	-36.409832	14.382122	71	Fag-Di2	primary
1305	13052	SP 4	0	-36.438743	14.310972	71	Fag-Di2	primary
1305	13051	SP 4	1	-36.438743	14.310972	71	Fag-Di2	primary
1302	13024	SP 4	0	-36.294649	14.257914	71	Fag-Di2	primary
1302	13023	SP 4	1	-36.294649	14.257914	71	Fag-Di2	primary
2302	23022	SP 1	1	-36.674709	13.778799	71	Fag-Di2	primary
2302	23023	SP 1	0	-36.674709	13.778799	71	Fag-Di2	primary
2305	23052	SP 1	1	-36.688094	13.659060	71	Fag-Di2	primary
2305	23053	SP 1	0	-36.688094	13.659060	71	Fag-Di2	primary
2302	23023	SP 2	0	-36.632971	13.594591	71	Fag-Di2	primary
2302	23022	SP 2	1	-36.632971	13.594591	71	Fag-Di2	primary
2305	23052	SP 2	1	-36.612627	13.496758	71	Fag-Di2	primary
2305	23053	SP 2	0	-36.612627	13.496758	71	Fag-Di2	primary
1305	13052	SP 3	1	-35.775107	13.053633	71	Fag-Di2	primary
1305	13053	SP 3	0	-35.775107	13.053633	71	Fag-Di2	primary
1302	13022	SP 3	1	-35.781919	12.985825	71	Fag-Di2	primary
1302	13023	SP 3	0	-35.781919	12.985825	71	Fag-Di2	primary

...continued

beam	element	pt	pos	L_{rest}	D_{hist}	$\Delta\sigma_C$	section	category
1305	13052	SP 4	1	-35.673607	12.944512	71	Fag-Di2	primary
1305	13053	SP 4	0	-35.673607	12.944512	71	Fag-Di2	primary
1302	13022	SP 4	1	-35.677879	12.861853	71	Fag-Di2	primary
1302	13023	SP 4	0	-35.677879	12.861853	71	Fag-Di2	primary
2302	23021	SP 1	1	-36.090400	12.211178	71	Fag-Di2	primary
2302	23022	SP 1	0	-36.090400	12.211178	71	Fag-Di2	primary
2305	23053	SP 1	1	-36.017367	12.129982	71	Fag-Di2	primary
2305	23054	SP 1	0	-36.017367	12.129982	71	Fag-Di2	primary
2302	23022	SP 2	0	-36.169569	12.117175	71	Fag-Di2	primary
2302	23021	SP 2	1	-36.169569	12.117175	71	Fag-Di2	primary
2305	23054	SP 2	0	-35.958638	11.965029	71	Fag-Di2	primary
2305	23053	SP 2	1	-35.958638	11.965029	71	Fag-Di2	primary
1305	13054	SP 3	0	-35.257056	11.872594	71	Fag-Di2	primary
1305	13053	SP 3	1	-35.257056	11.872594	71	Fag-Di2	primary
1302	13021	SP 3	1	-35.357638	11.819823	71	Fag-Di2	primary
1302	13022	SP 3	0	-35.357638	11.819823	71	Fag-Di2	primary
1305	13053	SP 4	1	-35.275514	11.812353	71	Fag-Di2	primary
1305	13054	SP 4	0	-35.275514	11.812353	71	Fag-Di2	primary
1302	13021	SP 4	1	-35.173174	11.744685	71	Fag-Di2	primary
1302	13022	SP 4	0	-35.173174	11.744685	71	Fag-Di2	primary
2302	23021	SP 1	0	-35.549179	11.050691	71	Fag-Di2	primary
2302	23021	SP 2	0	-35.338722	10.960035	71	Fag-Di2	primary
2305	23054	SP 1	1	-35.329596	10.905853	71	Fag-Di2	primary
2305	23054	SP 2	1	-35.199180	10.716212	71	Fag-Di2	primary
1305	13054	SP 3	1	-34.709197	10.643568	71	Fag-Di2	primary
1302	13021	SP 3	0	-34.649963	10.576809	71	Fag-Di2	primary
1305	13054	SP 4	1	-34.560912	10.475656	71	Fag-Di2	primary
1302	13021	SP 4	0	-34.586593	10.380441	71	Fag-Di2	primary
2305	23054	SP 3	1	-35.327166	9.040015	71	Fag-Di2	primary
2302	23021	SP 3	0	-35.323886	8.978215	71	Fag-Di2	primary
2305	23054	SP 4	1	-35.217953	8.845164	71	Fag-Di2	primary
2302	23021	SP 4	0	-35.221012	8.792281	71	Fag-Di2	primary
1302	13021	SP 1	0	-35.490639	8.372706	71	Fag-Di2	primary
1305	13054	SP 1	1	-35.473936	8.347832	71	Fag-Di2	primary
1302	13021	SP 2	0	-35.383997	8.222015	71	Fag-Di2	primary
1305	13054	SP 2	1	-35.312960	8.187988	71	Fag-Di2	primary
2302	23022	SP 4	0	-34.022143	7.680167	71	Fag-Di2	primary
2302	23021	SP 4	1	-34.022143	7.680167	71	Fag-Di2	primary
2305	23054	SP 3	0	-34.446255	7.645837	71	Fag-Di2	primary
2305	23053	SP 3	1	-34.446255	7.645837	71	Fag-Di2	primary
2305	23053	SP 4	1	-34.219622	7.609646	71	Fag-Di2	primary
2305	23054	SP 4	0	-34.219622	7.609646	71	Fag-Di2	primary
2302	23022	SP 3	0	-34.420869	7.608983	71	Fag-Di2	primary

. . . continued

beam	element	pt	pos	L_{rest}	D_{hist}	$\Delta\sigma_C$	section	category
2302	23021	SP 3	1	-34.420869	7.608983	71	Fag-Di2	primary
3224	32242	SP 1	1	-29.500993	7.425879	85	LB1	secondary
3225	32251	SP 1	0	-29.514255	7.412527	85	LB1	secondary
3225	32251	SP 2	0	-29.423919	7.409076	85	LB1	secondary
3224	32242	SP 2	1	-29.444439	7.404384	85	LB1	secondary
3202	32022	SP 1	1	-29.519232	7.355575	85	LB1	secondary
1302	13022	SP 1	0	-34.790054	7.355084	71	Fag-Di2	primary
1302	13021	SP 1	1	-34.790054	7.355084	71	Fag-Di2	primary
3203	32031	SP 1	0	-29.505340	7.343217	85	LB1	secondary
1305	13053	SP 1	1	-34.748691	7.324142	71	Fag-Di2	primary
1305	13054	SP 1	0	-34.748691	7.324142	71	Fag-Di2	primary
3203	32031	SP 2	0	-29.439056	7.318812	85	LB1	secondary
3202	32022	SP 2	1	-29.428411	7.309366	85	LB1	secondary
1302	13021	SP 2	1	-34.587979	7.228638	71	Fag-Di2	primary
1302	13022	SP 2	0	-34.587979	7.228638	71	Fag-Di2	primary
1305	13053	SP 2	1	-34.605599	7.199752	71	Fag-Di2	primary
1305	13054	SP 2	0	-34.605599	7.199752	71	Fag-Di2	primary
2305	23053	SP 3	0	-33.170599	6.718641	71	Fag-Di2	primary
2305	23052	SP 3	1	-33.170599	6.718641	71	Fag-Di2	primary
2302	23023	SP 3	0	-33.093614	6.699820	71	Fag-Di2	primary
2302	23022	SP 3	1	-33.093614	6.699820	71	Fag-Di2	primary
2305	23053	SP 4	0	-33.016059	6.633386	71	Fag-Di2	primary
2305	23052	SP 4	1	-33.016059	6.633386	71	Fag-Di2	primary
2302	23023	SP 4	0	-32.958197	6.596502	71	Fag-Di2	primary
2302	23022	SP 4	1	-32.958197	6.596502	71	Fag-Di2	primary
1302	13023	SP 1	0	-33.670892	6.408033	71	Fag-Di2	primary
1302	13022	SP 1	1	-33.670892	6.408033	71	Fag-Di2	primary
2406	24061	SP 1	0	-29.123579	6.377029	71	Fag-Ve4	primary
1302	13022	SP 2	1	-33.490296	6.376400	71	Fag-Di2	primary
1302	13023	SP 2	0	-33.490296	6.376400	71	Fag-Di2	primary
1305	13053	SP 1	0	-33.784746	6.350957	71	Fag-Di2	primary
1305	13052	SP 1	1	-33.784746	6.350957	71	Fag-Di2	primary
2406	24061	SP 2	0	-29.093967	6.348853	71	Fag-Ve4	primary
1305	13053	SP 2	0	-33.547102	6.257322	71	Fag-Di2	primary
1305	13052	SP 2	1	-33.547102	6.257322	71	Fag-Di2	primary
3102	31022	SP 1	1	-29.581589	6.216242	85	LB1	secondary
3103	31031	SP 1	0	-29.465620	6.205155	85	LB1	secondary
3124	31242	SP 1	1	-29.447102	6.030267	85	LB1	secondary
3125	31251	SP 1	0	-29.565196	6.018815	85	LB1	secondary
3103	31031	SP 2	0	-29.600726	5.949001	85	LB1	secondary
3102	31022	SP 2	1	-29.499104	5.887230	85	LB1	secondary
3124	31242	SP 2	1	-29.516365	5.816515	85	LB1	secondary
2302	23024	SP 3	0	-31.575199	5.801624	71	Fag-Di2	primary

...continued

beam	element	pt	pos	L_{rest}	D_{hist}	$\Delta\sigma_C$	section	category
2302	23023	SP 3	1	-31.575199	5.801624	71	Fag-Di2	primary
2305	23051	SP 3	1	-31.653018	5.794922	71	Fag-Di2	primary
2305	23052	SP 3	0	-31.653018	5.794922	71	Fag-Di2	primary
2305	23051	SP 4	1	-31.388763	5.788802	71	Fag-Di2	primary
2305	23052	SP 4	0	-31.388763	5.788802	71	Fag-Di2	primary
3125	31251	SP 2	0	-29.480929	5.765763	85	LB1	secondary
2302	23024	SP 4	0	-31.397534	5.721331	71	Fag-Di2	primary
2302	23023	SP 4	1	-31.397534	5.721331	71	Fag-Di2	primary
1302	13023	SP 1	1	-32.489988	5.683835	71	Fag-Di2	primary
1302	13024	SP 1	0	-32.489988	5.683835	71	Fag-Di2	primary
3217	32171	SP 1	0	-28.204608	5.669585	85	LB1	secondary
3216	32161	SP 1	1	-28.209002	5.668504	85	LB1	secondary
3220	32202	SP 1	1	-27.876133	5.639819	85	LB1	secondary
3221	32211	SP 1	0	-27.956007	5.635641	85	LB1	secondary
3221	32211	SP 2	0	-27.784153	5.599980	85	LB1	secondary
3220	32202	SP 2	1	-27.794048	5.589273	85	LB1	secondary
1305	13051	SP 1	1	-32.408107	5.572739	71	Fag-Di2	primary
1305	13052	SP 1	0	-32.408107	5.572739	71	Fag-Di2	primary
1302	13023	SP 2	1	-32.383655	5.565543	71	Fag-Di2	primary
1302	13024	SP 2	0	-32.383655	5.565543	71	Fag-Di2	primary
3216	32161	SP 2	1	-27.815351	5.548223	85	LB1	secondary
3217	32171	SP 2	0	-27.819959	5.547458	85	LB1	secondary
3207	32071	SP 1	0	-27.867361	5.546225	85	LB1	secondary
3206	32062	SP 1	1	-27.878835	5.537733	85	LB1	secondary
3207	32071	SP 2	0	-27.783358	5.510737	85	LB1	secondary
3206	32062	SP 2	1	-27.802433	5.508343	85	LB1	secondary
1305	13052	SP 2	0	-32.265172	5.505194	71	Fag-Di2	primary
1305	13051	SP 2	1	-32.265172	5.505194	71	Fag-Di2	primary

B.2 Tabulated results from Brummund bridge.

Table B2: Tabulated result of the 150 most damaged elements on the Brummund bridge.

beam	element	pt	pos	L_{rest}	D_{hist}	$\Delta\sigma_C$	section	category
3202	32023	SP 3	0	-46.866003	29.063693	85	LB2	secondary
3214	32143	SP 3	0	-46.866003	29.063693	85	LB2	secondary
3102	31022	SP 3	1	-46.866003	29.063693	85	LB2	secondary
3102	31022	SP 1	1	-46.866003	29.063693	85	LB2	secondary
3102	31023	SP 3	0	-46.866003	29.063693	85	LB2	secondary
3202	32022	SP 1	1	-46.866003	29.063693	85	LB2	secondary
3202	32022	SP 3	1	-46.866003	29.063693	85	LB2	secondary
3114	31143	SP 3	0	-46.866003	29.063693	85	LB2	secondary

. . . continued

beam	element	pt	pos	L_{rest}	D_{hist}	$\Delta\sigma$	section	category
3114	31143	SP 1	0	-46.866003	29.063693	85	LB2	secondary
3114	31142	SP 3	1	-46.866003	29.063693	85	LB2	secondary
3114	31142	SP 1	1	-46.866003	29.063693	85	LB2	secondary
3202	32023	SP 1	0	-46.866003	29.063693	85	LB2	secondary
3214	32142	SP 1	1	-46.866003	29.063693	85	LB2	secondary
3214	32142	SP 3	1	-46.866003	29.063693	85	LB2	secondary
3214	32143	SP 1	0	-46.866003	29.063693	85	LB2	secondary
3102	31023	SP 1	0	-46.866003	29.063693	85	LB2	secondary
3202	32023	SP 7	0	-46.866003	29.063693	85	LB2	secondary
3114	31142	SP 5	1	-46.866003	29.063693	85	LB2	secondary
3102	31023	SP 7	0	-46.866003	29.063693	85	LB2	secondary
3202	32023	SP 5	0	-46.866003	29.063693	85	LB2	secondary
3102	31023	SP 5	0	-46.866003	29.063693	85	LB2	secondary
3202	32022	SP 5	1	-46.866003	29.063693	85	LB2	secondary
3202	32022	SP 7	1	-46.866003	29.063693	85	LB2	secondary
3214	32142	SP 5	1	-46.866003	29.063693	85	LB2	secondary
3114	31143	SP 7	0	-46.866003	29.063693	85	LB2	secondary
3114	31142	SP 7	1	-46.866003	29.063693	85	LB2	secondary
3214	32142	SP 7	1	-46.866003	29.063693	85	LB2	secondary
3114	31143	SP 5	0	-46.866003	29.063693	85	LB2	secondary
3102	31022	SP 5	1	-46.866003	29.063693	85	LB2	secondary
3214	32143	SP 5	0	-46.866003	29.063693	85	LB2	secondary
3102	31022	SP 7	1	-46.866003	29.063693	85	LB2	secondary
3214	32143	SP 7	0	-46.866003	29.063693	85	LB2	secondary
3205	32053	SP 3	0	-45.835919	22.413618	85	LB2	secondary
3205	32053	SP 1	0	-45.835919	22.413618	85	LB2	secondary
3111	31112	SP 3	1	-45.835919	22.413618	85	LB2	secondary
3105	31053	SP 3	0	-45.835919	22.413618	85	LB2	secondary
3211	32112	SP 1	1	-45.835919	22.413618	85	LB2	secondary
3111	31113	SP 3	0	-45.835919	22.413618	85	LB2	secondary
3211	32113	SP 1	0	-45.835919	22.413618	85	LB2	secondary
3105	31053	SP 1	0	-45.835919	22.413618	85	LB2	secondary
3111	31113	SP 1	0	-45.835919	22.413618	85	LB2	secondary
3211	32112	SP 3	1	-45.835919	22.413618	85	LB2	secondary
3105	31052	SP 3	1	-45.835919	22.413618	85	LB2	secondary
3111	31112	SP 1	1	-45.835919	22.413618	85	LB2	secondary
3105	31052	SP 1	1	-45.835919	22.413618	85	LB2	secondary
3205	32052	SP 3	1	-45.835919	22.413618	85	LB2	secondary
3205	32052	SP 1	1	-45.835919	22.413618	85	LB2	secondary
3211	32113	SP 3	0	-45.835919	22.413618	85	LB2	secondary
3105	31052	SP 7	1	-45.835919	22.413618	85	LB2	secondary
3105	31053	SP 5	0	-45.835919	22.413618	85	LB2	secondary
3105	31053	SP 7	0	-45.835919	22.413618	85	LB2	secondary

...continued

beam	element	pt	pos	L_{rest}	D_{hist}	$\Delta\sigma$	section	category
3205	32052	SP 5	1	-45.835919	22.413618	85	LB2	secondary
3105	31052	SP 5	1	-45.835919	22.413618	85	LB2	secondary
3111	31113	SP 5	0	-45.835919	22.413618	85	LB2	secondary
3205	32052	SP 7	1	-45.835919	22.413618	85	LB2	secondary
3205	32053	SP 5	0	-45.835919	22.413618	85	LB2	secondary
3111	31113	SP 7	0	-45.835919	22.413618	85	LB2	secondary
3211	32112	SP 5	1	-45.835919	22.413618	85	LB2	secondary
3111	31112	SP 7	1	-45.835919	22.413618	85	LB2	secondary
3111	31112	SP 5	1	-45.835919	22.413618	85	LB2	secondary
3211	32113	SP 7	0	-45.835919	22.413618	85	LB2	secondary
3211	32113	SP 5	0	-45.835919	22.413618	85	LB2	secondary
3205	32053	SP 7	0	-45.835919	22.413618	85	LB2	secondary
3211	32112	SP 7	1	-45.835919	22.413618	85	LB2	secondary
3208	32083	SP 1	0	-45.504500	18.488305	85	LB2	secondary
3208	32083	SP 3	0	-45.504500	18.488305	85	LB2	secondary
3108	31083	SP 1	0	-45.504500	18.488305	85	LB2	secondary
3208	32082	SP 3	1	-45.504500	18.488305	85	LB2	secondary
3108	31082	SP 1	1	-45.504500	18.488305	85	LB2	secondary
3108	31083	SP 3	0	-45.504500	18.488305	85	LB2	secondary
3208	32082	SP 1	1	-45.504500	18.488305	85	LB2	secondary
3108	31082	SP 3	1	-45.504500	18.488305	85	LB2	secondary
3108	31082	SP 5	1	-45.504500	18.488305	85	LB2	secondary
3108	31083	SP 5	0	-45.504500	18.488305	85	LB2	secondary
3108	31082	SP 7	1	-45.504500	18.488305	85	LB2	secondary
3208	32083	SP 5	0	-45.504500	18.488305	85	LB2	secondary
3208	32083	SP 7	0	-45.504500	18.488305	85	LB2	secondary
3208	32082	SP 7	1	-45.504500	18.488305	85	LB2	secondary
3208	32082	SP 5	1	-45.504500	18.488305	85	LB2	secondary
3108	31083	SP 7	0	-45.504500	18.488305	85	LB2	secondary
3202	32022	SP 6	1	-45.546237	16.234113	85	LB2	secondary
3102	31023	SP 8	0	-45.546237	16.234113	85	LB2	secondary
3114	31142	SP 6	1	-45.546237	16.234113	85	LB2	secondary
3114	31143	SP 8	0	-45.546237	16.234113	85	LB2	secondary
3114	31143	SP 6	0	-45.546237	16.234113	85	LB2	secondary
3202	32022	SP 8	1	-45.546237	16.234113	85	LB2	secondary
3102	31022	SP 6	1	-45.546237	16.234113	85	LB2	secondary
3102	31022	SP 8	1	-45.546237	16.234113	85	LB2	secondary
3102	31023	SP 6	0	-45.546237	16.234113	85	LB2	secondary
3114	31142	SP 8	1	-45.546237	16.234113	85	LB2	secondary
3214	32143	SP 8	0	-45.546237	16.234113	85	LB2	secondary
3214	32143	SP 6	0	-45.546237	16.234113	85	LB2	secondary
3214	32142	SP 8	1	-45.546237	16.234113	85	LB2	secondary
3214	32142	SP 6	1	-45.546237	16.234113	85	LB2	secondary

...continued

beam	element	pt	pos	L_{rest}	D_{hist}	$\Delta\sigma$	section	category
3202	32023	SP 6	0	-45.546237	16.234113	85	LB2	secondary
3202	32023	SP 8	0	-45.546237	16.234113	85	LB2	secondary
3114	31142	SP 4	1	-45.546237	16.234113	85	LB2	secondary
3202	32022	SP 4	1	-45.546237	16.234113	85	LB2	secondary
3214	32143	SP 4	0	-45.546237	16.234113	85	LB2	secondary
3102	31022	SP 4	1	-45.546237	16.234113	85	LB2	secondary
3214	32143	SP 2	0	-45.546237	16.234113	85	LB2	secondary
3102	31022	SP 2	1	-45.546237	16.234113	85	LB2	secondary
3214	32142	SP 4	1	-45.546237	16.234113	85	LB2	secondary
3102	31023	SP 4	0	-45.546237	16.234113	85	LB2	secondary
3214	32142	SP 2	1	-45.546237	16.234113	85	LB2	secondary
3202	32022	SP 2	1	-45.546237	16.234113	85	LB2	secondary
3114	31142	SP 2	1	-45.546237	16.234113	85	LB2	secondary
3114	31143	SP 4	0	-45.546237	16.234113	85	LB2	secondary
3202	32023	SP 2	0	-45.546237	16.234113	85	LB2	secondary
3102	31023	SP 2	0	-45.546237	16.234113	85	LB2	secondary
3202	32023	SP 4	0	-45.546237	16.234113	85	LB2	secondary
3114	31143	SP 2	0	-45.546237	16.234113	85	LB2	secondary
3102	31021	SP 3	1	-45.328956	15.542987	85	LB2	secondary
3214	32143	SP 1	1	-45.328956	15.542987	85	LB2	secondary
3214	32143	SP 3	1	-45.328956	15.542987	85	LB2	secondary
3214	32144	SP 3	0	-45.328956	15.542987	85	LB2	secondary
3102	31022	SP 3	0	-45.328956	15.542987	85	LB2	secondary
3114	31143	SP 1	1	-45.328956	15.542987	85	LB2	secondary
3102	31022	SP 1	0	-45.328956	15.542987	85	LB2	secondary
3114	31143	SP 3	1	-45.328956	15.542987	85	LB2	secondary
3114	31144	SP 1	0	-45.328956	15.542987	85	LB2	secondary
3102	31021	SP 1	1	-45.328956	15.542987	85	LB2	secondary
3114	31144	SP 3	0	-45.328956	15.542987	85	LB2	secondary
3202	32021	SP 1	1	-45.328956	15.542987	85	LB2	secondary
3202	32022	SP 3	0	-45.328956	15.542987	85	LB2	secondary
3214	32144	SP 1	0	-45.328956	15.542987	85	LB2	secondary
3202	32021	SP 3	1	-45.328956	15.542987	85	LB2	secondary
3202	32022	SP 1	0	-45.328956	15.542987	85	LB2	secondary
3202	32021	SP 7	1	-45.328956	15.542987	85	LB2	secondary
3214	32143	SP 7	1	-45.328956	15.542987	85	LB2	secondary
3214	32144	SP 5	0	-45.328956	15.542987	85	LB2	secondary
3214	32144	SP 7	0	-45.328956	15.542987	85	LB2	secondary
3102	31022	SP 7	0	-45.328956	15.542987	85	LB2	secondary
3202	32022	SP 7	0	-45.328956	15.542987	85	LB2	secondary
3102	31022	SP 5	0	-45.328956	15.542987	85	LB2	secondary
3202	32022	SP 5	0	-45.328956	15.542987	85	LB2	secondary
3114	31144	SP 5	0	-45.328956	15.542987	85	LB2	secondary

...continued

beam	element	pt	pos	L_{rest}	D_{hist}	$\Delta\sigma$	section	category
3202	32021	SP 5	1	-45.328956	15.542987	85	LB2	secondary
3102	31021	SP 7	1	-45.328956	15.542987	85	LB2	secondary
3114	31143	SP 5	1	-45.328956	15.542987	85	LB2	secondary
3102	31021	SP 5	1	-45.328956	15.542987	85	LB2	secondary
3114	31143	SP 7	1	-45.328956	15.542987	85	LB2	secondary
3214	32143	SP 5	1	-45.328956	15.542987	85	LB2	secondary
3114	31144	SP 7	0	-45.328956	15.542987	85	LB2	secondary
3105	31051	SP 3	1	-44.501581	15.422708	85	LB2	secondary
3105	31051	SP 1	1	-44.501581	15.422708	85	LB2	secondary
3111	31114	SP 1	0	-44.501581	15.422708	85	LB2	secondary
3105	31052	SP 1	0	-44.501581	15.422708	85	LB2	secondary
3111	31113	SP 1	1	-44.501581	15.422708	85	LB2	secondary
3105	31052	SP 3	0	-44.501581	15.422708	85	LB2	secondary

B.3 Tabulated results from Saulidelva bridge.

Table B3: Tabulated result of the 150 most damaged elements on the Brummund bridge.

beam	element	pt	pos	L_{rest}	D_{hist}	$\Delta\sigma_C$	section	category
8108	81081	SP 2	0	-31.309430	72.194534	71	LB-Diag	secondary
8109	81094	SP 2	1	-31.306972	71.777690	71	LB-Diag	secondary
8201	82014	SP 2	1	-31.047688	68.718310	71	LB-Diag	secondary
8202	82021	SP 2	0	-31.098689	68.127747	71	LB-Diag	secondary
1403	14034	SP 2	1	-27.908922	26.254915	85	Fag 5-6	primary
1403	14034	SP 1	1	-27.690964	26.066209	85	Fag 5-6	primary
1407	14074	SP 2	1	-27.778411	25.925863	85	Fag 5-6	primary
1407	14074	SP 1	1	-27.803108	25.202244	85	Fag 5-6	primary
8109	81094	SP 1	1	-29.112125	24.256452	71	LB-Diag	secondary
8201	82014	SP 1	1	-29.130756	24.241826	71	LB-Diag	secondary
8108	81081	SP 1	0	-29.113122	24.153145	71	LB-Diag	secondary
8202	82021	SP 1	0	-29.089102	23.979883	71	LB-Diag	secondary
4103	41031	SP 2	1	-29.441462	21.558387	71	LB	secondary
4146	41461	SP 2	0	-29.686490	21.294663	71	LB	secondary
4103	41031	SP 3	1	-29.584127	21.084045	71	LB	secondary
4146	41461	SP 3	0	-29.556561	21.047782	71	LB	secondary
4104	41041	SP 2	0	-29.519699	20.887564	71	LB	secondary
4104	41041	SP 3	0	-29.454785	20.675228	71	LB	secondary
4145	41451	SP 3	1	-29.371921	20.462546	71	LB	secondary
4145	41451	SP 2	1	-29.421099	20.441158	71	LB	secondary
3702	37024	SP 2	1	-30.325728	19.762234	71	T Diag2_1	secondary
4102	41022	SP 2	1	-28.994375	19.642725	71	LB	secondary
4103	41031	SP 2	0	-28.994375	19.642725	71	LB	secondary

. . . continued

beam	element	pt	pos	L_{rest}	D_{hist}	$\Delta\sigma_C$	section	category
4102	41022	SP 3	1	-28.995550	19.580220	71	LB	secondary
4103	41031	SP 3	0	-28.995550	19.580220	71	LB	secondary
3708	37084	SP 1	1	-30.248586	19.558780	71	T Diag2$_1$	secondary
4147	41471	SP 3	0	-28.964322	19.421056	71	LB	secondary
4146	41461	SP 3	1	-28.964322	19.421056	71	LB	secondary
4146	41461	SP 2	1	-29.005681	19.290635	71	LB	secondary
4147	41471	SP 2	0	-29.005681	19.290635	71	LB	secondary
3702	37024	SP 1	1	-30.419693	18.460000	71	T Diag2$_1$	secondary
4104	41041	SP 1	0	-28.970979	18.216379	71	LB	secondary
3708	37084	SP 2	1	-30.337317	18.214531	71	T Diag2$_1$	secondary
4104	41041	SP 4	0	-28.860123	17.981536	71	LB	secondary
4145	41451	SP 4	1	-28.727007	17.975104	71	LB	secondary
4103	41031	SP 1	1	-28.878588	17.906041	71	LB	secondary
4145	41451	SP 1	1	-28.868694	17.899218	71	LB	secondary
4146	41461	SP 1	0	-28.666937	17.861968	71	LB	secondary
4146	41461	SP 4	0	-28.637111	17.543691	71	LB	secondary
4103	41031	SP 4	1	-28.735619	17.539168	71	LB	secondary
4103	41031	SP 1	0	-28.234360	16.954149	71	LB	secondary
4102	41022	SP 1	1	-28.234360	16.954149	71	LB	secondary
4102	41022	SP 4	1	-28.325173	16.904397	71	LB	secondary
4103	41031	SP 4	0	-28.325173	16.904397	71	LB	secondary
4104	41041	SP 3	1	-28.237355	16.823058	71	LB	secondary
4105	41051	SP 3	0	-28.237355	16.823058	71	LB	secondary
4146	41461	SP 4	1	-28.289781	16.811293	71	LB	secondary
4147	41471	SP 4	0	-28.289781	16.811293	71	LB	secondary
4147	41471	SP 1	0	-28.244263	16.799969	71	LB	secondary
4146	41461	SP 1	1	-28.244263	16.799969	71	LB	secondary
4144	41442	SP 3	1	-28.123920	16.781727	71	LB	secondary
4145	41451	SP 3	0	-28.123920	16.781727	71	LB	secondary
4104	41041	SP 2	1	-28.235023	16.658015	71	LB	secondary
4105	41051	SP 2	0	-28.235023	16.658015	71	LB	secondary
1401	14014	SP 3	1	-29.868767	16.548838	71	Fag 1-2	primary
4144	41442	SP 2	1	-28.169308	16.324049	71	LB	secondary
4145	41451	SP 2	0	-28.169308	16.324049	71	LB	secondary
2403	24034	SP 3	1	-25.935204	16.319583	85	Fag 5-6	primary
1503	15031	SP 2	0	-27.253770	16.225689	85	Fag 5-6	primary
1401	14014	SP 4	1	-29.903111	16.151930	71	Fag 1-2	primary
1503	15031	SP 1	0	-27.102326	16.135772	85	Fag 5-6	primary
2403	24034	SP 4	1	-25.895462	16.079366	85	Fag 5-6	primary
1507	15071	SP 2	0	-27.115220	15.978878	85	Fag 5-6	primary
2407	24074	SP 3	1	-25.929800	15.920354	85	Fag 5-6	primary
4110	41101	SP 3	0	-27.426909	15.889978	71	LB	secondary
2407	24074	SP 4	1	-25.956352	15.869843	85	Fag 5-6	primary

. . . continued

beam	element	pt	pos	L_{rest}	D_{hist}	$\Delta\sigma_C$	section	category
1507	15071	SP 1	0	-26.941943	15.820246	85	Fag 5-6	primary
1401	14014	SP 7	1	-29.517475	15.729833	71	Fag 1-2	primary
4109	41091	SP 3	1	-27.322981	15.503452	71	LB	secondary
4139	41391	SP 3	1	-27.282919	15.343674	71	LB	secondary
1401	14014	SP 8	1	-29.254939	15.231232	71	Fag 1-2	primary
4140	41401	SP 3	0	-27.191294	15.175082	71	LB	secondary
4104	41041	SP 4	1	-27.741689	14.953305	71	LB	secondary
4105	41051	SP 4	0	-27.741689	14.953305	71	LB	secondary
4110	41101	SP 2	0	-27.226864	14.946202	71	LB	secondary
4145	41451	SP 4	0	-27.738604	14.837656	71	LB	secondary
4144	41442	SP 4	1	-27.738604	14.837656	71	LB	secondary
4139	41391	SP 2	1	-27.193026	14.775465	71	LB	secondary
3702	37023	SP 2	1	-29.240208	14.666243	71	T Diag2_1	secondary
3702	37024	SP 2	0	-29.240208	14.666243	71	T Diag2_1	secondary
4105	41051	SP 1	0	-27.814880	14.594875	71	LB	secondary
4104	41041	SP 1	1	-27.814880	14.594875	71	LB	secondary
8108	81084	SP 2	1	-28.541015	14.560690	71	LB-Diag	secondary
3708	37083	SP 1	1	-29.215264	14.559095	71	T Diag2_1	secondary
3708	37084	SP 1	0	-29.215262	14.559095	71	T Diag2_1	secondary
8201	82013	SP 2	1	-27.630213	14.547076	71	LB-Diag	secondary
8201	82014	SP 2	0	-27.630213	14.547076	71	LB-Diag	secondary
4144	41442	SP 1	1	-27.697159	14.361569	71	LB	secondary
4145	41451	SP 1	0	-27.697159	14.361569	71	LB	secondary
8202	82021	SP 2	1	-27.599534	14.345725	71	LB-Diag	secondary
8202	82022	SP 2	0	-27.599534	14.345725	71	LB-Diag	secondary
8109	81091	SP 2	0	-28.441193	14.181997	71	LB-Diag	secondary
4140	41401	SP 2	0	-26.845717	14.051657	71	LB	secondary
4109	41091	SP 4	1	-27.244370	14.033116	71	LB	secondary
4109	41091	SP 2	1	-26.855204	14.022530	71	LB	secondary
4110	41101	SP 4	0	-27.164131	13.948230	71	LB	secondary
4109	41091	SP 3	0	-26.863634	13.871387	71	LB	secondary
4108	41082	SP 3	1	-26.863634	13.871387	71	LB	secondary
3702	37023	SP 1	1	-28.993617	13.795867	71	T Diag2_1	secondary
3702	37024	SP 1	0	-28.993617	13.795867	71	T Diag2_1	secondary
7103	71034	SP 2	1	-28.071015	13.773518	71	BF Diag	secondary
8108	81082	SP 2	0	-27.440036	13.767786	71	LB-Diag	secondary
8108	81081	SP 2	1	-27.440036	13.767786	71	LB-Diag	secondary
8109	81094	SP 2	0	-27.501660	13.739862	71	LB-Diag	secondary
8109	81093	SP 2	1	-27.501660	13.739862	71	LB-Diag	secondary
4140	41401	SP 4	0	-27.107205	13.736877	71	LB	secondary
3708	37084	SP 2	0	-28.972224	13.664621	71	T Diag2_1	secondary
3708	37083	SP 2	1	-28.972224	13.664621	71	T Diag2_1	secondary
4139	41391	SP 4	1	-27.051171	13.663535	71	LB	secondary

. . . continued

beam	element	pt	pos	L_{rest}	D_{hist}	$\Delta\sigma_C$	section	category
7104	71041	SP 2	0	-27.950017	13.586168	71	BF Diag	secondary
3802	38024	SP 1	1	-27.804516	13.579522	71	T Diag2_1	secondary
3808	38084	SP 2	1	-27.785993	13.499546	71	T Diag2_1	secondary
4140	41401	SP 3	1	-26.781656	13.495199	71	LB	secondary
4141	41411	SP 3	0	-26.781656	13.495199	71	LB	secondary
4110	41101	SP 1	0	-26.954589	13.342538	71	LB	secondary
4139	41391	SP 1	1	-26.965563	13.288702	71	LB	secondary
4110	41101	SP 3	1	-26.461002	13.194745	71	LB	secondary
4111	41111	SP 3	0	-26.461002	13.194745	71	LB	secondary
4139	41391	SP 3	0	-26.300576	12.917157	71	LB	secondary
4138	41382	SP 3	1	-26.300576	12.917157	71	LB	secondary
4116	41161	SP 2	0	-26.453901	12.871760	71	LB	secondary
1405	14054	SP 1	1	-26.785851	12.819067	85	Fag 9-10	primary
4133	41331	SP 2	1	-26.363344	12.767571	71	LB	secondary
1409	14094	SP 8	1	-28.897432	12.760102	71	Fag 1-2	primary
4128	41281	SP 4	0	-26.725109	12.723929	71	LB	secondary
4121	41211	SP 4	1	-26.734294	12.700386	71	LB	secondary
3802	38024	SP 2	1	-27.643796	12.690752	71	T Diag2_1	secondary
4109	41091	SP 4	0	-26.625397	12.663384	71	LB	secondary
4108	41082	SP 4	1	-26.625397	12.663384	71	LB	secondary
3808	38084	SP 1	1	-27.612564	12.651351	71	T Diag2_1	secondary
4128	41281	SP 3	0	-26.430859	12.635285	71	LB	secondary
4140	41401	SP 1	0	-26.731937	12.602931	71	LB	secondary
1405	14054	SP 2	1	-26.910549	12.592994	85	Fag 9-10	primary
7102	71024	SP 2	1	-27.291174	12.578694	71	BF Diag	secondary
4121	41211	SP 3	1	-26.429735	12.576596	71	LB	secondary
2401	24014	SP 1	1	-27.780180	12.548031	71	Fag 1-2	primary
4109	41091	SP 1	1	-26.799854	12.545952	71	LB	secondary
7101	71011	SP 2	0	-27.276007	12.526024	71	BF Diag	secondary
1403	14034	SP 2	0	-26.537823	12.478194	85	Fag 5-6	primary
1403	14033	SP 2	1	-26.537823	12.478194	85	Fag 5-6	primary
1403	14034	SP 1	0	-26.371724	12.421564	85	Fag 5-6	primary
1403	14033	SP 1	1	-26.371724	12.421564	85	Fag 5-6	primary
4115	41151	SP 2	1	-26.301539	12.416383	71	LB	secondary
4133	41331	SP 3	1	-26.391205	12.371279	71	LB	secondary
2401	24014	SP 2	1	-27.431717	12.332128	71	Fag 1-2	primary
4109	41091	SP 2	0	-26.204466	12.331429	71	LB	secondary
4108	41082	SP 2	1	-26.204466	12.331429	71	LB	secondary
4141	41411	SP 4	0	-26.544998	12.321479	71	LB	secondary
4140	41401	SP 4	1	-26.544998	12.321479	71	LB	secondary
4134	41341	SP 2	0	-26.275737	12.293085	71	LB	secondary

C Discretisation of Lerelva bridge.

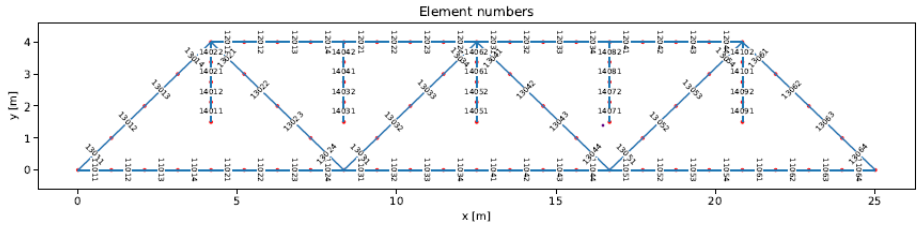

(a) Left side trusses on the Lerelva bridge.

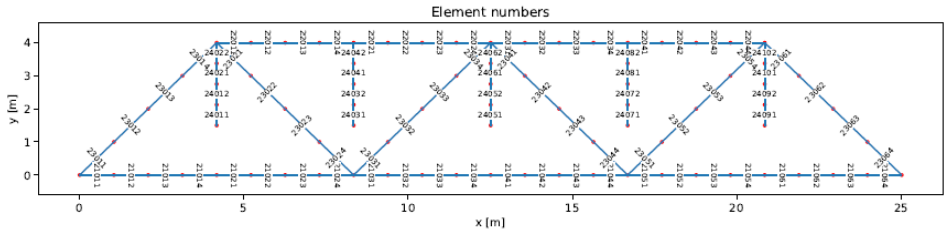

(b) Right side trusses on the Lerelva bridge.

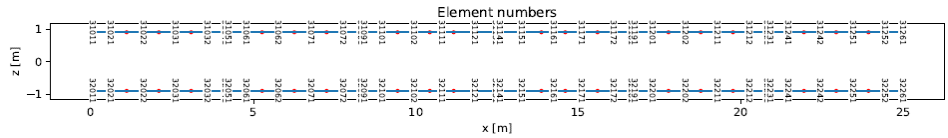

(c) Longitudinal grillages on the Lerelva bridge.

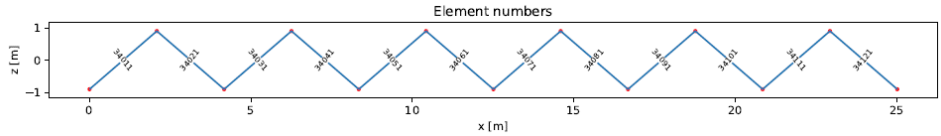

(d) Diagonal longitude grillages on the Lerelva bridge.

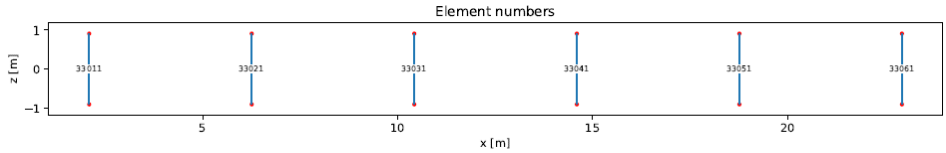

(e) Transverse longitudinal grillages on the Lerelva bridge.

Figure C1: Discretisation of the element numbers on the Lerelva bridge.

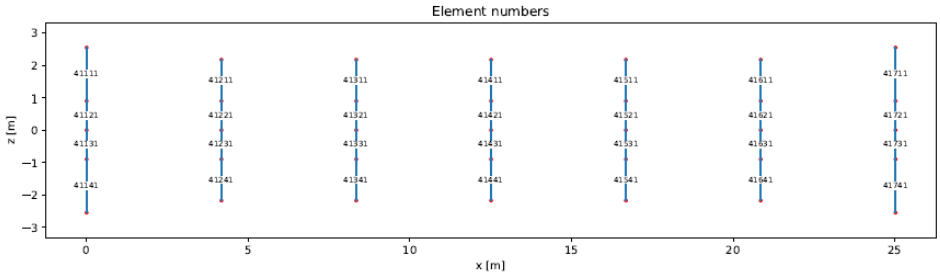

(f) Element numbers of the diagonal longitude grillages on the Lerelva bridge.

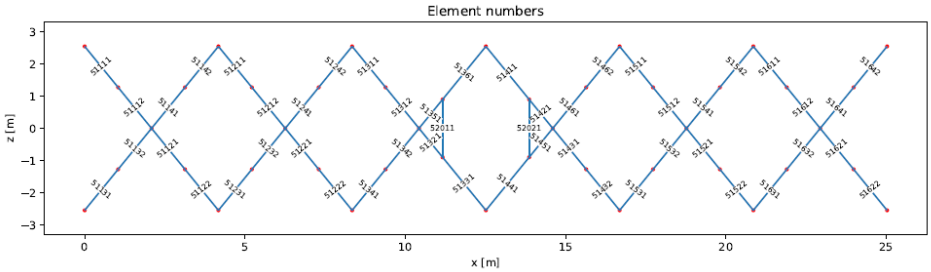

(g) Element numbers of the diagonal longitude grillages on the Lerelva bridge.

Figure C1: Discretisation of the element numbers on the Lerelva bridge.

D Discretisation of Brummund bridge.

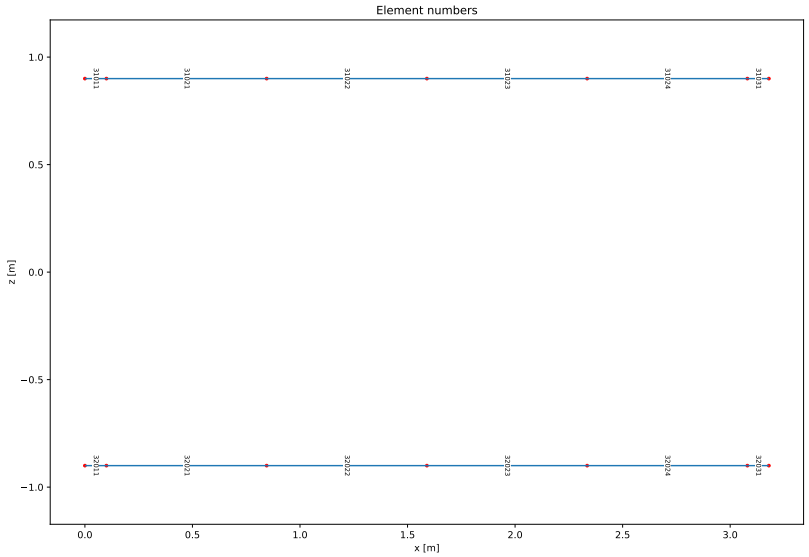

(a) Longit. grillage - part 1

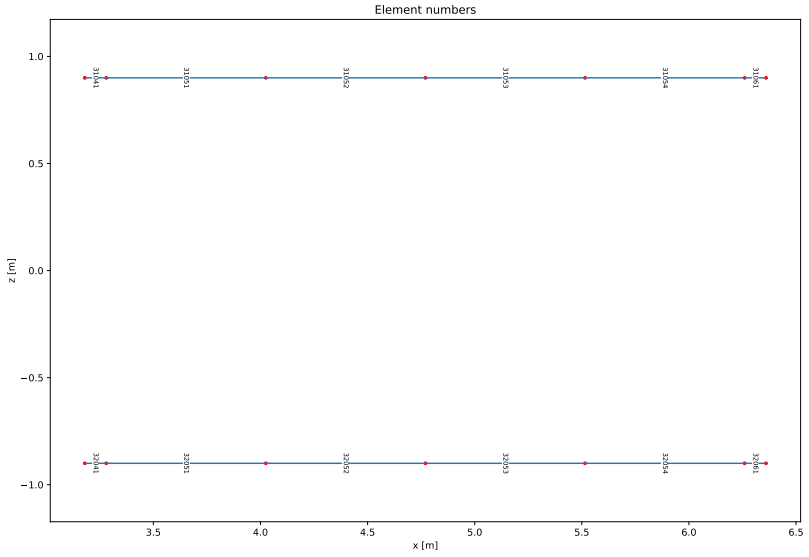

(b) Longit. grillage - part 2

Figure D1: Discretisation of the element numbers on the Brummund bridge.

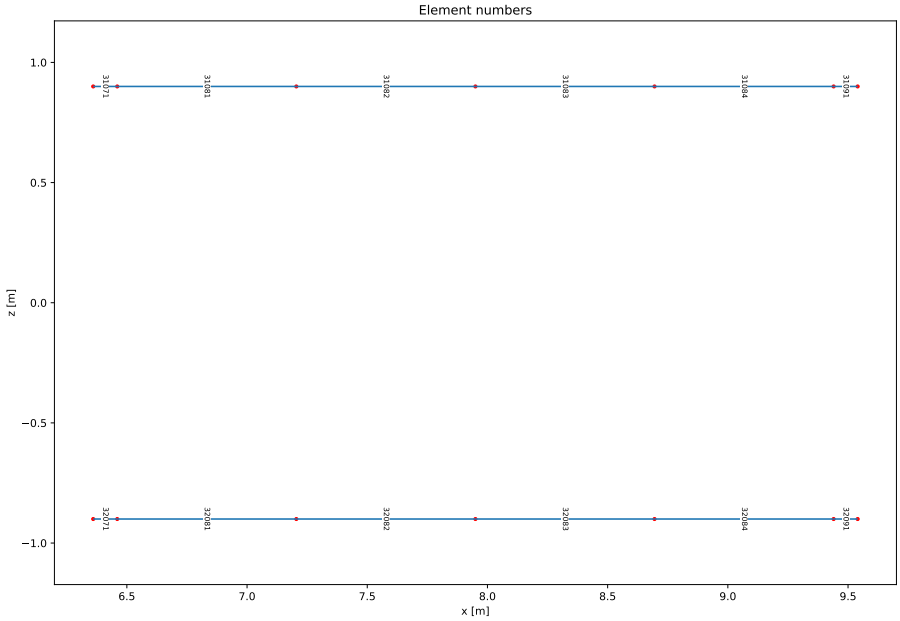

(c) Longit. grillage - part 3

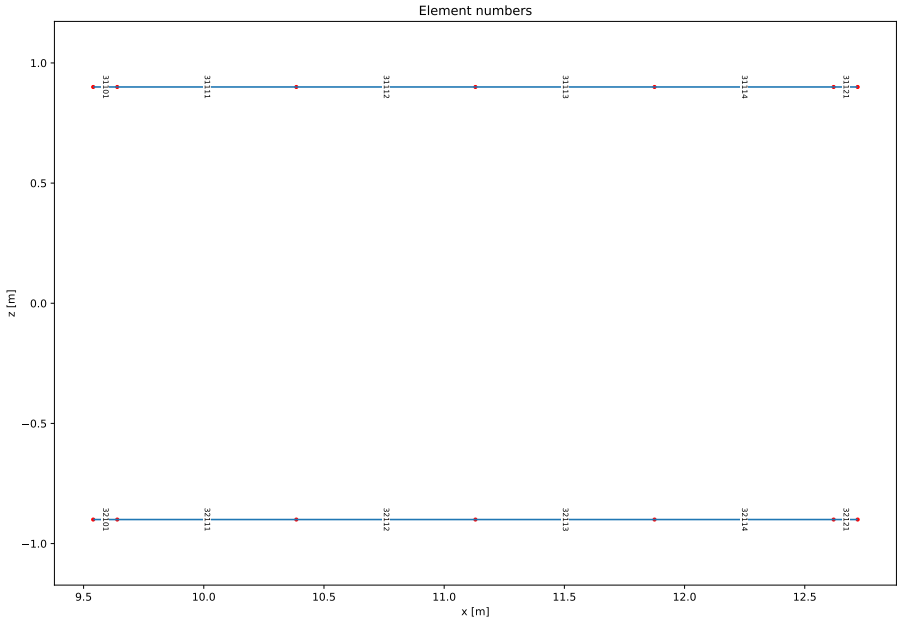

(d) Longit. grillage - part 4.

Figure D1: Discretisation of the element numbers on the Brummund bridge.

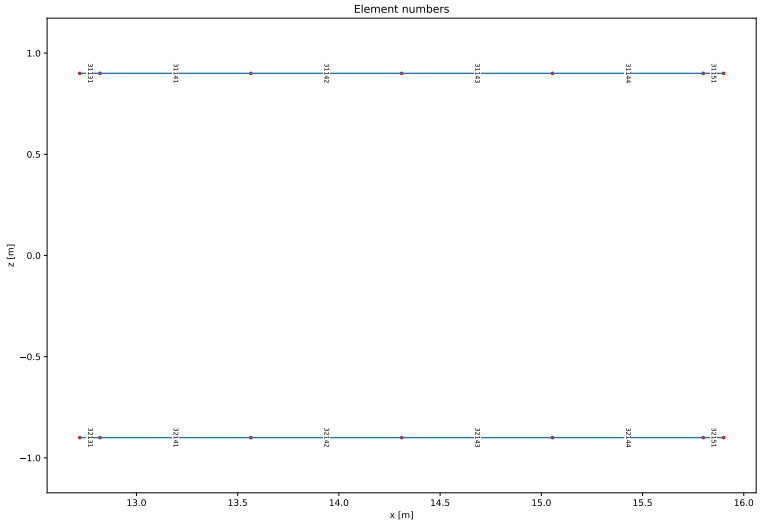

(e) Longit. grillage - part 5

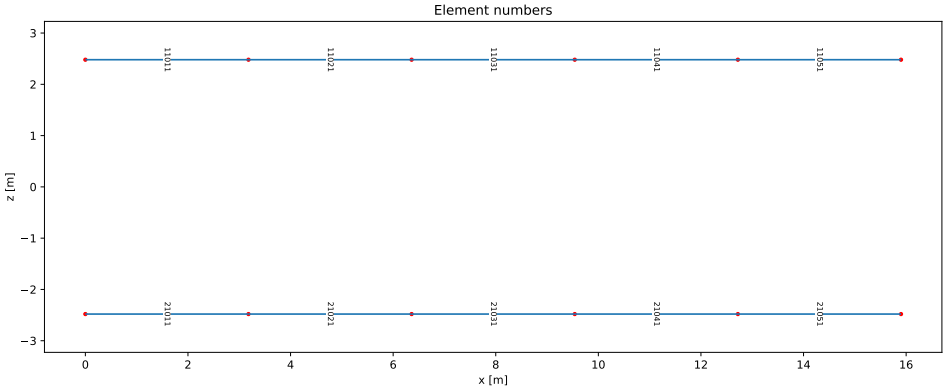

(f) Main girders

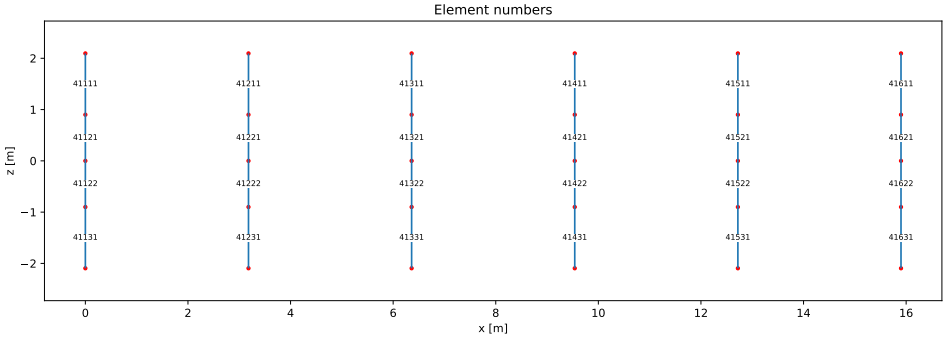

(g) Transverse grillage

Figure D1: Discretisation of the element numbers on the Brummund bridge.

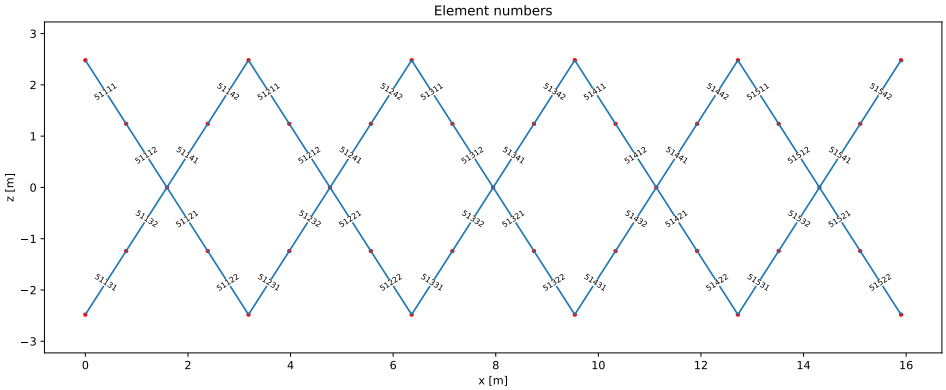

(h) Wind diagonals

Figure D1: Discretisation of the element numbers on the Brummund bridge.

E Discretisation of Saulidelva bridge.

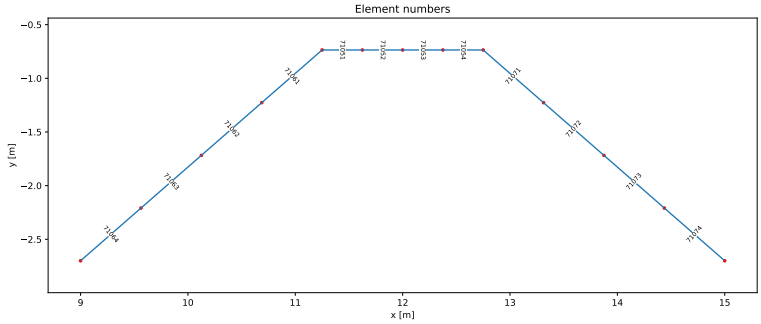

(a) Braking structure

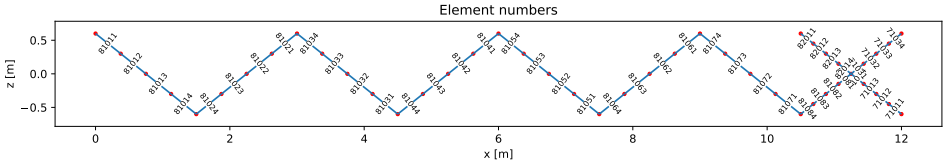

(b) Longitudinal diagonal part 1

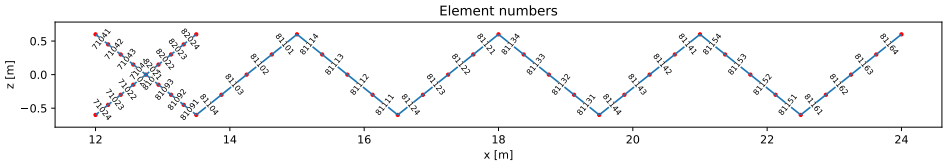

(c) Longitudinal diagonal part 2

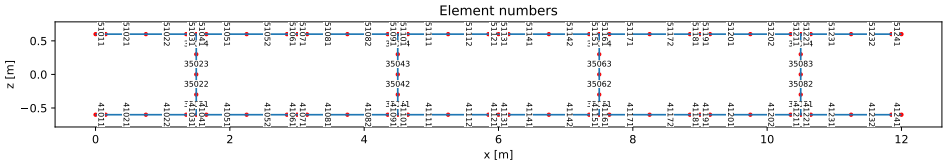

(d) Longtudinal grillage part 1

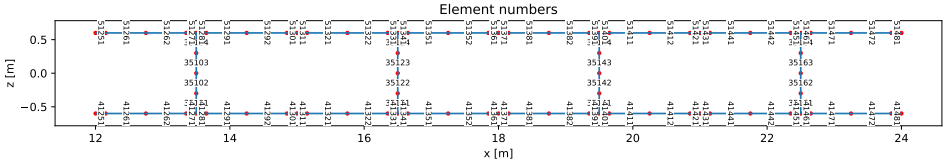

(e) Longitudinal grillage part 2

Figure E1: Discretisation of the element numbers on the Saulidelva bridge.

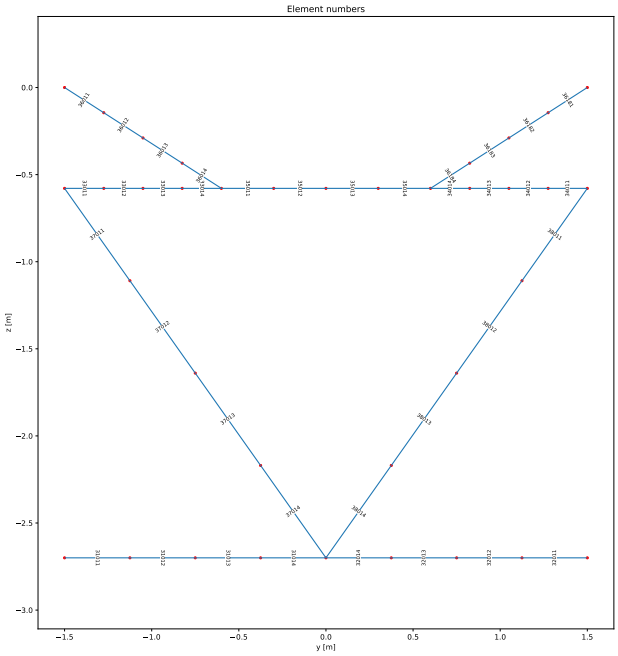

(f) Transverse grillage part 1

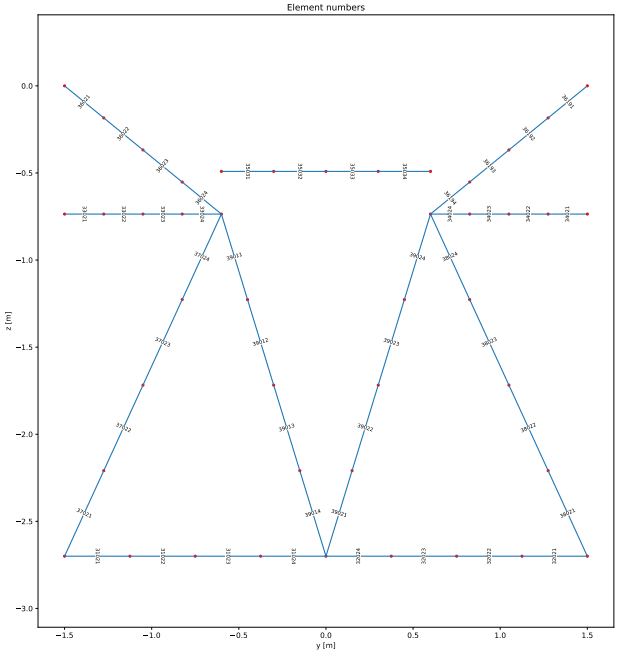

(g) Transverse grillage part 2

Figure E1: Discretisation of the element numbers on the Saulidelva bridge.

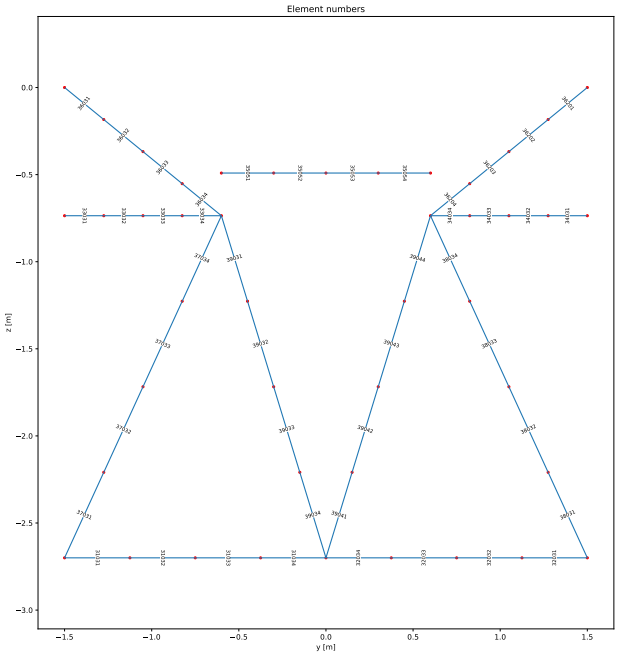

(h) Transverse grillage part 3

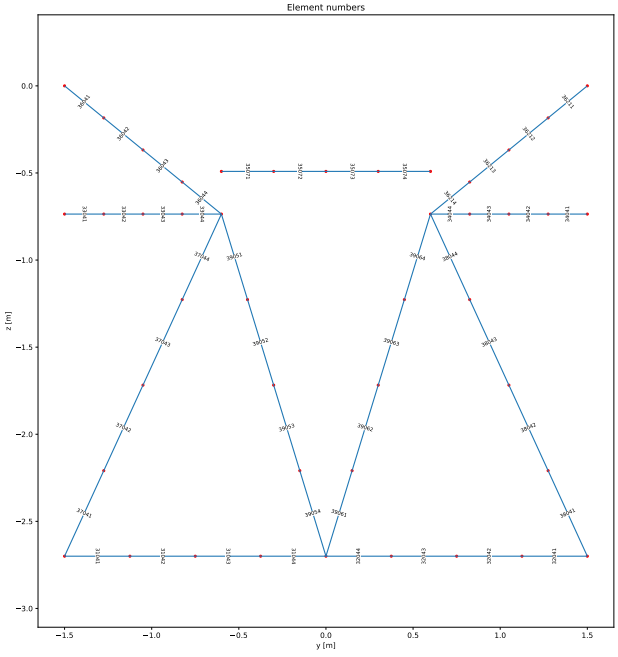

(i) Transverse grillage part 4

Figure E1: Discretisation of the element numbers on the Saulidelva bridge.

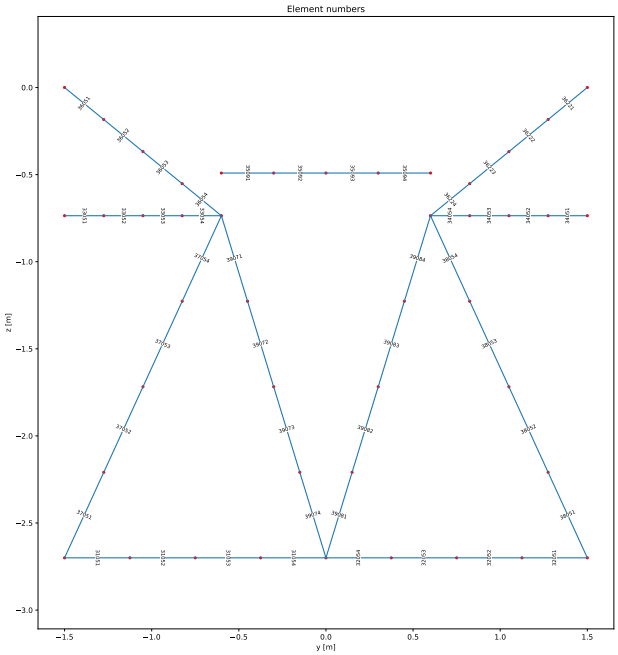

(j) Transverse grillage part 5

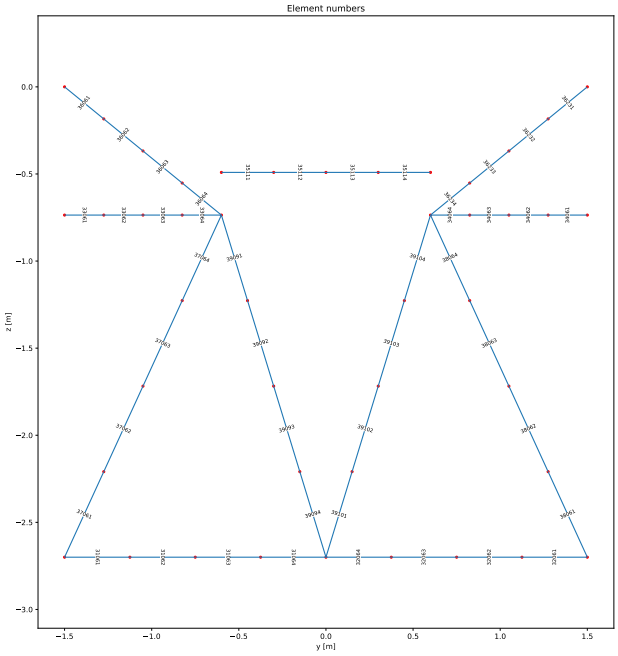

(k) Transverse grillage part 6

Figure E1: Discretisation of the element numbers on the Saulidelva bridge.

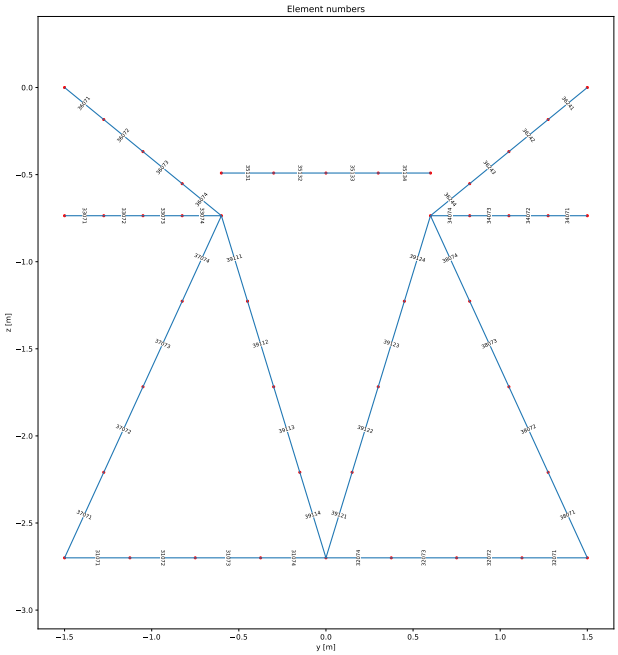

(l) Transverse grillage part 7

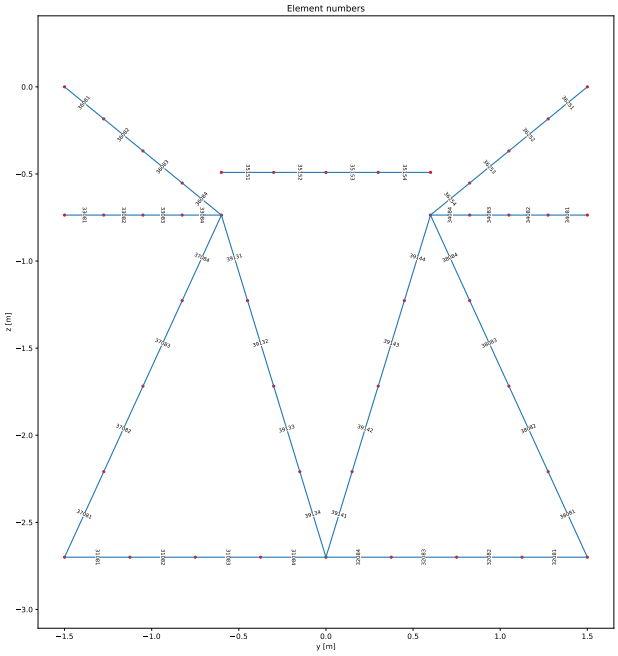

(m) Transverse grillage part 8

Figure E1: Discretisation of the element numbers on the Saulidelva bridge.

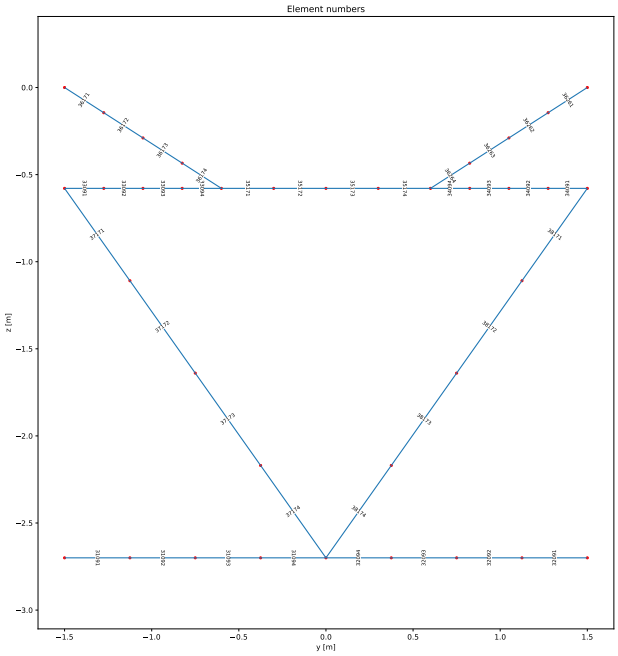

(n) Transverse grillage part 9

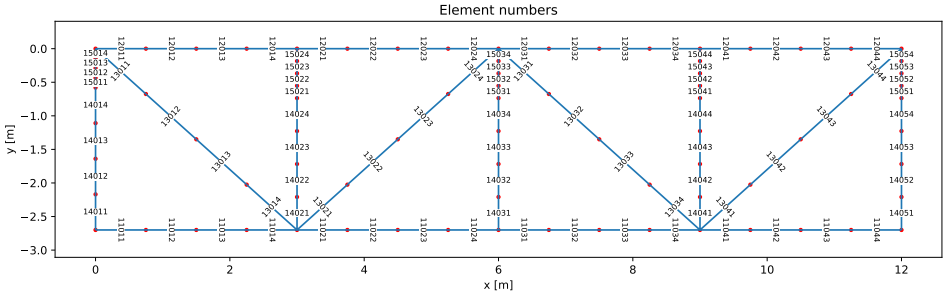

(o) Trusses left side part 1

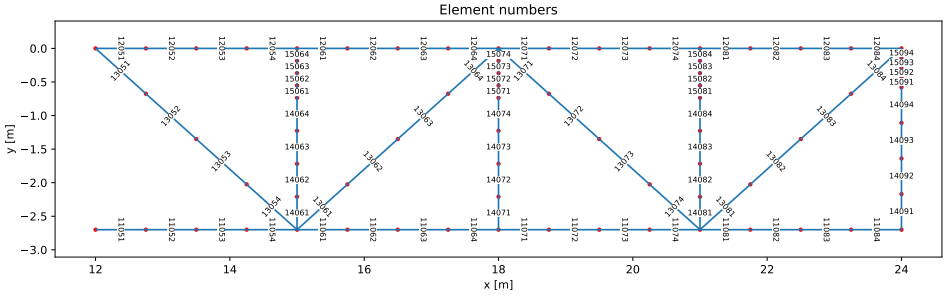

(p) Trusses left side part 2

Figure E1: Discretisation of the element numbers on the Saulidelva bridge.

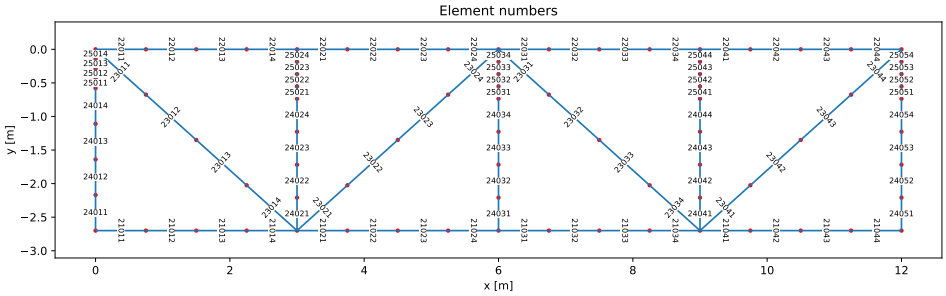

(q) Truss right side part 1

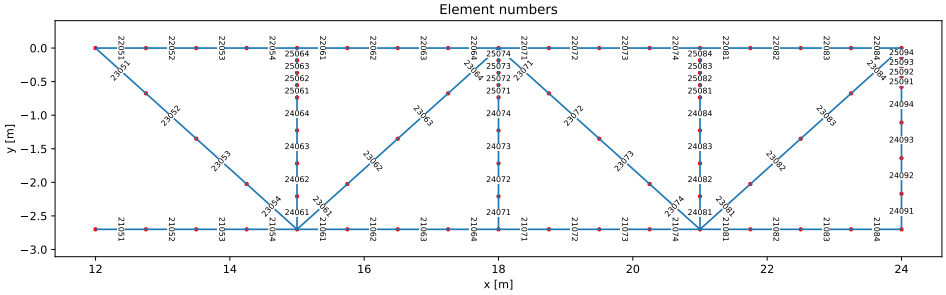

(r) Truss right side part 2

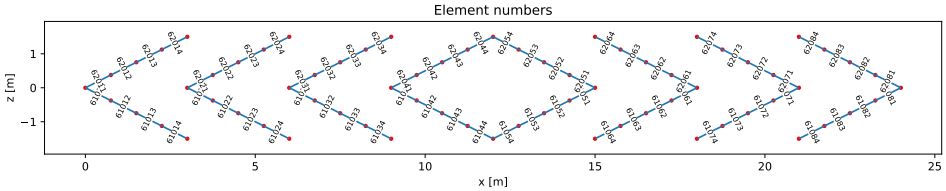

(s) Wind diagonals

Figure E1: Discretisation of the element numbers on the Saulidelva bridge.

Bibliography

[1] Beregningsrapport utmatting, Bru over Brummund elv. Technical Report KU-027955-000, Bane NOR, 2018.

[2] Beregningsrapport utmatting, Lerelva. Technical Report KU-027954-000, Bane NOR, 2018.

[3] Generelle prosjektforutsetninger. Technical Report KU-027972-000, Bane NOR, 2018.

[4] Beregningsrapport utmatting, Saulidelva. Technical Report KU-027943-000, Bane NOR, 2018.

[5] C. Amzallag, J. Gerey, J. Robert, and J. Bahuaud. Standardization of the rainflow counting method for fatigue analysis. *International Journal of Fatigue*, 16(4):287 – 293, 1994. doi: 10.1016/0142-1123(94)90343-3.

[6] CEN/TC250. *EN 1991-2: Eurocode 1: Actions on structures - Part 2: Traffic loads on bridges*. 2002.

[7] CEN/TC250. *EN 1993-1-9 (2005) (English): Eurocode 3: Design of steel structures - Part 1-9: Fatigue*. 2005.

[8] A. Fatemi and L. Yang. Cumulative fatigue damage and life prediction theories: A survey of the state of the art for homogeneous materials. *International Journal of Fatigue*, 20:9–34, 01 1998. doi: 10.1016/S0142-1123(97)00081-9.

[9] G. T. Frøseth. Load model of historic traffic for fatigue life estimation of norwegian railway bridges, 2019. ISBN: 9788232637485.

[10] G. Marsh, C. Wignall, P. R. Thies, N. Barltrop, A. Incecik, V. Venugopal, and L. Johanning. Review and application of rainflow residue processing techniques for accurate fatigue damage estimation. *International Journal of Fatigue*, 82:757 – 765, 2016. ISSN 0142-1123. doi: https://doi.org/10.1016/j.ijfatigue.2015.10.007.

[11] A. Taras and R. Greiner. Development and application of a fatigue class catalogue for riveted bridge components. *Structural Engineering International*, 20:91–103, 02 2010. doi: 10.2749/101686610791555810.

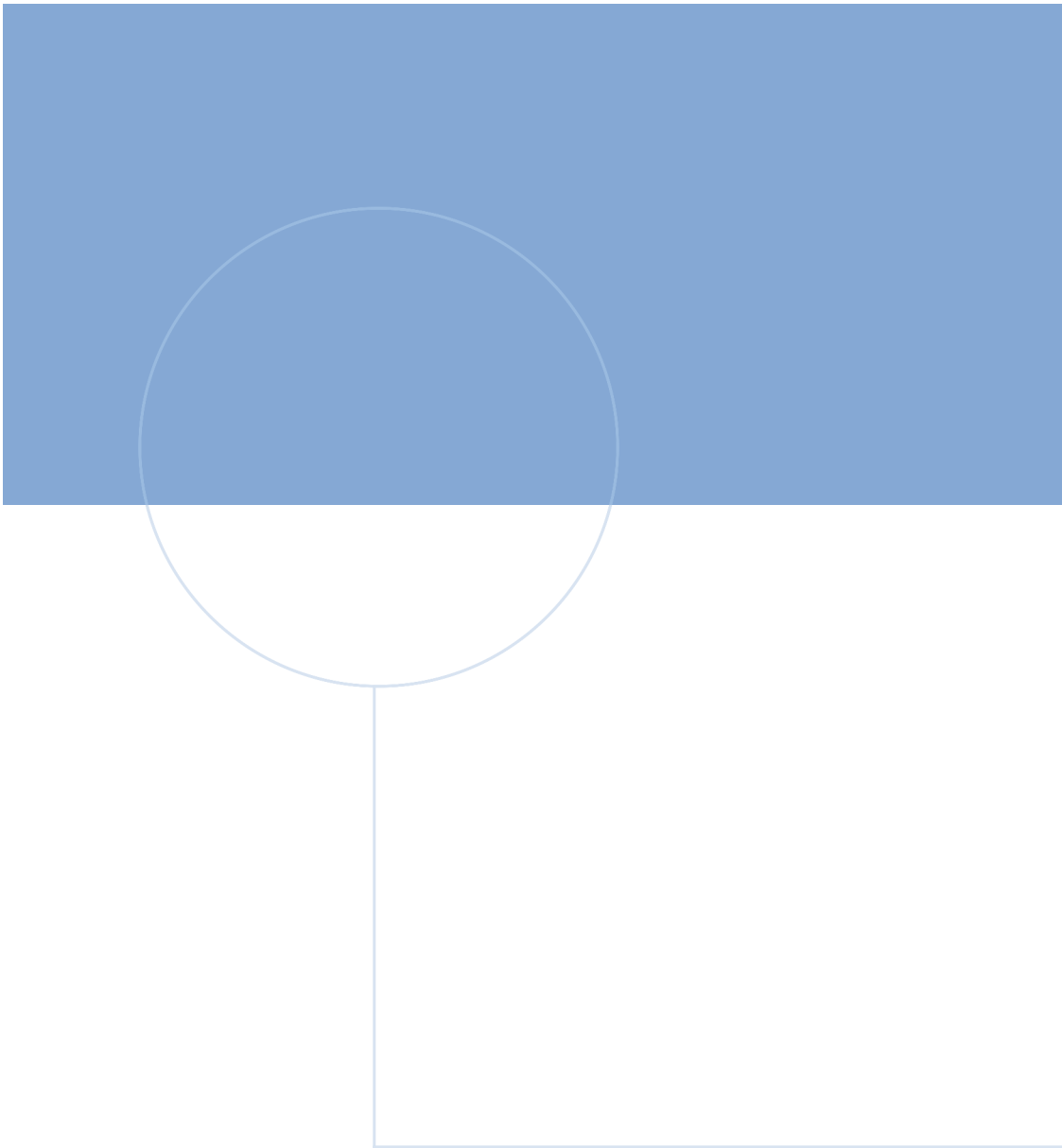

NTNU

Norwegian University of
Science and Technology